Yang *et al. Energy Mater* 2022;2:200006
DOI: 10.20517/energymater.2022.02

Energy Materials

Review

Open Access

Check for updates

Multi-dimensional correlation of layered Li-rich Mn-based cathode materials

Zhe Yang[1], Chaoliang Zheng[1], Zhicheng Wei[1], Jianjian Zhong[1], Huirong Liu[1], Jiameng Feng[1], Jianling Li[1,*], Feiyu Kang[2]

[1]State Key Laboratory of Advanced Metallurgy, School of Metallurgical and Ecological Engineering, University of Science and Technology Beijing, Beijing 100083, China.
[2]Tsinghua Shenzhen International Graduate School, Tsinghua University, Shenzhen 518055, Guangdong, China.

***Correspondence to:** Dr. Jianling Li, State Key Laboratory of Advanced Metallurgy, School of Metallurgical and Ecological Engineering, University of Science and Technology Beijing, Beijing 100083, China. E-mail: lijianling@ustb.edu.cn

How to cite this article: Yang Z, Zheng C, Wei Z, Zhong J, Liu H, Feng J, Li J, Kang F. Multi-dimensional correlation of layered Li-rich Mn-based cathode materials. *Energy Mater* 2022;2:200006. https://dx.doi.org/10.20517/energymater.2022.02

Received: 11 Jan 2022 **First Decision:** 9 Feb 2022 **Revised:** 16 Feb 2022 **Accepted:** 18 Feb 2022 **Published:** 28 Feb 2022

Academic Editors: Yuping Wu, Wei Tang **Copy Editor:** Xi-Jun Chen **Production Editor:** Xi-Jun Chen

Abstract

Lithium-rich manganese-based cathode materials are expected to promote the commercialization of lithium-ion batteries to a new stage by virtue of their ultrahigh specific capacity and energy density advantages. However, they are still restricted by complex phase transitions and electrochemical performance degradation caused by labile anion charge compensation. A deep understanding of the electrochemical properties contained in their intrinsic structures and the key driving factors of structural deterioration during cycling are crucial to guide the preparation and optimization of lithium-rich materials. Considering recent progress, this review introduces the intrinsic properties of Li-rich manganese-based cathode materials from interatomic interactions to particle morphology at multiple scales in the spatial dimension. The charge compensation mechanism and energy band reorganization of the initial charge and discharge, the structural evolution during cycling and the electrochemical reaction kinetics of the materials are analyzed in the temporal dimension. Based on the relationship between structure and electrochemical performance, preparation methods and modification methods are introduced to guide and design cathode materials. Effective characterization methods for studying anion charge compensation behavior are also demonstrated. This review provides important guidance and suggestions for making full use of the high specific capacity in these materials derived from anion redox and the maintaining of its stability.

Keywords: Li-ion batteries, Li-rich Mn-based cathodes, anion redox, structure-activity relationships, multiple dimensions

INTRODUCTION

The energy revolution is in the ascendancy. With the current global climate deteriorating, the reduction of carbon emissions has become an important measure to address climate change[1]. The main measures to reduce carbon emissions are to reduce the use of fossil energy and vigorously develop sustainable clean energy. As state-of-the-art electrochemical energy storage and conversion devices, lithium-ion batteries (LIBs) have been widely used in all aspects of modern society, including 3C products, electric vehicles and energy storage, and are an important link in achieving energy optimization and transformation[2].

High energy density is the eternal development direction for LIBs. From the 80 Wh kg^{-1} energy density of the first generation of commercial LIBs launched by Sony in the 1990s, LIBs have gone through several innovations in every aspect, from materials to assembly[3]. Cathode materials account for the largest cost and proportion of LIBs and are therefore significant limiting factors in reducing costs and increasing energy density. Current commercial cathode materials, including layered $LiCoO_2$, $LiNi_xCo_yMn_{1-x-y}O_2$ (NCM) and $LiNi_xCo_yAl_{1-x-y}O_2$, spinel $LiMn_2O_4$ and olivine $LiFePO_4$[4], have gradually reached their theoretical capacity energy density. In order to break through the energy bottleneck of LIBs, electrode materials need to be reformed in the electrochemical reaction system. Compared with the traditional cationic charge compensation mechanism, the unique anion redox mechanism of lithium-rich manganese-based layered oxides (LRMOs), $xLiMO_2 \cdot (1-x)Li_2MnO_3$ (M = Ni, Co, Mn, $Ni_{1/2}Mn_{1/2}$, $Ni_{1/3}Co_{1/3}Mn_{1/3}$ and so on), creates conditions for achieving higher specific capacity and energy density. These materials can achieve a high specific capacity exceeding 250 mAh g^{-1} in a large voltage range of 2.0-4.8 V, thereby making them ideal candidates for the next generation of LIB cathode materials[5].

Nevertheless, LRMOs still face a series of challenges that seriously hindered their commercialization. These challenges include: (1) a lack of systematic understanding in their intrinsic structure-activity relationships at multiple spatial scales; (2) low Coulombic efficiency and serious voltage hysteresis caused by the violent structural reorganization during the initial charge-discharge cycle; (3) capacity attenuation and voltage decay due to phase transformations and the dissolution of active Mn with deposition on the anode electrode[6,7]; (4) poor rate performance limited by sluggish electrode reaction kinetics[8]; and (5) reasonable and efficient materials preparation, modification and characterization methods that require substantial organization and improvement.

With extensive surveying and the employment of more advanced atomic-scale *in-situ*/*ex-situ* characterization technologies, the in-depth mechanisms behind the above-mentioned problems and their optimization/modification have achieved remarkable progress. Based on research of model materials, such as Li_2MO_3 (M = Mn[9], Ru[10], Ir[11], Mo[12] and Ti[13]), the trigger mechanism and reversibility of anion redox and its influence on the structure and electrochemical performance have been gradually clarified. For LRMO cathodes, the monolithic materials undergo a series of complex phase evolutions during electrochemical cycling, including irreversible migration of in-plane/out-of-plane transition metals (TMs)[14], evolution of the superlattice structure, generation and diffusion of oxygen vacancies, lattice structure distortion and deterioration and the continuous transition of redox couples[15]. In addition, more serious O_2 release, element dissolution, electrolyte erosion and structure densification occur in the near-surface interlayer of the material particles. In view of the above, surface modification[16], bulk doping[17], morphology control[18], element ratio[19], local structure[20], electrode/electrolyte[21] and so on, have been

considered to improve the structural stability and electrochemical performance of these cathode materials from different perspectives.

Based on the traditional view and recent research progress into LRMOs[22-24], this review elaborates the intrinsic structure, electrochemical properties and their relationship in the scope of multiple spatial scales (atomic scale, local structure, particle morphology and so on). The temporal clues of these materials in electrochemical processes also demonstrate the structure and energy band changes that cause inconsistency in the initial charge-discharge behavior, the influence of the local structural evolution on the electrochemical performance during cycling and the restrictive factors of the sluggish electrode reaction kinetics. The effective means for improving the electrochemical performance of LRMOs are reported from the aspects of materials preparation and modification. Classical electrochemistry and advanced physical characterization methods are introduced to comprehensively study the electrochemical reaction, structural evolution and anion charge compensation mechanism of LRMOs. Finally, various challenges that still exist in current research, countermeasures and future research directions are proposed (Scheme 1).

SPATIAL DIMENSION

The derivation of cathode performance depends on its structure and the understanding of structure-activity relationships is an ever-important topic. In order to clarify the electrochemical characteristics and the evolution laws of lithium-rich cathode materials, it is necessary to consider them from a multiscale perspective with regards to electron/energy band configuration, local microstructure and particle morphology.

Spatial coordination of elements

Li-O-Li configuration

LRMO cathode materials consist of $LiMO_2$ (M = Ni, Co, Mn and so on) and Li_2MnO_3 components, where Li and TM atoms are located at the center of octahedra surrounded by six oxygen atoms and the atom layer alternately arranges as O/Li/O/TM along the *c* axis. The occupation of extra Li atoms at the TM sites results in a $\sqrt{3}a \times 3a$ $LiMn_6$ superstructure, which gives rise to a change in the coordination environment of oxygen, i.e., three Li-O-TM configurations transform into two Li-O-TM configurations and a special Li-O-Li configuration[25] (shown in Figure 1A). The intense interaction of Li-O ionic bonds leaves the distribution of coordination electrons between Li and O closer to the oxygen element, forming an isolated unhybridized O 2p orbital. The Li-O-Li configurations stimulate a higher energy band, enabling the charge compensation of oxygen during charging (the downward shift of the Fermi level). TM-O bonds rotate along the other directions, resulting in the coplanar arrangement of adjacent unhybridized O 2p orbitals, which interact with each other to ultimately form O-O dimers. The unhybridized oxygen orbitals caused by the Li-O-Li configurations can also be triggered by other configurations[26] (such as Li-O-vacancy and Li-O-Na configurations).

TM-O hybridization

The charge compensation of anions is more closely associated with TMs coordinated by oxygen atoms[27], which is attributed to the two Li-O-TM configurations and one Li-O-Li configuration. For the typical Mn-based material Li_2MnO_3, Mn bonds with oxygen in a form where the non-bonding oxygen energy band with high activity is separated from the Mn t_{2g} energy band and electrons directly escape from it, contributing to the severe irreversible release of oxygen[28]. The introduction of Fe into the inert structure of Li_2TiO_3 successfully motivates the anion redox activity[13]. This can be attributed to the fact that electron holes tend to be selectively generated on oxygen ions bonded to Fe atoms instead of Ti atoms. The mechanism can also be extended to the stimulation of anions in Co-doped Li_2TiS_3.

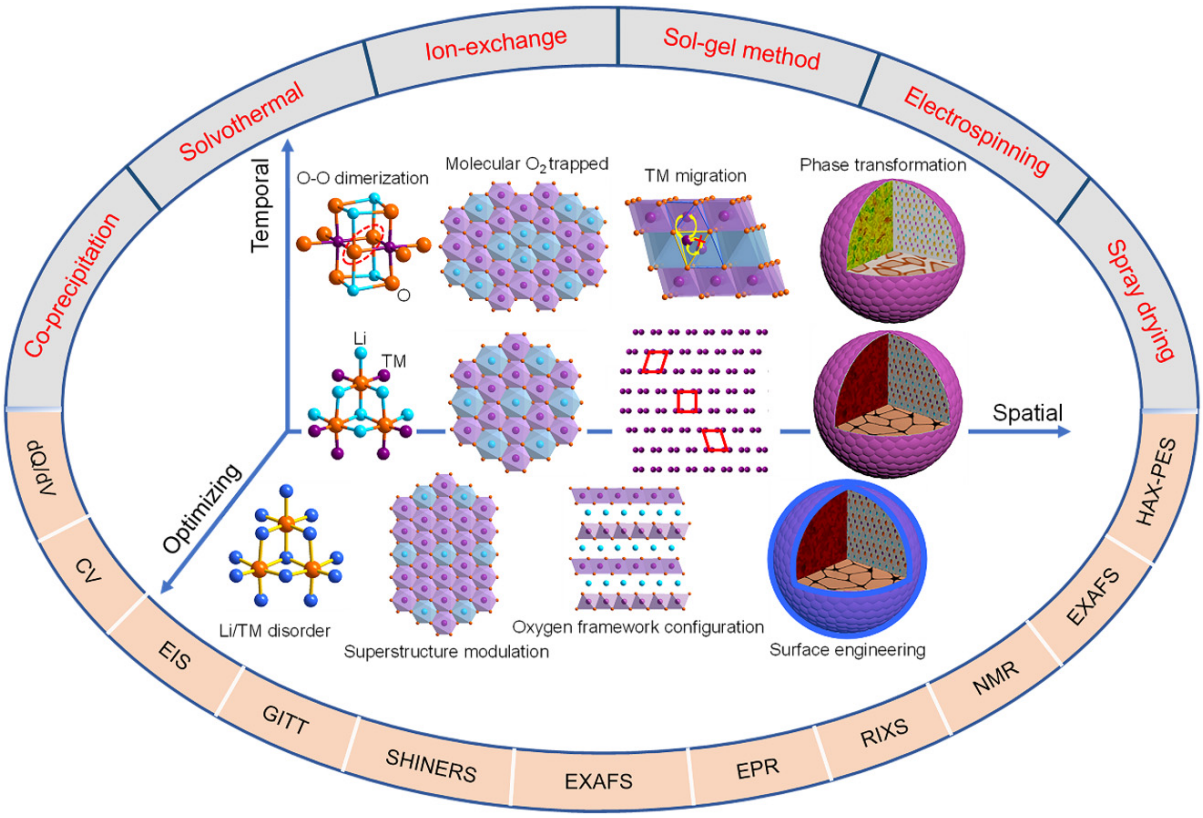

Scheme 1. Summary of layered Li-rich Mn-based cathode materials in multiple dimensions.

In the model Li_2RuO_3 material, the strong covalent interaction between Ru and oxygen causes overlap of the Ru 4d and O 2p non-bonding bands, exhibiting a competitive anion-cation redox coupling reaction with highly reversible anion redox[10]. The redox activity of Li_2RuO_3 can be regulated by the weaker covalency of the Sn-O bond. Furthermore, the intensely bonding Ir-O immensely suppresses the charge compensation ability of oxygen for Li_2IrO_3 and all the capacity derives from the redox reaction of Ir hybridized with oxygen[29]. When Ir is partially replaced by Sn, the lower number of valence electrons at the end of charging significantly promotes the ligand-to-metal charge transfer, resulting in short Ir-O π bonds and O-O dimers with a bond length of 1.4 Å. In Li_2RhO_3, with an intense π-type interaction [Figure 1B], the weaker difference in electronegativity between Rh and oxygen causes a more intense TM-O interaction and increases the contribution of O 2p to the high-energy π^* orbital. Oxygen exhibits high reactivity under the occupied anti-bonding state as the π electron donor of the central Rh, displaying a novel oxygen redox reaction at low voltages[30] (which is different from the redox of non-bonding oxygen), where oxygen participates in the reaction prior to Rh. The functional mechanism is demonstrated to be triggered by the oxygen-dominated π^* hybrid states.

As a result, the non-bonding O energy band is subtly regulated by the varieties and numbers of adjacent TM elements, owing to the π-type interaction between Li-O-Li configuration and TM t_{2g} bands. The hybridization state of TM-O is key for adjusting the anion charge compensation ability. The ability to resist oxygen loss and structural deterioration is promoted with the increase in M-O covalent bonds[31]. The redox mechanism derived from the 3d metals and more heavy metals with a d^0 electron configuration in Li_2MnO_3 is related with the lone-pair electron consumption of oxygen (locally non-bonding O 2p state), which leads to irreversible anion redox. Electrode materials formed by the coordination hybridization between oxygen

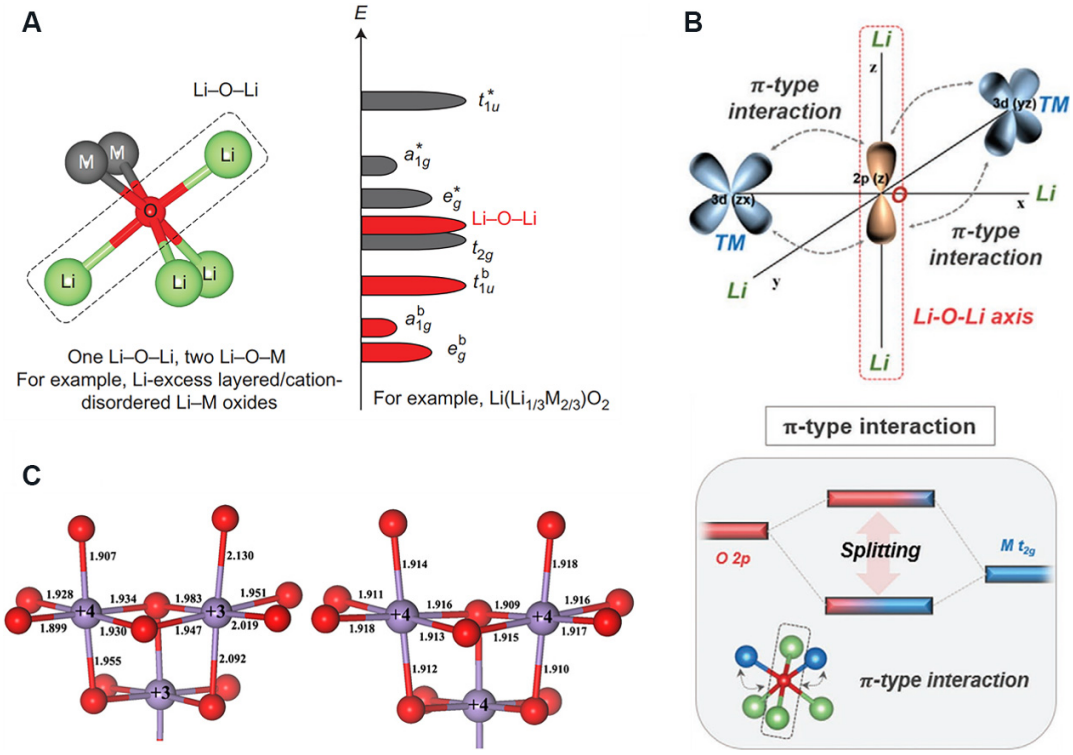

Figure 1. (A) Local coordination of oxygen with one Li-O-Li and two Li-O-M configurations and a schematic of the band structure for Li-rich layered oxides[25]. (B) Schematic of π-type hybridization of the Li-O-Li axis with neighboring TM and the band structure for the π-type hybridized state of the Li-O-Li axis interacted with M t_{2g}[27]. (c) Local coordination around Mn^{3+} and Mn^{4+} in $LiMn_2O_4$ (left) and λ-MnO_2 (right) obtained from theoretical calculations. The gray and red spheres represent Mn and oxygen atoms, respectively[33].

and 4d and 5d metals with intermediate d^n electron configurations are able to induce reversible cation and anion redox activity to realize reversible extra capacity.

The anion and cation redox ability can be visibly judged according to a Zaanen-Sawatzky-Allen diagram via the comparison of U (Coulombic interaction, depending on the d metal) and D (energy difference between (M-O) and (M-O)*, known as the charge transfer parameter)[32]. When U << D, the d band established in the (MO)* state locates first on the Fermi level, resulting in pure cation redox. When U > > D, the O 2p state on the p band lies at the Fermi level, thereby motivating anion redox that leads to the generation of highly unstable electron holes and highly activated free radicals in localized states. O-O dimers then form and escape from the lattice, giving rise to the serious irreversible release of oxygen. When U ≈ D/2, the d bands in the antibonding (MO)* states overlap with the O 2p non-bonding band, which stimulates the anion/cation redox mechanism and stabilizes the Fermi level via the decrease in local symmetry in the case of electron loss. Therefore, it is necessary to choose appropriate TM-O hybridization, local coordination and a combination to improve the possibility of reversible anion redox in the actual electrochemical window.

Jahn-Teller effect

The $LiMn_6$ superstructure formed by Mn plays an important role in motivating anion redox in LRMO cathode materials. Simultaneously, the anions in turn activate Mn to participate more in the redox reaction. The coupling of Mn and oxygen is supposed to have significant synergistic effects on stabilizing $(O_2)^{n-}$ species and activating more Mn ions to participate in the electrochemical process. However, the valence of

Mn undergoes a deep evolution in a wide voltage window of 2.0-4.8 V. The layer structure of LRMOs gradually transforms into the Li_2MnO_4 spinel phase with cycling, which induces Jahn-Teller distortion[33] [Figure 1C] that seriously influences the structural stability and electrochemical performance.

The Jahn-Teller effect refers to the asymmetric occupation of electrons in degenerate orbitals that causes a distortion of the geometric configuration, thus reducing the symmetry of the molecule and the orbital degeneracy, and further decreasing the energy of the system. In a $Mn^{3+}O_6$ octahedron, there is only one electron in the doubly degenerate e_g orbitals ($d_{x^2-y^2}$ and d_{z^2} orbitals) for high-spin Mn^{3+}[34], which leads to asymmetry of the electron distribution. To reduce the energy of the system, the bond length of Mn-O along the z-axis is elongated and four Mn-O bonds in the horizontal direction are shortened, causing a structural distortion that is not observed in the $Mn^{4+}O_6$ octahedron. It is generally considered that the critical mean valence of Mn is 3.5+ when Jahn-Teller distortion occurs. Moreover, unstable Mn^{3+} is prone to undergo a disproportionation reaction of $Mn^{3+} \rightarrow Mn^{4+} + Mn^{2+}$. Mn^{2+} dissolves into the electrolyte and deposits on the anode, resulting in a loss of active material and an increase in the electrochemical impedance on the electrode interface. Therefore, it is necessary to regulate the variation of Mn valence during the electrochemical process to decrease the content of Mn^{3+}.

Local structure

Crystal structure and nanodomains

Owing to the composition of the *R*$$\bar 3$$*m* $LiMO_2$ phase and *C*2/*m* Li_2MnO_3 component, LRMO materials display complex structural characteristics. The (001) crystal plane of the *C*2/*m* phase just overlaps with the (003) crystal plane of the *R*$$\bar 3$$*m* phase and both the interplanar spacings are close to 4.7 Å, which causes the two components to appear dissolved at the atomic scale and mixed at the nanometer scale [Figure 2A]. Interestingly, weak peaks at 20-25° appear in the X-ray diffraction (XRD) patterns, owing to the loss of the systematic absence for the $LiMn_6$ superstructure. Jarvis *et al.*[35] demonstrated that $Li[Li_{0.2}Ni_{0.2}Mn_{0.6}]O_2$ was composed of a solid solution with *C*2/*m* monoclinic symmetry and multiplanar defects via the combination of atomic-scale high-angle annular dark-field aberration-corrected scanning transmission electron microscopy (HAADF-STEM) and XRD. In particular, there are two-phase regions, owing to the loss of ordering between Li^+ and Mn^{4+} in the TM layer with less lithium. Yu *et al.*[36] also clarified the coexistence of $LiMO_2$ and Li_2MnO_3 with sizes of 2-4 nm in $Li_{1.2}Ni_{0.15}Co_{0.1}Mn_{0.55}O_2$. Yu *et al.*[37] revealed the symbiotic heterogeneous interface of rhombohedral $LiMO_2$/monoclinic Li_2MnO_3 at the atomic scale in $Li_{1.2}Mn_{0.567}Ni_{0.166}Co_{0.067}O_2$ via aberration-corrected STEM and computer simulations. The two structures were separated by the $(003)_{rh}$ and $(001)_{mon}$ crystal planes along the *c*-axis [Figure 2B].

In addition, stacking faults[38,39] along the *c*-axis exist both in the two-phase symbiotic heterogeneous interface and simple structure, which is the root cause of broadened superstructure diffraction peaks. Shunmugasundaram *et al.*[40] discovered that the location of the superstructure diffraction peaks varied monotonously with the Ni content, while the probability of stacking faults increased monotonously with the content of Ni according to the XRD patterns fitted by FAULTS. Therefore, the presence of heterovalent ions, such as Ni^{2+}, disturbs the stacking order along the *c*-axis and broadens the superstructure peaks of the material [Figure 2C]. Similarly, House *et al.*[41] determined 20% stacking faults in a pristine $Li_{1.2}Ni_{0.13}Co_{0.13}Mn_{0.54}O_2$ material. These widespread stacking faults result in local segregation of Li/Mn, expansion of the interplanar spacing and local heterodomains[42], which influence the extraction/insertion of Li^+, the structure size in the direction vertical to the TM/Li layer, the coordination environment of lattice oxygen and the distribution of 2p electrons, thereby changing the reaction behavior and activity of LRMOs.

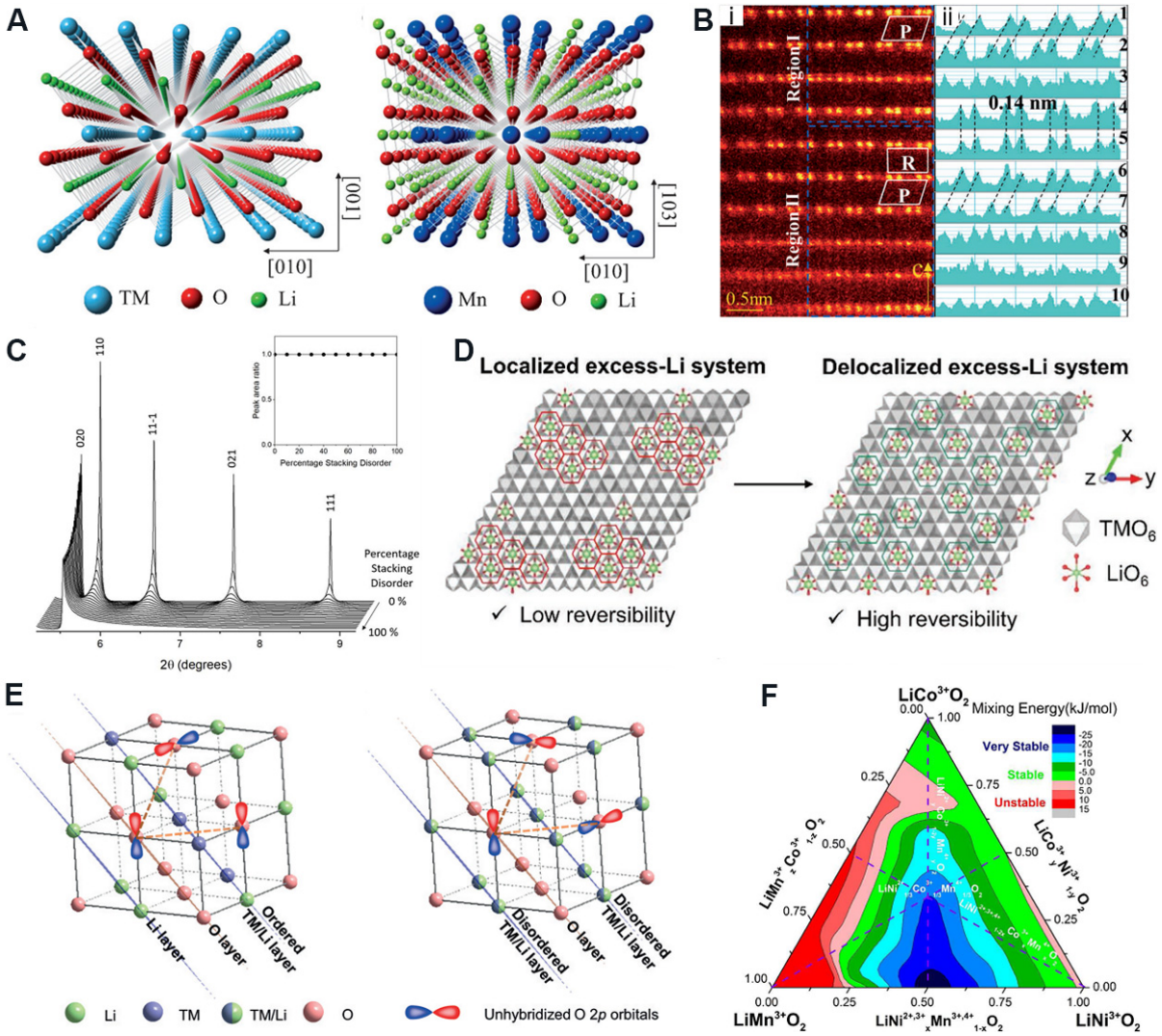

Figure 2. (A) Crystal structure of rhombohedral $LiMO_2$ (left) and monoclinic Li_2MnO_3 (right)[37]. (B) HAADF images (i) and intensity profiles (ii) of the two-phase intergrowth and heterointerface along the $[001]_{rh}$ zone axis direction[37]. (C) Increasing stacking disorder results in asymmetric peak broadening with no decrease in the peak area ratio between the superstructure peaks and the 001 direction (inset)[41]. (D) Morphological and structural designs for a delocalized excess Li system for enabling high electrode density and reversibility[20]. (E) 2D-ordered cation layered structure with coplanar unhybridized O 2p orbitals (left) and 3D-disordered cation framework with a random spatial distribution of unhybridized O 2p orbitals (right)[49]. (F) Mixing energy predicted from bonding model for the solid-solution $LiMO_2$ (M = Ni, Co and Mn) phase[51]. HAADF: High-angle annular dark-field.

Cation arrangement

The $LiMn_6$ superstructure is the key factor to induce anion redox and O-O dimers in the TM layer and its distribution deeply affects the whole structural evolution and electrochemical performance of the material[43]. Hwang *et al.*[20] discovered that $Li_{1.11}Mn_{0.49}Ni_{0.29}Co_{0.11}O_2$ with a relatively delocalized distribution of the superstructure exhibited more stable lattice oxygen [Figure 2D], which was attributed to the more dispersed distribution of highly active oxygen in an oxidized state that effectively suppressed the polymerization of O-O dimers and the release of O_2 during the extraction of Li^+. In addition, Song *et al.*[44] found that a disordered distribution of Li/Mn in the TM layer improved the symmetry of LRMOs and substantially adjusted the redox activity of oxygen, which helped to realize the reversibility of the structure, thereby alleviating the Jahn-Teller effect, decreasing the band gap and expanding the two-dimensional (2D)

diffusion channel of Li^+. The Li vacancy in the superstructure inhibited the dimerization of O-O in anion redox. This disordered arrangement is also universally applicable to other Li-rich systems. For Li_2RuO_3, the local symmetry around the oxygen ions is adjusted by the disordered arrangement in the Li/TM layer, so that the response structure to anion redox of the material transforms from the original O-O dimers to the retractable O-Ru-O configurations[45], thereby inhibiting the significant release of oxygen and promoting the cycle stability.

The cation arrangement between the TM and Li layers profoundly influences the coordination environment of oxygen and the whole structural stability of the material[46-48]. In LRMO materials with 2D cation arrays, the oxygen ions in Li-O-Li configurations interact with adjacent oxygen ions to reduce the O-O distance and their energy in the oxidized state. The interaction of different oxygen ions leads to a decrease in the bond angle of O-TM-O and the overlap of TM e_g and O 2p orbitals[49], which weakens the bonding of TM-O and damages the stability of the structural framework. Two unhybridized O 2p orbitals are non-coplanar in the structure with disordered three-dimensional (3D) cation arrays and the lack of interaction and bonding between the two orbitals inhibits the dimerization of O-O. This results in a relatively stable lattice structure of oxygen [Figure 2E] that hinders the diffusion and migration paths of Li^+. Liu *et al.*[47] synthesized Ti-doped $Li_{1.2}Ti_{0.26}Ni_{0.18}Co_{0.18}Mn_{0.18}O_2$, where Li^+ was partially replaced by Ti^{4+}, and the Li/Ti cation disorder structure strengthened the tolerance of deformation and restricted the migration of TM ions in the TM layer during the delithiation process. This contributed to lowering the electrochemical reaction potential and improving the reversibility of anion redox. Lee *et al.*[50] certified that the structural stability of the bulk and surface was enhanced with an increasing degree of cation disorder in $Li_{1.2}Ni_{0.2}Mn_{0.6}O_2$ during the initial activation process. This ultimately inhibited the structural deterioration with subsequent cycling and maintained the electrochemical activity and rate performance even in the case of cation disorder.

Distribution of elements

The distribution of elements in pristine particles affects the structure and electrochemical properties of LRMOs. Liang *et al.*[51] proposed a TM bond model and predicted the order of the strength of TM-TM bonds ($Mn^{4+}Mn^{4+}$ > $Ni^{2+}Mn^{4+}$ > $Ni^{3+}Mn^{4+}$ > $Co^{3+}Mn^{4+}$ > $Co^{2+}Mn^{4+}$ > $Ni^{2+}Ni^{4+}$) by studying the interaction and distribution of TM elements [Figure 2F]. It was found that Co and Mn could easily segregate to form clusters in the Ni environment, which was a significant reason for the deterioration of the structure and the degradation of the electrochemical performance during cycling. Adjusting the interaction of TM elements and promoting the uniformity of elements can prominently promote the structural stability of layered NCM materials. This mechanism is also applicable to LRMO cathode materials, with the segregation of Ni on the surface impeding the migration channel of Li^+ and weakening the interaction of Ni-Mn, thereby causing the reduction of manganese ions and the fast degradation of voltage and capacity. In contrast, the uniform distribution of elements at the atomic scale enhances the interaction of TM elements, stabilizes the crystal structure and contributes to excellent capacity retention and more smaller voltage degradation[52,53].

For LRMOs, the distribution of elements can be locally adjusted to produce outstanding electrochemical performance[54,55]. The gradient structure that Mn gradually decreases and Ni and Co gradually increase from the center to the surface with a certain slope inhibits the transformation to the spinel phase and the Jahn-Teller effect, thereby markedly reducing the degradation of voltage, which promotes the cycle performance. In Ni-rich layered materials, reducing the content of Ni in the surface layer and increasing the concentration of Mn[56] not only maintains the high capacity of the center of the material but also improves the stability of the surface layer. This seems to imply that a similar content of TM components can improve the structural tolerance of the material. The inhomogeneous distribution of Li also significantly influences local anion redox. Zhu *et al.*[57] synthesized an LRMO material with a Li-poor shell, which inhibited the

generation of O-O dimers on the surface and the release of O_2.

Stoichiometry

C2/m:R$$\bar 3$$m

The Li_2MnO_3 phase with the *C*2/*m* space group as the sole component of an LRMO endows the material with the "Li-excess" characteristic and profoundly affects its structure and electrochemical performance[9]. Li is extracted from the lattice in the form of "Li_2O" and leaves the MnO_2 phase to stabilize the structure, enabling the composite LRMO layered material to maintain good tolerance to high voltage. Yang and Xia[58] doped NCM811 cathode materials with a certain Li_2MnO_3 component to sufficiently inhibit the phase transition between the H2 and H3 hexagonal phases with distinctly different cell parameters, which dramatically decreased the variation of the structure volume and alleviated the drastic structural deterioration and capacity degradation. More importantly, the non-activated Li_2MnO_3 can store the excess lithium, so that Li^+ in the TM layer migrates to the adjacent Li-deficient layer during charging to stabilize the structure and realize the sufficient release of carriers and capacity.

The pristine layered structure of Li_2MnO_3 transforms to the spinel phase during cycling and the capacity source changes to maintain the capacity. However, the difference in the voltage plateau between the two phases leads to voltage degradation, which is a unique phenomenon and problem of LRMOs. The intrinsic atomic structure and arrays of the Li_2MnO_3 component significantly influence the electrochemical performance. Song *et al.*[59] found that the structural defects in different orientations and the imperfect atomic arrays of the Li_2MnO_3 component caused an increase in atomic defects and the concentration of vacancies, ultimately leading to the breaking of grains and performance degradation. The sluggish electrochemical kinetics of the Li_2MnO_3 phase restrict the rate performance and also limit the performance release of the *R*$$\bar 3$$*m* component. However, the control of the current density can regulate the activation of Li_2MnO_3 to improve the electrochemical performance.

The introduction of the *R*$$\bar 3$$*m* component into Li_2MnO_3 (via the doping of Ni or Co) can significantly improve the irreversible oxygen loss. It has been shown that the intrinsic charge compensation of anions for Li_2MnO_3 leads to the completely irreversible release of O_2, but the irreversible oxygen loss accounts for 25% in $Li_{1.2}Ni_{0.13}Co_{0.13}Mn_{0.54}O_2$ with a Li_2MnO_3 ratio of 50%. This means that Ni and Co play an important role in stabilizing lattice oxygen in the bulk material. Liu *et al.*[60] studied the electrochemical properties of $xLi_2MnO_3\cdot(1\text{-}x)0.5LiNi_{1/3}Co_{1/3}Mn_{1/3}O_2$ (x = 0.3, 0.5 or 0.7) and found that materials with a medium Li_2MnO_3 content had higher initial specific capacity. The materials with higher Li_2MnO_3 contents showed better cycling performance and more significant voltage attenuation due to the stable electrode/electrolyte interface and structural rearrangement at high potentials [Figure 3]. In addition, Shi *et al.*[61] replaced the *R*3*m* component in $0.5Li_2MnO_3\cdot0.5LiNi_{1/3}Co_{1/3}Mn_{1/3}O_2$ with $LiNi_{0.8}Co_{0.1}Mn_{0.1}O_2$, which increased the average discharge voltage from 3.5 to 3.8 V and the specific energy from 912 to 1033 Wh kg^{-1}. Thus, it is necessary to appropriately adjust the component and ratio of the *C*2/*m* and *R*$$\bar 3$$*m* phases to enhance the degree of uniformity and arrangement rules at the atomic level, improve the stability of Mn octahedra and balance the coordination effect of Mn valence, reversible capacity and the Jahn-Teller effect.

Ratio of Ni, Co, Mn and Li/O

Every element and stoichiometric ratio play a critical role in determining the whole structure and electrochemical activity[62]. Hua *et al.*[63] systematically studied the relationship between Li content and the structure of $Li_xNi_{0.2}Mn_{0.6}O_y$ by matching the Li content with the precursor. When $x < 0.4$, the material was indexed to the spinel phase (*Fd*$$\bar 3$$*m*), while at $0.4 < x < 1.2$, the material was a complex of the spinel (*Fd*$$\bar 3$$*m*) and rock salt (*Fm*$$\bar 3$$*m*) phases, including Li and the layered monoclinic phase (*C*2/

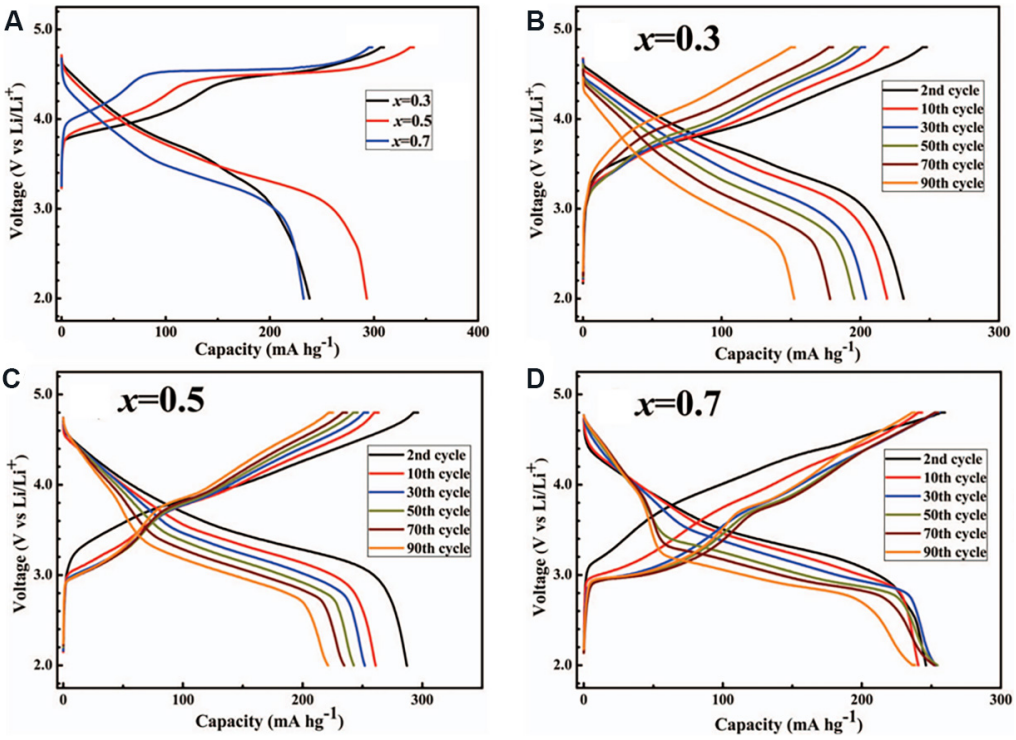

Figure 3. Typical charge-discharge curves of (A) initial and (B-D) cycling process for $xLi_2MnO_3 \cdot (1-x)LiNi_{1/3}Co_{1/3}Mn_{1/3}O_2$ (x = 0.3, 0.5 or 0.7) cathode materials[60].

m). At 1.20 < x < 1.52, the material was indexed to the pure monoclinic phase (*C*2/*m*). The ratio of Li/O represents the content of Li-O-Li configurations in the LRMO material, thereby affecting the anion redox and the structure of the energy bands[64]. The lower ratio of Li/O means the TM-O hybridization and non-bonding O 2p bands move to lower energy levels, which contributes to a higher potential of redox reaction that promotes the electrode reaction kinetics, reversibility and energy efficiency [Figure 4A]. The higher ratio of Li/O accelerates the anion redox reaction, inevitably introducing an excess disordered structure that is regarded as the buffer regulating the conflict between oxygen evolution and the crystal structure and making the LRMO more stable and flexible[65].

The regulation of lithium and oxygen is also applied to other cathode materials. Xiao *et al.*[38] designed different cooling technologies and synthesized Li_2MnO_3 with various nonstoichiometric oxygen defects and stacking faults. These defects decreased the valence of Mn and the increase in Mn^{3+} content accelerated the activation of Li_2MnO_3, but this simultaneously led to a more rapid structure deterioration to the spinel and capacity degradation. Wu *et al.*[66] introduced an appropriate excess of lithium into NCM811, resulting in the reduction of partial Ni^{3+} to Ni^{2+} and the decrease of Li/Ni disorder, which improved the electrochemical stability and structural robustness during cycling. Ji *et al.*[67] designed a novel cathode material with excellent rate performance and reversible redox of oxygen via the introduction of excess Li into spinel $LiMn_2O_4$. The cations over stoichiometric ratio and the derived local disorder eliminated the typical first-order phase transition reaction of the ordered spinel material and realized higher practical capacity.

The oxidation of oxygen in Li_2MnO_3 during charging generally causes the irreversible loss of lattice oxygen. However, the introduction of Ni and/or Co can dramatically inhibit the loss of oxygen, which results in the formation of $Li[Li_{0.2}Ni_{0.2}Mn_{0.6}]O_2$ and $Li[Li_{0.2}Ni_{0.13}Co_{0.13}Mn_{0.54}]O_2$. The introduced Ni is enriched on the

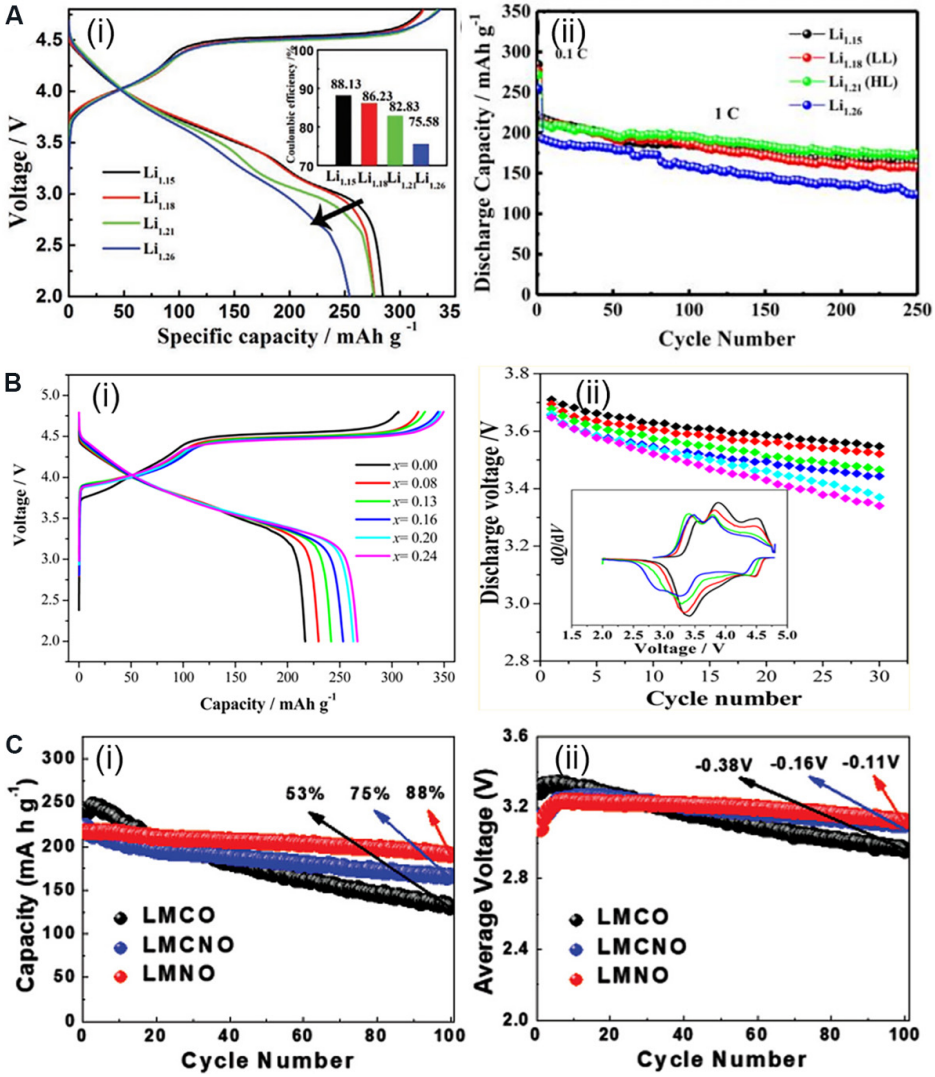

Figure 4. (A) Initial charge-discharge plots with Coulombic efficiency (i) and cycle performance (ii) of the as-prepared $Li_xMn_{0.56}Ni_{0.16}Co_{0.08}O_2$ samples[64]. (B) Initial charge-discharge curves (i) and average discharge voltage during cycling with the differential capacity curve (d*Q*/d*V*) (ii) of the $Li[Li_{0.2}Ni_{0.2-x/2}Mn_{0.6-x/2}Co_x]O_2$ ($0 \le x \le 0.24$) samples[70]. (C) Capacity (i) and average voltage retention (ii) of as-prepared $Li_{0.7}Mn_{0.78}Co_{0.22}O_2$ (LMCO), $Li_{0.75}Mn_{0.78}Co_{0.11}Ni_{0.11}O_2$ (LMCNO) and $Li_{0.74}Mn_{0.78}Ni_{0.22}O_2$ (LMNO) during cycling[69].

particle surface to form Li-deficient and Ni-rich rock salt shells as protection layers to inhibit oxygen loss[68]. Though the addition of Co cannot cause the formation of the rock salt phase, it still restricts the oxygen loss overall. In addition, the overlap of the $Co^{3+/4+}$ t_{2g} and O 2p bands and the intense covalency of Co-O in LRMO can promote the coupling between Co and O and the anion redox[69]. Nevertheless, this leads to an increase in Mn^{3+} content, a decrease in electrochemical reaction potential, the generation of oxygen vacancies and the migration of TM ions to the Li layer[70], which accelerates the capacity and voltage degradation [Figure 4B]. Accordingly, the appropriate increase in Ni content and a lower ratio of Co/Ni can efficiently adjust the coordination environment and local electron structure of oxygen to reduce the proportion of Mn^{3+}/Mn^{4+} redox couples at low voltages and enhance the operation voltage[19]. This also enables the TM-O and non-bonding O 2p bands to move down to lower energy levels, thereby inhibiting anion redox and the corresponding phase transition and efficiently improving the structural stability and capacity/voltage retention. Enhancing the Ni content not only changes the center of redox in LRMO

cathode materials but also promotes the reversibility of Mn migration[71] by a shielding effect, where the random transition of Mn is restricted in a certain region by the electrostatic shielding effect of Ni ions [Figure 4C].

Particle morphology

The particle morphology of a cathode material plays an important role in the transportation of Li^+, the release of capacity, the stability of the structure and the stress-strain relationship. At present, the mainstream particle morphology of layered cathode materials includes irregular single-crystal particles (nano- and microscales), secondary spherical particles consisting of primary single-crystal particles and other single-crystal or polycrystalline particles with special morphologies. Submicron single-crystal particles possess high specific surface area and shorter Li^+ diffusion path, which enables sufficient contact with the electrolyte and inhibits the generation of local nanodomains inside the particles. These advantages contribute to the sufficient release of electrochemical activity to ultimately realize excellent reversible capacity and rate performance. However, the severe release of O_2 on the surface and the side reaction with the electrolyte lead to the formation of a cathode-electrolyte interface (CEI) that impedes the transportation of Li^+. The oxygen vacancies on the surface cause destruction of the lattice and densification of the structure, giving rise to a serious solution of TM ions that further deteriorates the capacity retention and rate performance. With cycling, the smaller particles also undergo severe structural deterioration and performance degradation. Smaller sized particles cannot meet the requirements of tap density in industry. Microscale single-crystal particles efficiently alleviate the side reaction with the electrolyte at the interface via a decrease in the specific surface area, thereby maintaining the structural integrity of the inner component. However, the poorer Li^+ mobility limits the release of capacity and the utilization of the material, which may induce the generation of local domain[72,73] boundaries that hinder the transportation of Li^+, leading to structural deterioration. Thus, it is necessary to balance the particle size and the electrochemical performance.

In typical layered cathode materials, the diffusion path of Li^+ is the 2D channel vertical to the *c*-axis in the Li layer, i.e., the migration direction of Li^+ is vertical to {010} crystal plane, including the (010), ($$\bar 1$$10), ($$\bar 1$$00), (0$$\bar 1$$0), (1$$\bar 1$$0) and (100) crystal planes. However, the close packing of TM and O in the (001) planes severely hinders the transportation of Li^+. Therefore, the exposed planes in the particles are key to determining the extraction/insertion rate of Li^+[74]. In order to obtain excellent Li^+ migration rates, the {010} crystal planes should be more exposed and the proportion of (001) planes reduced[75] [Figure 5A]. However, the thermodynamic surface energy of the close-packed (001) plane is the lowest and generally the proportion of the exposed (001) plane is the largest, which creates difficulties in providing fast transportation channels and planes for Li^+. To enhance the exposure rate of {010} crystal planes, it is necessary to reduce the surface energy of {010} and increase the surface energy of the (001) plane during the nucleation and growth process. The exposure of special planes enables the particles to exhibit special morphologies, such as nanosheet-/plate-like single crystals and their stacked spherical[18] [Figure 5B], 3D orthogonal and cubic maze-like polycrystals[76].

Currently, secondary spherical particles consisting of primary single-crystal particles are widely applied and their advantages include the side reaction at the interface, owing to the low specific surface area, and the better rate performance than that of single-crystal particles of the same size. In addition, the stacking of particles with different sizes leaves the spatial occupation denser, thereby exhibiting a higher tap density. The connection between the primary particles is also worthy of consideration. Appropriate pores are conducive to the sufficient contact between the electrode particles and the electrolyte. It can also ensure the effective connection between particles, so that electrons and ions can be facilely transferred in solid-phase materials[77,78]. However, the anisotropic volume changes of the primary single-crystal particles during

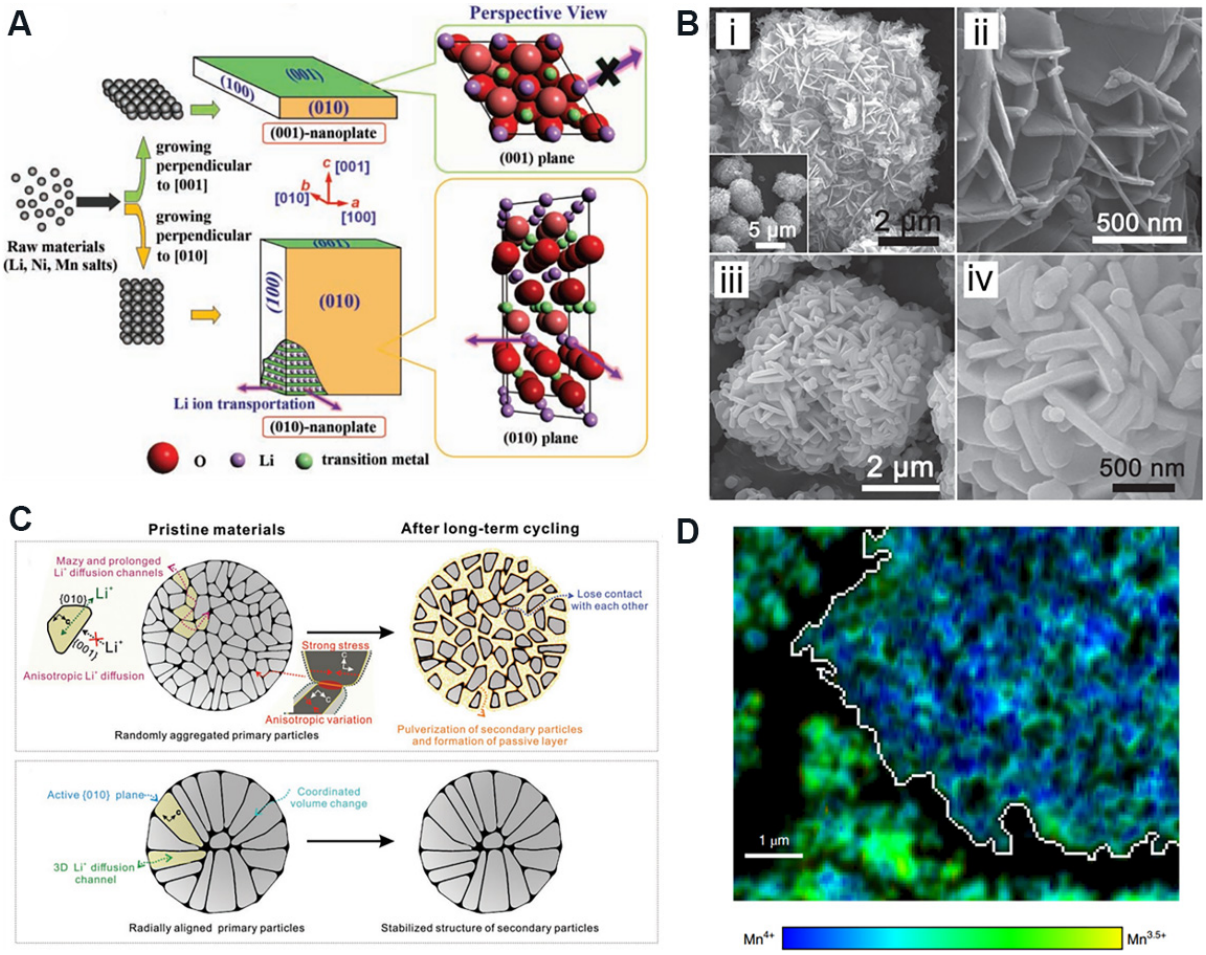

Figure 5. (A) Schematic illustration of two kinds of nanoplates and the microstructure of their surfaces[75]. (B) Field emission scanning electron microscopy images of (i) precursors and (ii) their magnified image, (iii) hierarchical structured lithium-rich material after pre-heating at 500 °C and (iv) its magnified image[18]. (C) Schematic illustration of the structure and characteristics of commercial NCM (top) and the materials with radially aligned single-crystal primary particles (bottom)[79]. (D) A single large agglomerate (to the right of the image, outlined in white) that is substantially more oxidized than the surrounding areas[80].

charging cause stress/strain and cracks in the whole polycrystalline particles, leading to an obstruction in Li^+ diffusion and an increase in impedance. Ultimately, the particles become broken, resulting in the dissociation of active materials in the electrolyte and dramatic performance deterioration. The anisotropic volume change can be improved by the morphological control of the primary particles.

Xu *et al.*[79] synthesized radially-oriented single-crystal primary nanosheets for Ni-rich cathode materials via the optimization of synthesis technology [Figure 5C]. The exposed {010} planes and the morphology extending from the surface to the center ensure the rapid diffusion of Li^+. The radially-oriented primary particles with consistent crystal orientation can regulate the volume change during cycling to alleviate the stress/strain, contributing to excellent structural stability and cycle performance. Furthermore, the permeation of the liquid electrolyte in broken particles results in a larger contact area between the active material and electrolyte, decreasing the charge transfer resistance and enhancing the apparent diffusion coefficient of Li^+, eventually realizing high reversible capacity and outstanding rate performance. This special primary particle morphology is also worthy of study and applying to the morphological design of LRMO materials. In addition, Csernica *et al.*[80] analyzed the oxygen evolution in cross sections of LRMO

particles with different sizes in both the inner section and on the surface. It was found that the degree of oxygen evolution of the single primary particles was highly dependent on their place in the secondary structure, i.e., the closer the primary particle approached to the surface, the severer the oxygen evolution and structural transformation [Figure 5D]. Primary particles may be important factors in determining the overall capacity of a material compared with secondary particles from a morphological perspective. It was supposed to explore much larger secondary LRMO material particles to relieve the release of oxygen.

TEMPORAL DIMENSION

In this section, we focus on the charge compensation, element migration, phase transformation and reconstruction of the energy band structures of LRMO materials during the charge and discharge process.

Initial charge and discharge

Charge compensation mechanism

The LRMO cathode material $xLi_2MnO_3 \cdot (1-x)LiMO_2$ possesses a superior discharge capacity of over 250 mAh g^{-1} and a complex crystal structure, so that the charge-discharge mechanism is difficult to reasonably explain through the escaping/embedding mechanism of typical LIB layered materials. The initial charge-discharge curves of the typical lithium-rich material $Li_{1.2}Ni_{0.13}Co_{0.13}Mn_{0.54}O_2$ mainly include two parts: a slope below 4.4 V indexed to the solid solution reaction and a voltage plateau at 4.5 V. The discharge curve acts as a slope with a large voltage span. The material exhibits completely inconsistent charge/discharge behavior with a Coulombic efficiency of ~80%, which is different from other cathode materials with good reversibility (e.g., $LiFePO_4$, $LiCoO_2$, $LiMn_2O_4$, $LiNi_xCo_yMn_{1-x-y}O_2$ and so on). The dramatic irreversible phase transition of $Li_{1.2}Ni_{0.13}Co_{0.13}Mn_{0.54}O_2$ inevitably occurs in the initial cycle, which strongly influences the subsequent charge and discharge cycles. Therefore, the initial charge/discharge behavior is an important scientific problem that cannot be ignored in the study of LRMO materials.

According to the absorption edge analysis of each element at different states of charge [Figure 6A], it is found that the slope below 4.4 V during charging corresponds to the charge compensation of Ni^{2+}/Ni^{4+} and Co^{3+}/Co^{4+} without the variation of the Mn^{4+} valence, which is attributed to the charge compensation mechanism of the $LiMO_2$ component[9]. The absorption edge of the TM at 4.5 V shows that there is no change in the K edge of Ni and Co[81]. The Mn K-edge X-ray absorption near-edge structure spectrum indicates that the environment of Mn changes at 4.5 V according to the continuous variation of the absorption edge, which results from the distortion of MnO_6 octahedra. Hence, the lattice oxygen coordinated with Mn can more easily participate in charge compensation and generate electron holes. The unique anion charge compensation of LRMOs occurs in the plateau region at 4.5 V (the triggering condition has been discussed above), which is ascribed to the Li-O-Li configurations and the hybridization conditions of TM-O.

In the initial cycle, oxygen evolution occurs in the Li_2MnO_3 component with the extraction of Li^+ manifesting as the first-order phase transition reaction in the form of "Li_2O" net loss [Figure 6B], which involves the nanodomains and dislocations formed by localized uneven delithiation[82]. It is clarified that CO_2 gas forms at the beginning of the voltage plateau by operando mass spectrometry and oxygen isotope labeling[83], which can be attributed to the oxidic lattice oxygen with high activity reacting with the electrolyte (possibly including the decomposition of residual Li_2CO_3 on the surface). Subsequently, O_2 escapes from the lattice at the end of the voltage plateau[84], which does not derive from the oxidation of the electrolyte [Figure 6C]. However, the amount of oxygen release is considerably lower than the estimated value generated by the activation of the Li_2MnO_3 component. Considering that O_2 cannot migrate from the bulk to the surface, the emission of O_2 occurs only at the near surface. According to calculations, the

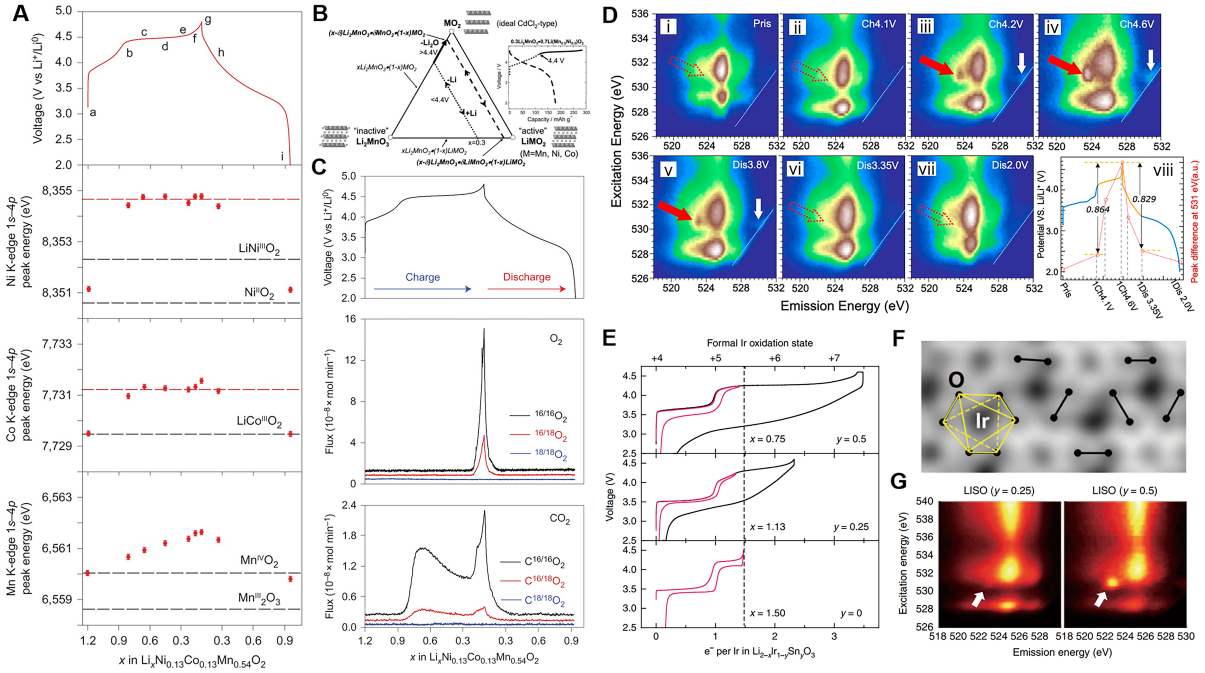

Figure 6. (A) 1s-4p peak energy in the initial cycle showing almost no change in the environment around Ni and Co on charging across the 4.5 V plateau[83]. (B) Compositional phase diagram showing the electrochemical reaction pathways for a $xLi_2MnO_3 \cdot (1-x)LiMO_2$ electrode[9]. (C) Operando mass spectrometry of ^{18}O-labelled $Li_{1.2}Ni_{0.13}Co_{0.13}Mn_{0.54}O_2$ cathode during the initial cycle[83]. (D) O K-edge mRIXS of a series of Li_2RuO_3 electrodes at different electrochemical states. The solid red arrows indicate the striking, sharp features of oxidization at the high voltage state. (i-vii) represent the mRIXS of Li_2RuO_3 at the state of the pristine, charged to 4.1 V, charged to 4.2 V, charged to 4.6 V, discharged to 3.8 V, discharged to 3.35 V, and discharged to 2.0 V, respectively. (viii) Summary of Ru and O redox during the initial cycling profile with blue for lattice $Ru^{4+/5+}$ and yellow for lattice oxygen redox[28]. (E) Charge-discharge profiles of $Li_{2-x}Ir_{1-y}Sn_yO_3$ for a full cycle (black) and for ~1.5 e^- in Ir per cycle (pink)[29]. (F) Enlarged ABF-STEM image. The O-O pairs arise from twisting the opposite triangular faces of the IrO_6 octahedra (shown in yellow)[11]. (G) O K-edge mRIXS of $Li_2Ir_{0.75}Sn_{0.25}O_2$ and $Li_2Ir_{0.75}Sn_{0.25}O_2$ charged to 4.60 V showing a localized RIXS feature at 530.7 eV excitation energy and 522.8 eV emission energy[29]. mRIXS: Mapping of resonant inelastic X-ray scattering.

equivalent thickness of the surface where oxygen is released is ~2-3 nm[85].

The anion charge compensation mechanism is distinct for different lithium-rich materials[28]. For Li_2RuO_3, the cation Ru^{4+}/Ru^{5+} and anion O^{2-}/O_2^{n-} couples reversibly participate in charge compensation [Figure 6D], owing to the d-sp hybridization related to the redox coupling without irreversible oxygen evolution. For Li_2IrO_3, only the Ir^{4+}/Ir^{5+} and Ir^{5+}/Ir^{6+} couples participate in the charge compensation without anion redox via the high-efficiency mapping of resonant inelastic X-ray scattering (mRIXS) results. Though it was demonstrated that the IrO_6 octahedron is distorted with the generation of analogous O-O dimers, the distance of O-O is much larger than ~1.5 Å for the generation of peroxide and superoxide groups[11] [Figure 6F]. However, the substitution of Sn^{4+} can promote the reaction activity of anions [Figure 6E and G] by the local coordination environments.

Energy band reconstruction

The inconsistency of the initial charge/discharge curves certainly means the reconstruction of the bulk structure and the corresponding energy band. According to the above discussion, the redox of Ni and Co is the same as the charge compensation of $LiMO_2$ with good reversibility, which cannot influence the structure and energy band. Therefore, it is the key to defining the anion charge compensation mechanism. It is found that the valence of Ni and Co remains unchanged at the beginning and the end of discharge and the

variation of valence during discharging is reversible via the comparison of the absorption edge for Ni, Co and Mn. However, the valence of Mn decreases slightly, which may be ascribed to the activation of Mn in the Li_2MnO_3 component[86]. Based on the test and calculation results, more than half the discharge capacity (~280 mAh g^{-1}) is still unidentified. If we exclude the side reaction with the electrolyte, this part of the capacity can be regarded as the contribution from the reduction of oxygen.

In order to verify the reversibility of anion redox, Li *et al.*[87] determined the reversible evolution of O-O dimers during charging for the first time via *in-situ* surface enhanced Raman spectroscopy. The results seemed to suggest the reversibility of the redox behavior of oxygen but failed to explain why the reduction plateau of oxygen disappeared during discharging. Yabuuchi *et al.*[84] considered that oxygen was electrochemically reduced on the electrode surface below 3 V during discharging. Sun *et al.*[64] demonstrated that there was larger voltage hysteresis (≈ 0.5 V) during the anion redox via adjusting the cut-off voltage. Gent *et al.*[88] revealed that the strong couple effect between anion redox and the partially reversible cation migration contributed to the decrease over 1 V in the reduction potential of the bulk oxygen, causing the rearrangement of the anion and cation redox potentials.

However, this does not seem to explain intuitively and thoroughly the root cause of the energy band structure rearrangement. Considering the irreversible release of O_2 in the near-surface region of the lithium-rich material during the first charging process, it should be questioned whether O^{2-} will also dimerize to form O_2 molecules after being oxidized inside the particle body, which are restricted in the crystal lattice and cannot escape. This assumption seems more reasonable. Recently, House *et al.*[41] used high-resolution RIXS and ^{17}O magic angle spinning nuclear magnetic resonance (NMR) spectroscopy to successfully confirm the existence of O_2 molecules in the crystal lattice instead of O_2^{2-}, longer peroxide-like O-O bonds or electron holes on O^{2-}. In addition, they calculated and simulated the intralayer migration and disordered arrangement of TM elements in the fully charged state, which destroyed the $LiMn_6$ honeycomb ordered superstructure and formed vacant clusters that can accommodate O_2 [Figure 7]. The migration in the TM layer is irreversible. During the discharge process, the coordination environment of active oxygen changes from O-Li_4Mn_2 to O-Li_6 with the insertion of Li^+, which increases the number of oxygen non-bonded orbitals and increases the energy level[14]. Therefore, the reduction of oxygen occurs in the low voltage stage, which leads to a larger voltage hysteresis. The above perspective is currently the most satisfactory conclusion of the reconstruction of the structure and the rearrangement of the energy band during the first cycle of LRMO materials, but it still requires the unremitting efforts of researchers to verify and improve it.

Element migration

The topological reaction occurs before 4.4 V, where Li^+ ions are extracted from the $LiMO_2$ component with no variation in the frameworks[89]. During the electrochemical process, the Li^+ ions in the $LiMO_2$ component are gradually consumed, so the Li^+ ions in Li_2MnO_3 migrate from octahedral sites in the Mn layer to tetrahedral sites in the Li layer to participate in charge compensation, which provides extra binding energy to stabilize the structure. Li^+ ions continue to be extracted from the Li_2MnO_3 component with a series of complicated element migrations and phase transition processes at the 4.5 V voltage plateau[90,91]. The charge compensation of oxygen ions at the 4.5 V plateau leads to TMO_6 octahedral distortion[92] and even the formation of oxygen vacancies. Taking the $Li_{1.5}MnO_3$ model containing Li vacancies, Yu *et al.*[93] found that the migration energy of Mn from the 4g site to the 2b Li site was ~3.07 eV through theoretical calculations. With the introduction of oxygen vacancies, the migration energy was rapidly reduced to 1.86 eV, which promotes the migration of Mn ions.

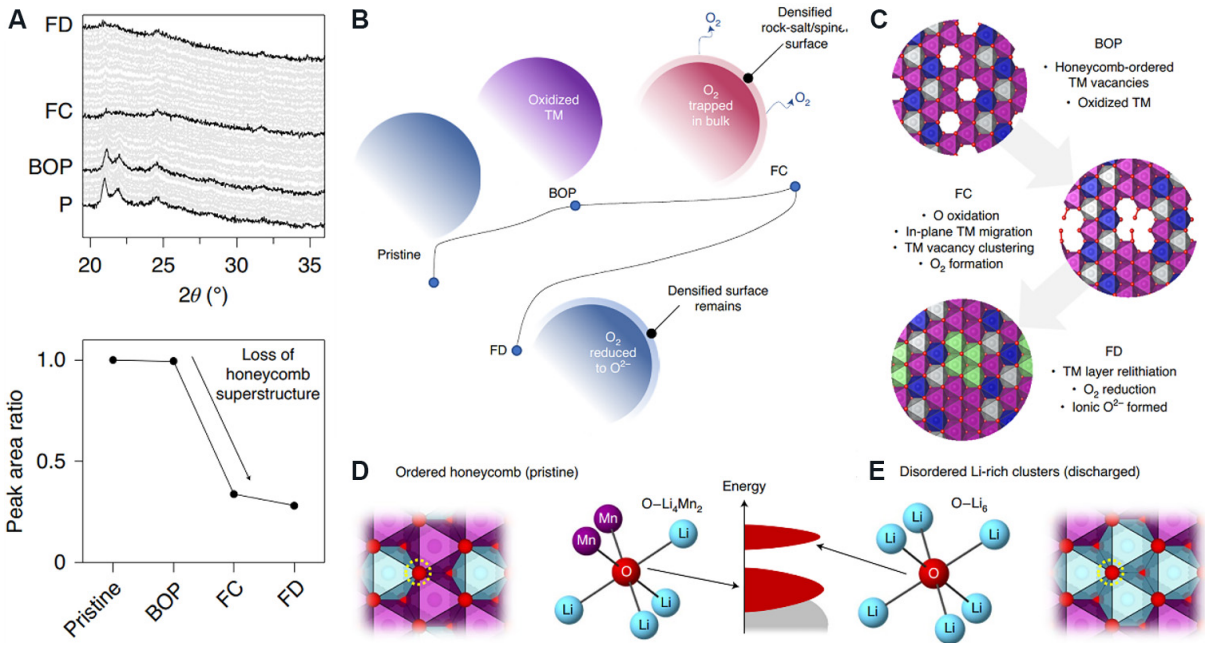

Figure 7. (A) Operando XRD of $Li_{1.2}Ni_{0.13}Co_{0.13}Mn_{0.54}O_2$ at different stages of the initial cycle, where P is pristine, BOP is the beginning of the plateau, FC is full charge and FD is full discharge. The peak area ratio of the superstructure peaks relative to the 001 peak decreases across the plateau, which indicates the loss of the honeycomb structure[41]. (B) Macroscale changes of the cathode particles during the first cycle[41]. (C) Structures of atomic-scale ordering changes within the TM layer modeled by DFT[41]. (D) Local coordination environment around oxygen in pristine honeycomb-ordered O-Li_4Mn_2 [14]. (E) Local coordination around oxygen in disordered Li-rich cluster O-Li_6 after the first cycle. O 2p states belonging to O and that have six coordinating Li are higher in energy than those that have four coordinating Li, which results in the initial voltage hysteresis[14]. XRD: X-ray diffraction.

It is generally considered that partial Mn ions migrate from octahedral sites to the coplanar tetrahedral sites in the Li layer and ultimately from tetrahedral sites to Li sites at this stage. Radin *et al.*[94] claimed that the Mn migration to tetrahedral sites was actually indexed to the oxidation of Mn^{4+}/Mn^{7+} simultaneously triggering the generation of O_2 molecules and peroxide ions [Figure 8A] according to first-principles calculations based on the Li-Mn-O phase diagram. Mn^{7+} was then reduced and returned to the original octahedral sites and there were also Mn^{7+} ions in tetrahedral sites at the end of charging. Kleiner *et al.*[95] quantified the migration track of TMs via synchrotron radiation XRD differential Fourier fitting. It was found that ~8% TMs occupied the tetrahedral sites in the Li layer during charging and ~2%-5% TMs occupied Li octahedral sites without the occupation of tetrahedral sites after discharge. Their results strongly suggested that 3%-6% TMs can reversibly migrate from the tetrahedral sites to the original TM octahedral sites during delithiation [Figure 8B].

The TM ions partially migrate to Li sites, leading to the formation of localized spinel-like phases. Therefore, the electrochemical activity of Mn is activated and Mn will be excessively reduced to Mn^{3+} below 3 V. This tends to stimulate the Jahn-Teller effect, as well as the disproportionation of Mn^{3+}, resulting in structural deterioration and element dissolution. In particular, in the near-surface layer of LRMOs, TM migration and structural reorganization are more serious due to the O_2 release and the destruction of the oxygen framework, resulting in the formation of disordered rock-salt phases and surface densification[91]. Therefore, irreversible element migration is a vital reason for the phase transition and the degradation of electrochemical performance. It is particularly important to suppress the irreversible migration of TMs, especially the migration process from the transition-state tetrahedral site to the Li octahedral site. The O2-type cathode material[96,97] then emerges and the special oxygen stack (ABCBA) enables TM ions to undergo

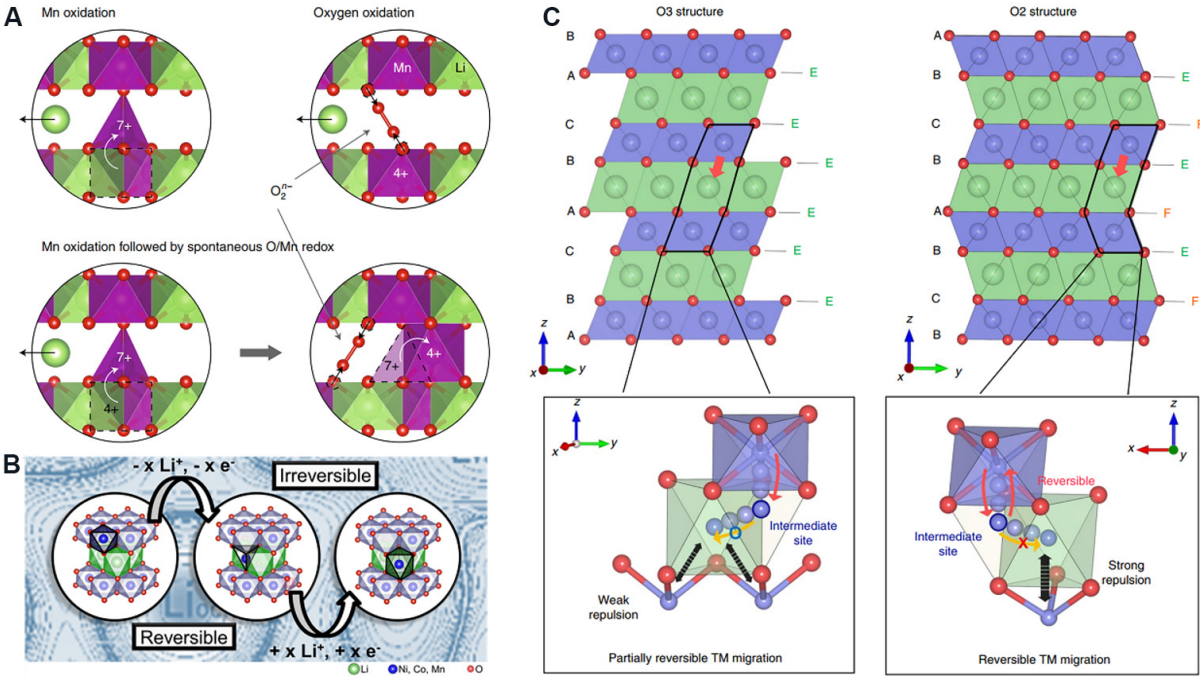

Figure 8. (A) Alternative charge mechanisms in LRMO cathode materials. Oxidation of Mn^{4+} to Mn^{7+}, followed by the spontaneous formation of peroxide or trapped oxygen molecules accompanied by the reduction of Mn[94]. (B) TM migration in an LRMO from the octahedral TM sites via tetrahedral sites into octahedral Li sites[95]. (C) Comparison of crystal structures. Schematic illustrations of crystal structures of O3-type (left) and O2-type (right) LRMOs with TM migration paths. Although the TM ions in the O3 structure can readily occupy Li sites that share only edges with neighboring cations, the TM ions in the O2 structure are subject to strong repulsion when they occupy Li sites that face share with neighboring cations[98]. LRMOs: Lithium-rich manganese-based layered oxides.

intense electrostatic repulsion when occupying the octahedral Li sites coplanar with adjacent TM cations. This effectively suppresses the irreversible TM migration and phase transition[98] [Figure 8C]. Furthermore, if the TMs can realize reversible migration between the TM and Li layers during the charge-discharge process, it is also worthy of affirmation. Ma *et al.*[99] clarified that Mo can reversibly migrate between the Li and TM layers in Li_2MoO_3, with the material maintaining good structural and electrochemical stability with the "unit cell breathing"[12] mechanism.

Electrochemical cycling

Although the anion redox mechanism in LRMO cathode materials provides considerable specific capacity, its instability and irreversible damage to the structure have a profound impact on the cycle performance of the materials and cause serious problems, including capacity attenuation, voltage decay and hysteresis. The following sections describe the key issues during cycling from different perspectives.

Oxygen vacancy transfer and element segregation

As LRMOs are cycled under a wide voltage range of 2-4.8 V and high voltage conditions, the lattice oxygen redox and complex structural evolution can continue to exist. From the above discussion, the TMs in the TM layer not only migrate to the Li layer after the first activation but will also migrate in the layer to form localized nanopores to restrain O_2 molecules. Moreover, the oxygen ions around the nanopores become more active due to the change in the coordination environment and the increase in the number of non-bonded 2p orbitals, which in turn makes it easier to form oxygen vacancies and promote the migration of TMs[100]. The nanopores gradually expand and merge [Figure 9A], and around the pores, the continuous transfer of TMs leads to segregation and densification of the structure. This phenomenon continues with

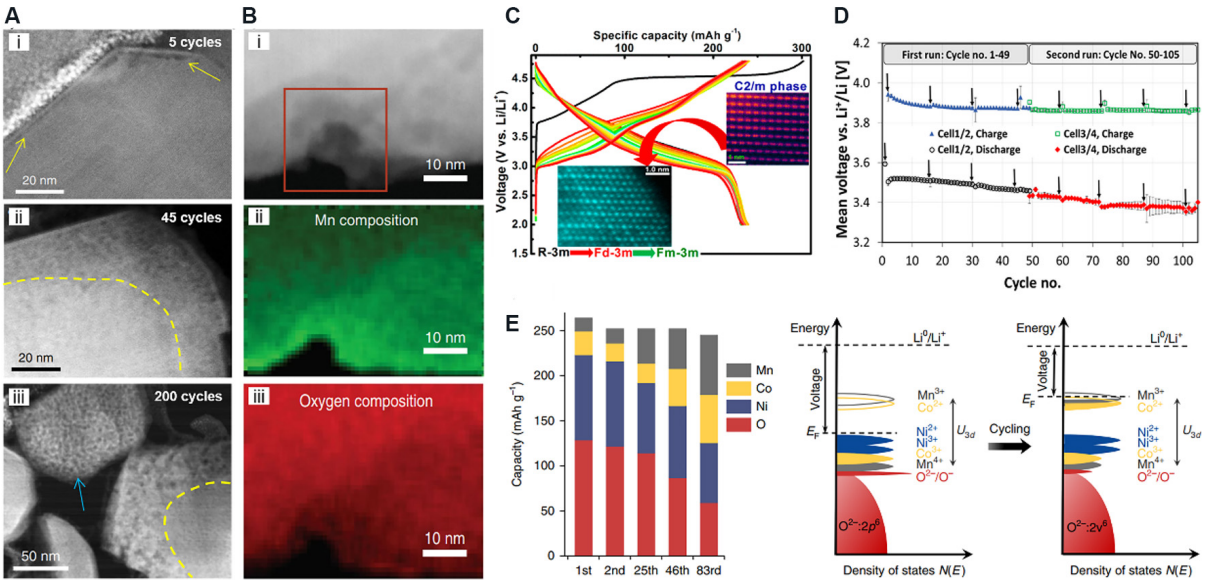

Figure 9. (A) HAADF-STEM images of $Li_{1.2}Mn_{0.6}Ni_{0.2}O_2$ cathode showing the gradual propagation of the nanovoid-populated zone from the particle surface towards the interior of the particle with increasing cycles[101]. (i-iii) Represent the HAADF-STEM images of the material after different cycles (5 cycles, 45 cycles, 200 cycles, respectively). (B) Annular dark-field STEM image (i) of an opened pore. Mn (ii) and oxygen (iii) composition extracted from the quantification of the electron energy-loss spectroscopy map[15]. (C) Charge-discharge curves and phase structural evolution of LRMO during electrochemical cycling[105]. (D) Mean discharge/charge voltage of the two cells cycled simultaneously (cell 1/2: 22 °C, cycles 1-49; cell 3/4: 25 °C, cycles 1-49; 22 °C, cycles 49-105), with the error bars representing the standard deviation between the two cells[95]. (E) Contribution towards the discharge capacity from each element at various cycles (left). An illustration of the Fermi level being lifted up as a result of the electronic structure change (right)[15]. HAADF-STEM: High-angle annular dark-field aberration-corrected scanning transmission electron microscopy.

charge and discharge cycling. In this case, the active lattice oxygen gradually forms O_2 molecules and gathers in large pores, which cannot provide capacity. The densified rock salt phase structure around the pores is also electrochemically inert, leading to continuous capacity attenuation, which also hinders Li^+ transport and charge transfer and increases electrochemical impedance and voltage hysteresis. Grenier *et al.*[100] used small-angle X-ray scattering to observe the formation of characteristic nanopores during the initial oxygen oxidation of lithium-rich materials (rather than other traditional layered cathode materials) and believed that cation migration and disorder may promote the formation of nanopores. The 3D electron tomography reconstruction method was employed by Hu *et al.*[15] and it was detected that $Li_{1.2}Ni_{0.15}Co_{0.1}Mn_{0.55}O_2$ produces obvious holes inside after 15 cycles. The decrease in oxygen content and the segregation of Mn were found in the host material around the pores [Figure 9B].

In addition, there are differences in oxygen release on the surface and inside of LRMO particles. Csernica *et al.*[80] used transmission-based X-ray absorption spectroscopy and ptychography on a mechanically cross-sectioned $Li_{1.18x}Ni_{0.21}Mn_{0.53}Co_{0.08}O_{2-\delta}$ electrode to quantitatively analyze its oxygen deficiency during cycling. It was found that the degree of oxygen release was more serious on the surface of the material particles and under the conditions of the same size of the primary particles, larger secondary particles can alleviate the problem of oxygen release and maintain the electrochemical capacity. This seems reasonable because oxygen released at the material interface will diffuse into the electrolyte, leading to a series of side reactions and HF erosion, thereby aggravating element dissolution, O_2 release and structural deterioration near the surface of the cathode. Yan *et al.*[101] found that the pores of the material are more inclined to the particle surface distribution and exhibit a larger pore size. They then gradually diffuse and expand into the material and the diffusion ability of oxidized O^{n-} into the material is significantly higher

than that of O^{2-} by theoretical calculations. Similarly, Lin *et al.*[102] also found abnormal segregation of Ru on the surface in $Li_2Ru_{0.5}Mn_{0.5}O_3$ after cycling. The surface layered structure was replaced by 1-2 nm metal clusters and the overall structure also became loose and porous. In other materials, such as spinel $LiMn_2O_4$ and layered $LiCoO_2$, the original oxygen vacancies and TMs continuously migrate during non-equilibrium charging and discharging. Along the direction of the close-packed oxygen layer, stacking faults are particularly prone to large lattice strains and stress concentrations[103], which also cause the generation and evolution of cracks and gaps.

Local phase structural transformation

During the cycling of LRMO materials, the layered structure gradually becomes unstable with the generation of oxygen vacancies and the migration of TMs. When the TM, especially Mn, occupies the octahedral site of the Li layer, the surrounding re-embedded sites of Li^+ are transferred to the tetrahedral vacancy, forming a spinel-like $LiMn_2O_4$ phase of a sub-nanodomain. Although a considerable amount of Mn will reversibly return to the original position after it migrates from its own octahedral position to the tetrahedral position of the Li layer in each charge and discharge process and the recurring spinel nanodomain proposed by Xiao *et al.*[104] appears, there is still some Mn irreversibly migrated to the Li layer. This process continues to accumulate, from the first charge and discharge Li site octahedra are occupied by TMs (mainly Mn) at ~2%, which gradually increases to ~5% after 100 cycles[95]. In the wide voltage range of 2-4.8 V, the Mn ions undergo a profound valence state change. When discharged to ~2.8 V, Li^+ ions are excessively embedded in the 16c octahedral position of the cubic spinel $LiMn_2O_4$ phase, forming a tetragonal spinel $Li_2Mn_2O_4$ phase, and the valence state of Mn decreases from +3.5 to +3, resulting in Jahn-Teller distortion and the dissolution of Mn^{2+} caused by the disproportionation reaction of Mn^{3+}. This leads to further deterioration of the material structure and eventually an inactive disordered rock salt structure (Fm$$\bar 3$$m space group). On the surface of the material, due to the loss of Mn and the migration of Ni, a large number of maligned NiO rock salt phases will be formed[105] [Figure 9C].

The series of phase structural transformations mentioned above lead to a decrease in electrochemically active materials that can accommodate the reversible deintercalation of Li^+. In addition, the local disordered rock-salt phase of cations, especially on the surface, seriously hinders the migration of Li^+ and charge transfer and increases the electrochemical impedance and voltage hysteresis. Although the production of the active spinel phase during cycling compensates to a certain extent for the capacity decline caused by the gradually weakened anion charge compensation, this leads to another unfavorable factor where the $O^{2-}/O^{(2-n)-}$ electrochemical couple with the high-voltage reaction is replaced by the Mn^{3+}/Mn^{4+} couple with the low-voltage reaction [Figure 9E]. The continuous TM valence decreases as the oxygen vacancy increases, which also leads to a decline in the redox potential of Co and Ni. Although there is a small energy level difference between the Ni^{2+}/Ni^{3+} and Ni^{3+}/Ni^{4+} redox couples, the difference between Co^{2+}/Co^{3+} and Co^{3+}/Co^{4+} is quite large. Therefore, the reduction of the electrochemical reaction potential of the redox couples during cycling and the aforementioned kinetic factors are the direct causes of the voltage decay[15]. It is noteworthy that the charge/discharge average voltage changes during the cycle are inconsistent and the charge average voltage changes very little[95] compared with the serious attenuation of the discharge average voltage [Figure 9D], which can also be attributed to the combined effects of kinetics and thermodynamics. Because electrochemical polarization increases the potential during the charging process, the thermodynamically driven redox couples change will lower the electrode potential. In addition, TMs mainly migrate to the tetrahedral position during the charging process and partially irreversibly migrates to the octahedral Li position during the discharge process, which may also cause a difference in the thermodynamic electrode potential during charging and discharging.

Electrochemical reaction kinetics

Li^+ migration

In layered cathode materials, Li^+ mainly carries out 2D interlayer migration in the Li layer. There are two migration paths for Li^+ from one octahedral position to the next octahedral position[106] [Figure 10A]. The first is that Li^+ directly passes through the center of O-O on the common edge of two octahedrons, which is known as oxygen dumbbell hopping (ODH). The second is to migrate to the tetrahedral site coplanar with the two octahedral by relying on the vacancy left by other Li^+ diffusion. It then moves to another octahedral position to complete a migration process known as tetrahedral site hopping (TSH). The diffusion barrier of the TSH path is much lower than that of the ODH path through theoretical calculations. Therefore, when the material is charged in the early stage, Li^+ migrates in the ODH path first because there are not many vacancies. With the continuous emergence of Li^+ and the increase of vacancies, the migration path of Li^+ gradually changes from ODH to TSH and the migration rate is gradually accelerated. Liu *et al.*[107] pre-introduced Li vacancies in Li-rich materials, which not only reduced the energy barrier of Li^+ in the initial ODH diffusion path but also accelerated the transition from difficult ODH to facile TSH.

When a TM occupies the Li site in the crystal structure of the material (especially after cycling and near the surface of the material), the migration channel of Li^+ gradually deteriorates from 0-TM to 3-TM[108] [Figure 10B] and the diffusion path of Li^+ will not only be blocked, but also suffer from the electrostatic repulsion of the high-valence TM, which greatly increases the migration energy barrier of Li^+. Huang *et al.*[109] found that Cr can realize the non-topotactic reaction of reversible octahedral to tetrahedral migration in the process of delithiation in lithium-rich disordered rock salt materials. Octahedral TMs are the main obstacle to Li^+ diffusion. When Cr migrates to the tetrahedral position, it will correspondingly provide a tetrahedral vacancy for Li^+, which improves the migration conditions of Li^+ [Figure 10C]. This principle can be used for reference to alleviate the deterioration of Li^+ diffusion kinetics caused by the deterioration of the layered oxide structure. In addition to Cr, other electronic configurations, such as d^5 and d^{10}, are also conducive to the migration to the tetrahedral position, but the matching between the TM size and tetrahedral pores needs to be considered simultaneously.

Anion reaction kinetics

In the first charging activation process, our previous work[110] found that the diffusion coefficient of Li^+ (D_{Li^+}) increases slightly at the initial charging stage, which corresponds to the release of Li^+ from the $LiMO_2$ component. However, D_{Li^+} drops sharply at the 4.5 V plateau [Figure 10D], which corresponds to the charge compensation process of oxygen in the Li_2MnO_3 component. This anomalous behavior cannot be explained from the perspective of the Li^+ migration channel. Although a small amount of TM migration occurred during the process, which hindered the migration of Li^+, the generation of Li vacancies and the expansion of *c*-axis layer spacing were still favorable for Li^+ diffusion. Considering the electrochemical redox reaction with both electron and ion conduction, the above apparent decrease in D_{Li^+} only represents a decrease in the electrochemical reaction rate rather than a decrease in the diffusion capacity of Li^+. Therefore, the electron transfer of anions is likely to be a limiting factor.

Nayak *et al.*[111] used electrochemical impedance spectroscopy (EIS) to test the reaction kinetics of a LRMO at various reaction steps at different potentials and found that the charge transfer resistance increased significantly at voltages of > 4.4 V [Figure 10E], indicating that the electrode reaction kinetics at high potentials were controlled by anionic charge transfer rather than Li^+ diffusion. Yu *et al.*[36] used time-resolved X-ray absorption spectroscopy (XAS) to determine the characteristic reaction kinetics of each element. Compared with Ni and Co, the reaction kinetics of the Mn site before and after the initial activation of Li_2MnO_3 was much worse. These results suggest that Li_2MnO_3 (anionic charge transfer) is a key component in limiting the rate capacity of LRMOs. Moreover, the anion reaction kinetics in the O2-type

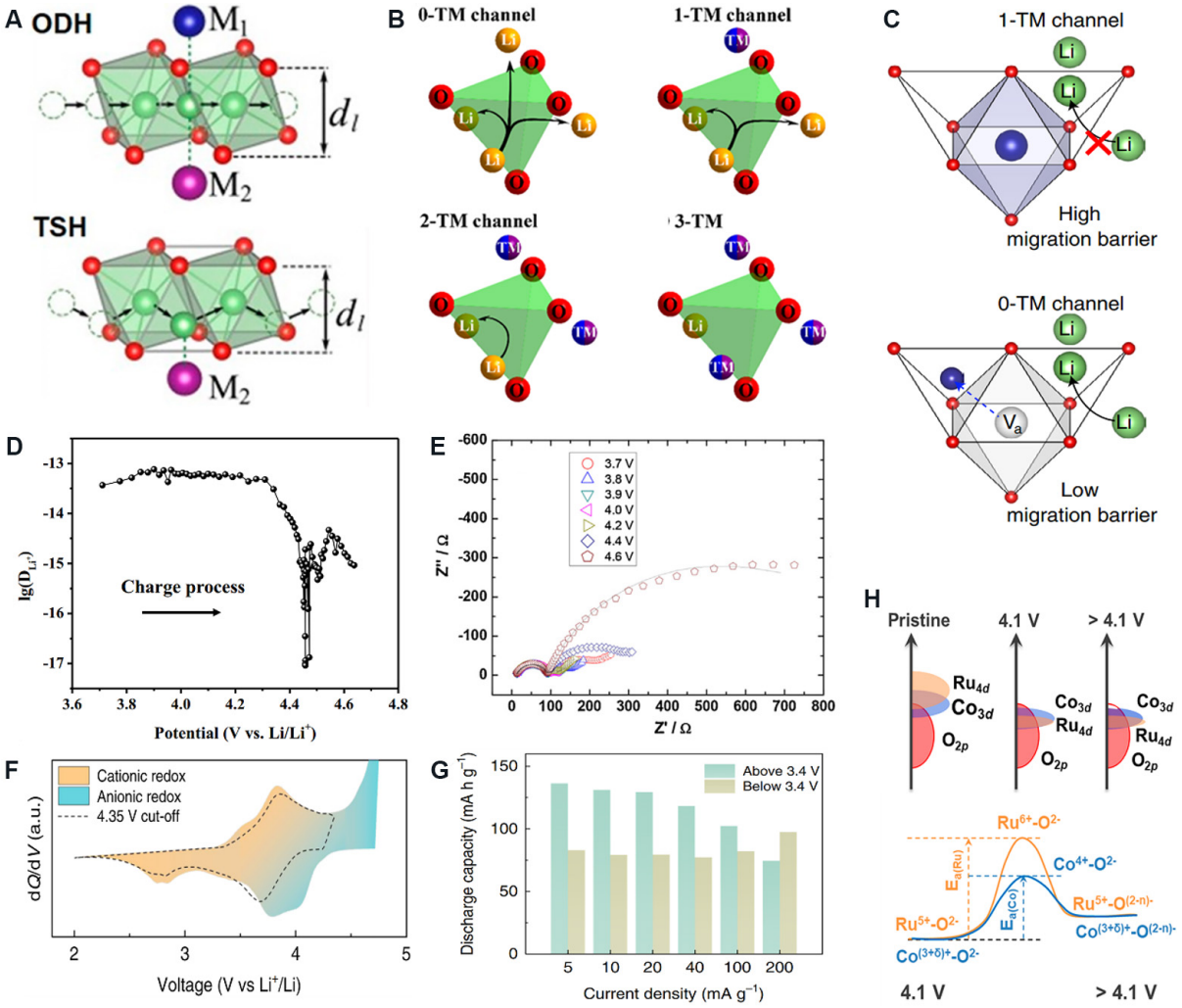

Figure 10. (A) Illustration of ODH and TSH types of Li^+ diffusion pathways[106]. (B) Schematic diagram of Li^+ distributions around tetrahedral sites in the cation-disordered oxide: 0-TM; 1-TM; 2-TM; 3-TM[108]. (C) Illustration of a TMO_6 octahedron with two face-sharing tetrahedral sites. Migration of the TM from the octahedron transforms a 1-TM channel into a 0-TM channel[109]. (D) D_{Li}^+ of a LRMO material under different states during the initial charge[110]. (E) Nyquist plots of $Li_{1.2}Mn_{0.56}Ni_{0.16}Co_{0.08}O_2$ electrodes at various potentials[111]. (F) d*Q*/d*V* curve of O2-LRMO measured at a current density of 5 mA g^{-1}, which proves the reaction mechanism of anions at high potential[98]. (G) Variation of discharge capacity as a function of current density is estimated for the two classified voltage ranges of 2.0-3.4 and 3.4-4.8 V[98]. (H) Schematic diagrams of density of states at different states of charge (top) and anionic oxygen oxidation coupled with cationic reduction (bottom), showing the effect of different activation energy in the intermediate states on anionic kinetics in $Li_{1.2}Ru_{0.4}Co_{0.4}O_2$[112]. ODH: Oxygen dumbbell hopping; TSH: tetrahedral site hopping.

LRMO cathode material are also slower than that of the cations. Eum *et al.*[98] analyzed the d*Q*/d*V* of different potential ranges and found that the charge compensation of the anion in O2-type materials during charge and discharge occurs at a high potential [Figure 10F], which is different from the anion reduction in the O3-type material at a low potential. This creates the conditions for simply examining the reaction kinetics of anions and cations by controlling the applied current and analyzing the capacity evolution at different potential ranges [Figure 10G]. In order to improve the reaction kinetics of the anions, Li *et al.*[112] found that the strong covalent property of Co and O enables the charge compensation of oxygen to occur in advance before the complete oxidation of Co^{3+} to Co^{4+}. This strong coupling effect makes the rapid redox of $Co^{(3+\delta)+}/Co^{4+}$ a medium to improve the kinetics of anion redox in lithium-rich materials [Figure 10H]. Other anions, such as S^{2-}, exhibit faster reaction kinetics and lower voltage hysteresis than O^{2-} but also lower the

redox potential[113] and affect the energy density due to the weaker electronegativity.

PREPARATION AND MODIFICATION

Preparation method

Co-precipitation method

Generally, various metal salts are prepared into a mixed solution according to the target stoichiometric ratio and the metal salt solution and the precipitating agent (e.g., OH^-, CO_3^{2-}, $C_2O_4^{2-}$ and so on) are added dropwise to deionized water simultaneously. An appropriate amount of chelating agent (e.g., ammonia) is added to coordinate with metal ions to buffer the precipitation reaction. Meanwhile, the pH and stirring speed are controlled at a certain temperature to allow metal cations to co-precipitate. The precursor and lithium source (e.g., LiOH, Li_2CO_3 and so on) are then uniformly ground and then calcined at a high temperature to obtain the final lithium-rich oxide. This method can realize ion mixing on the nanometer scale and the subsequent formation of the phase structure at high temperature does not require long-range diffusion of TM ions and avoids problems such as uneven cation distribution and lattice defects. This simple and quick synthesis process is suitable for large-scale promotion and application.

Among them, hydroxide precipitation, especially $Mn(OH)_2$, is easily oxidized in an alkaline environment and an inert protective gas is required to isolate oxygen. However, compared to other carbonates and oxalates, hydroxides have higher reactivity and promote a better crystal structure. During the precipitation process, the nucleation and growth of crystals should be controlled by adjusting the conditions, such as pH and chelating agent. The morphology of the primary and secondary particles formed by aggregation is controlled by adjusting the temperature and stirring speed[79]. During the preparation of the precursor, the sheet morphology can be controlled by adjusting the ammonia concentration, thereby synthesizing particles with specific {010} crystal planes dominantly exposed to promote the rapid diffusion of Li^+. Furthermore, primary particles with a radially ordered arrangement can be generated in the final secondary spherical particles by optimizing the ammonia concentration and stirring speed during co-precipitation, so that the radial primary particles of the material undergo a coordinated volume change during circulation to reduce stress, strain and the formation of microcracks. It is also possible to prepare precursor materials with a concentration gradient (or core-shell structure)[114,115] by adding pre-designed metal salt solutions of different concentrations in batches [Figure 11A], thereby preparing gradient materials with special element distributions and better performance. However, it is necessary to pay attention to the the phenomenon that the gradient distribution would be weakened in the high-temperature calcination process.

The calcination temperature and time have an important influence on the crystallinity and morphology of a material. The higher the calcination temperature and the longer the hold time, the larger the particle size of the primary particles[116-118], and even the transformation from polycrystalline secondary particles to large single crystal particles occurs, with the structure with a special morphology being more susceptible to damage during the calcination process. It may also cause excessive oxidation of TMs and a loss of Li/O, leading to increased cation mixing and phase transformation[119]. In contrast, a lower calcination temperature and time also reduce the crystallinity of the material. Considering the special morphology and high crystallinity, Chen *et al.*[18] heated the precursor with the special morphology at a low temperature in advance to pre-oxidize the TM, thereby reducing the reaction temperature and time, while maintaining the crystallinity of the material during the calcination process. The pre-oxidation process can also remove part of CO_2 or H_2O from the precursor in advance to form a particle morphology with a multilayer hollow core-shell structure. The rate of heating and cooling also affects the morphology and crystal structure of the material. A lower heating rate is more conducive to the maintenance of the particle morphology and a faster cooling method causes more stacking faults, cation disorder and other lattice defects[38].

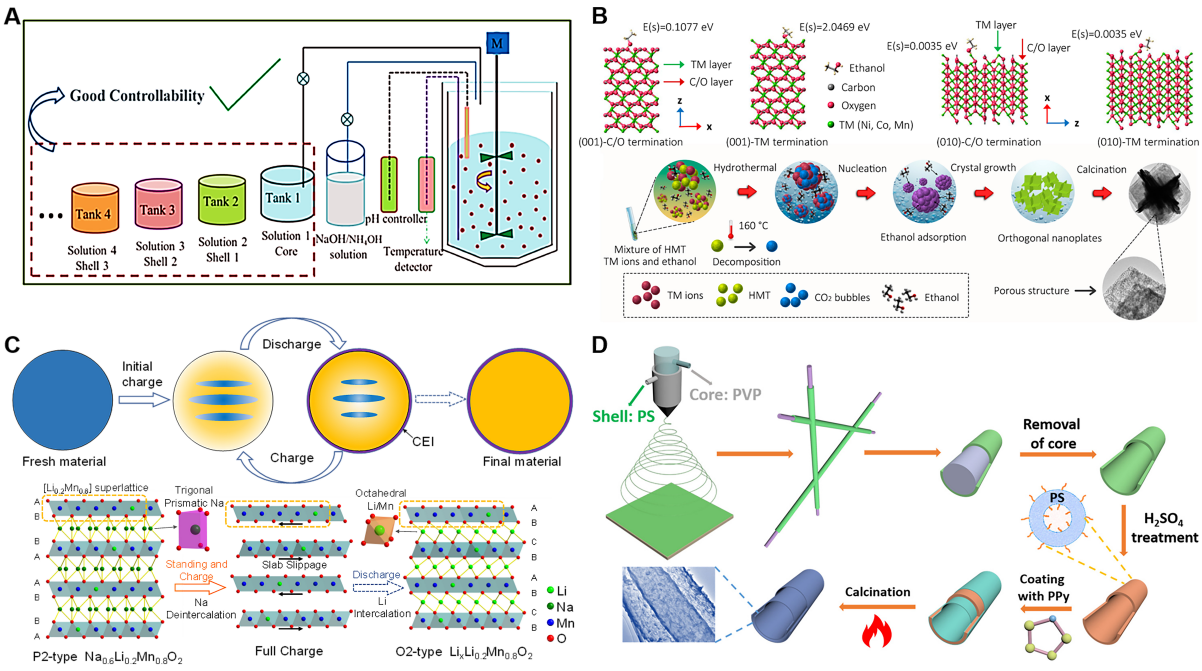

Figure 11. Schematic diagram of (A) materials preparation with gradient distribution of elements by step-by-step co-precipitation method[114]. (B) Controlling nucleation growth to prepare special exposed crystal faces and morphologies by solvothermal method[123]. (C) One-step preparation of O2-type Mn-based cathode material by electrochemical ion exchange[127]. (D) Synthesis process of one-dimensional core-shell structure by electrospinning method[139].

Solvothermal method

The solvothermal method refers to the rearrangement/recrystallization of ions in the liquid phase at a certain temperature and pressure, which can realize some reactions that are difficult to complete in solid or normal liquid phase reactions. Some new materials with special structures or morphologies can be prepared[120-122]. Specifically, the corresponding molar ratio of metal salt and lithium salt is dissolved in a single or mixed solvent[120] (e.g., deionized water, alcohol, dimethyl formamide and so on) with a certain additive, such as acetic acid[75] and hexamethylenetetramine (HMT)[76]. Subsequently, the prepared solution is transferred to a stainless-steel reactor. The precursor can be collected after reacting at a certain temperature and then calcined at a certain calcination condition to obtain the final material. Among them, the Li source can also be introduced after the solvothermal reaction. The morphology of the materials prepared by the solvothermal method is complex and diverse, including spherical secondary particles, single crystal nanosheets, microrods and 3D layered morphology, formed by orthogonal stacking of nanosheets. Microwave assistance can accelerate the reaction rate in the solvothermal process and increase the pores between the spherical secondary particles for promoting the migration of Li^+[77]. The microwave heating method can also be applied to the high-temperature calcination process, which greatly shortens the reaction time.

During the nucleation process, some additives or solvent molecules have the lowest adsorption energy on the {010} crystal plane and tend to be adsorbed on the surface of the crystal plane[123], which results in slower crystal growth in the direction of the crystal plane and promotes the continuous accumulation and growth of atoms along the *c*-axis direction [Figure 11B]. This promotes the final particle to exhibit more exposed {010} crystal planes. Liu *et al.*[76] synthesized a series of precursors with a controllable morphology by a solvothermal method, where HMT acts as the precipitant and a mixture of dimethyl formamide and deionized water acts as the solvent. The prepared 3D cube-maze-like $Li_{1.2}Mn_{0.54}Co_{0.13}Ni_{0.13}O_2$ material

exhibited excellent Li^+ diffusion ability and cycle stability by virtue of its unique 3D structure.

Ion-exchange method

The ion-exchange method means that after the material is placed in the designed solution, a certain ion in the material is spontaneously exchanged with the corresponding ion in the solution and the basic framework of the material is maintained to achieve the preparation of new materials. Among them, the number of ions in the solution must exceed the number of ions in the material to be replaced several times to be completely exchanged. At present, the Li/Na ion exchange reaction is usually used to prepare LIB cathode materials, which can obtain unique structural characteristics based on the precursor with a layered structure[124]. However, the large difference between the Li^+ and Na^+ radii causes drastic changes in the interlayer spacing and structure of the material, which may be accompanied by partial lattice distortion and particle breakage[125].

The conspicuous O2-type LRMO materials are prepared by molten salt ion exchange based on the precursor of P2-type Na-ion battery cathode materials[126]. Specifically, the P2-type precursor is mixed with an excessive amount of composite lithium salt ($LiNO_3$:LiCl = 88:12 w/w) with a lower eutectic point and then heated to melt the composite lithium salt and cause the Li/Na ion exchange to occur. After a period of the reaction, it is cooled to room temperature, washed clean to remove impurities and the O2-type material is finally obtained. This kind of O2-type structure cannot be obtained with the traditional high-temperature calcination process and can only be obtained using the characteristics of the P2-type material, where the oxygen array slips easily at high potential to generate the O2-type structure.

Furthermore, we have developed an electrochemical ion exchange method[127] based on the working principle of alkaline-ion batteries [Figure 11C]. By assembling the precursor into a hetero-type battery, the ions in the electrolyte and bulk material can be exchanged through the electrochemical driving force by continuous charge and discharge. This method generally needs to circulate the material a certain number of times to achieve a relatively complete exchange. A relatively complete ion exchange will be achieved after certain electrochemical cycles by this method, which is simple to realize one-stop ion exchange and enhanced performance. Ion exchange can also occur when the precursor material is immersed in an organic or inorganic solution[128,129] containing a relatively high concentration and excess of Li^+ at room temperature.

Other preparation methods

The sol-gel method[130-132] refers to the stoichiometric ratio of metal salts dissolved in water to prepare a solution, with a certain proportion of complexing agents (e.g., glucose, citric acid and so on) added and heating and stirring to evaporate the solvent. During this process, the metal salt is gradually hydrolyzed or complexed to form a sol and finally dehydrated to form a gel. The gel is dried and calcined to obtain a metal oxide precursor. It is then calcined at a high temperature to obtain the final cathode material after the precursor is uniformly ground. This method can realize the mixing of target ions at the ion/nanoscale, lower the subsequent calcination temperature and is beneficial to realizing the elemental distribution of the cathode material with high uniformity.

The electrospinning method is used to jet-spin the target metal salt polymer solution in a strong electric field to produce a polymer filament precursor with a nanometer diameter and then perform high-temperature sintering to prepare the cathode with one-dimensional nanowires[133-137]. Other petal-shaped nanosheets and nano-block particles can also be prepared by adjusting the sintering temperature and time[138]. In addition, using different preparation processes, such as changing the nozzle structure and controlling the experimental conditions, the precursors with solid, hollow or core-shell structures can be

obtained, and finally the preparation of materials with special morphologies or an *in-situ* coating can be realized [Figure 11D][139].

The spray drying method is used to spray the mixed solution, sol or suspension and other fluid materials that need to be dried under high pressure and dispersed into mist-like droplets. The droplets are sprayed into the drying chamber with fluid hot air, which can instantly remove the moisture and a dry powder particle with uniform mixing of elements will be obtained. The precursor material is then sintered and finally the layered cathode material is prepared. The nanoscale primary particles dispersed in the solution can be spray-dried to produce secondary spherical particles and a more uniform coating can also be achieved by spray drying the coating material[140], such as graphene, and the electrode material. Herein, the properties of different preparation methods and their advantages and disadvantages are prepared in Table 1.

Modification technology

Despite the in-depth research into LRMOs, their drawbacks still need to be resolved to meet commercial applications. The irreversible O_2 release generated near the surface layer after the initial activation of the material poses a severe challenge to the stability and safety of the electrode interface. The destruction of the $LiMn_6$ superlattice and the evolution of the local structure caused by the migration of bulk TMs and oxygen vacancies exert a profound impact on the structure and electrochemical performance. For this reason, a large number of targeted modification measures have been taken for LRMOs to solve the above-mentioned problems.

Regulating activation

When an LRMO is charged to ~4.5 V for the first time, the charge compensation of oxygen occurs, accompanied by the in-plane/out-of-plane migration of TMs and the reorganization of the energy band structure. The irreversible structural changes that partly occur during this process to the subsequent electrochemical behavior and structural evolution are affected profoundly. Watanabe *et al.*[141] and Ito *et al.*[142,143] carried out voltage regulation, reducing the upper voltage to 4.5 V during the initial activation and gradually increasing the upper cut-off voltage to 4.8 V, which can significantly improve the cycle performance of the material. After thorough research, this stepwise pre-cycling treatment can inhibit the microcracks on the particle surface and the periodic distortion of the crystal structure, significantly improving the cycle resistance of the material. In our previous work [Figure 12A], we also found that pre-cycling can alleviate the severe lattice distortion and the formation of spinel-like phases during the activation process and rationalize the intercalation/deintercalation interval of Li^+[110].

The range of the voltage test is also related to the evolution of electrochemical performance and structure[144]. TMs migrate from the TM layer to the vacancy in the Li layer at a high charging voltage (> 4.5 V), tending to form a more favorable spinel structure. The Mn will be excessively reduced to a charge below +3.5 at low discharge voltages (< 2.8 V), which promotes the Jahn-Teller effect and the disproportionation reaction of Mn^{3+}. For this purpose, Yang *et al.*[145] used an LRMO to perform charge and discharge cycles in the range of 2.8-4.4 V, which effectively inhibited the phase transition at high and low voltages and showed excellent cycle stability. Nayak *et al.*[146] studied the effect of electrochemical activation on the performance of the material. It was found that the materials that have not undergone activation show the equivalent capacity of $LiMO_2$ at 2.3-4.3 V but still show a voltage decay of > 0.1 V after 100 cycles. The activated material exhibits a capacity exceeding the non-activated conditions by 50 mAh g^{-1} with a lower and more stable discharge average voltage. Pradon *et al.*[147] evaluated the influence of the constant voltage method adopted in industry to eliminate dynamic polarization of the materials. It was found that the more time spent at high potentials, the more structural defects that were formed. Yin *et al.*[148] also studied the

Table 1. Summary of the properties of different preparation methods and their advantages and disadvantages

	Cost	Process	Production	Morphology	Performance
Co-precipitation method	Low	Simple	Huge	Spheroidal	General
Solvothermal method	High	Complex	low	Multiple	Good
Ion-exchange method	High	Simple	Huge	Irregular	Good
Sol-gel method	Low	Complex	low	Irregular	Good
Electrospinning method	High	Complex	low	Fibrous	Good
Spray drying method	Low	Simple	Huge	Spheroidal	General

structural evolution of the material during a constant voltage of 5 h after being fully charged to 4.8 V and found a new phase produced under continuous oxidation at this stage, which aggravated the migration of Mn and the deterioration of capacity and voltage.

Kaewmala *et al.*[149] studied the influence of current density on the structural changes and cycle stability of an LRMO and found that the activation of the Li_2MnO_3 components was affected by the current density. High-current cycling can effectively reduce the activation of Li_2MnO_3 and the formation of the spinel phase to obtain better cycling performance and faster Li^+ diffusion. Yu *et al.*[93] studied the influence of activation temperature on the phase structural transformation [Figure 12B] and found that the remaining proportion of the Li_2MnO_3 component after activation at 25 °C is 17%, while the remaining Li_2MnO_3 component after activation at 55 °C only remains 7%. This shows that the activation process of LRMOs is very sensitive to temperature and will be aggravated with increasing temperature. Therefore, the activation process, voltage range, current density and other factors are very important for LRMOs. Appropriate working conditions need to be designed to make the electrochemical performance of the material reasonable.

Surface modification

In the process of electrochemical charge-discharge, there are serious problems, such as oxygen release, holes, microcracks, particle powdering, TM dissolution and irreversible phase change of the surface structure, which are the main reasons for the decay of electrochemical properties, so it is necessary to focus on improving the stability of the surface of the material.

Coating is a common means to modify the surface of a material. Coating materials are generally divided into oxides[150-152], phosphates[153], fluorides[154,155] and conductive polymers[156], and the surface treatment object can be an electrode material or precursor. Inert oxides, such as Al_2O_3[157] and SnO_2[158], can only build an inactive isolation layer on the surface of the materials to avoid the side reactions caused by direct contact with the electrolyte, but they may reduce the electron/ion conductivity and affect the rate performance. Other functional oxides enriched with oxygen vacancies, such as $Ce_{0.8}Sn_{0.2}O_{2-\sigma}$[159], MoO_x[160] and so on, not only avoid direct contact between the host material and the electrolyte, but also provide oxygen vacancies to capture oxygen radicals, a fast ionic conductor reacting with surface Li to improve rate performance[161,162], additional charge compensation to improve the capacity and other functions[163] [Figure 13A]. Fluoride coatings provide F-O bonds on the surface, thus reducing oxygen loss and the decomposition of the electrolyte. Phosphates can also stabilize the surface lattice oxygen to reduce oxygen loss and PO_4^{3-} can form covalent bonds with metal ions to inhibit TM migration. Conductive polymer coating layers can significantly improve the electrochemical performance due to its high electronic conductivity and good coating uniformity. In addition, the binding force between the surface coating layer and the host material cannot be ignored. It is a good choice to choose a coating that is structurally compatible with a bonding effect[164].

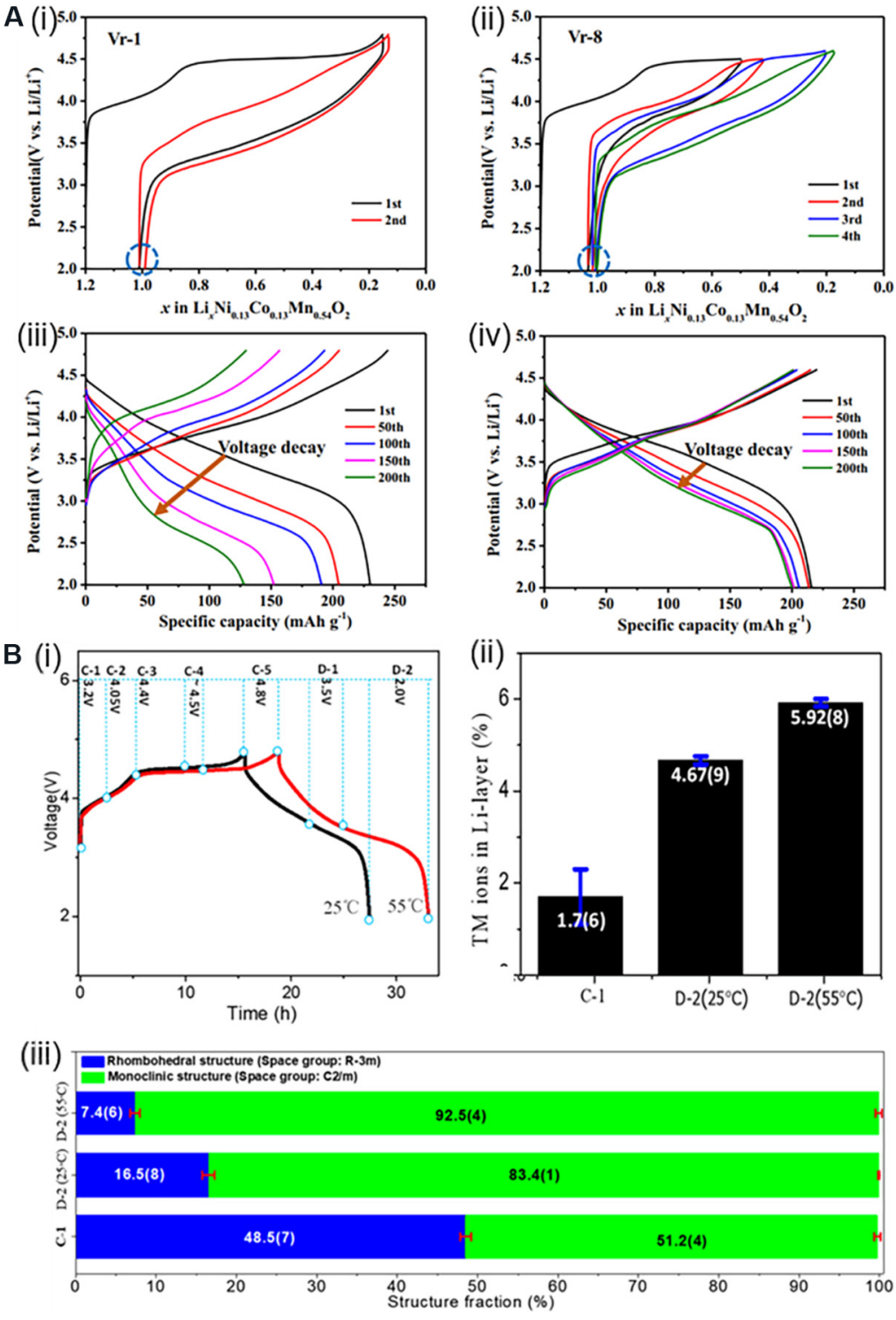

Figure 12. (A) Charge-discharge curves and electrochemical performance of LRMO materials under different voltage systems. (i) Initial two cycles of charge-discharge curves under the condition of Vr-1 (tested between 2.0 and 4.8 V). (ii) Initial four cycles of charge-discharge curves under the condition of Vr-8 (pre-cycled at 2.0 to 4.5 V for two cycles and tested between 2.0 and 4.6 V). (iii and iv) Cycle performance of materials under Vr-1 and Vr-8, respectively[110]. (B) Initial charge-discharge curves (i), the evolution of TM occupancy in Li layer (ii) and two-phase content by Rietveld refinement (iii) for $Li_{1.2}Mn_{0.567}Ni_{0.167}Co_{0.078}O_2$ at 25 and 55 °C[93]. LRMO: Lithium-rich manganese-based layered oxide.

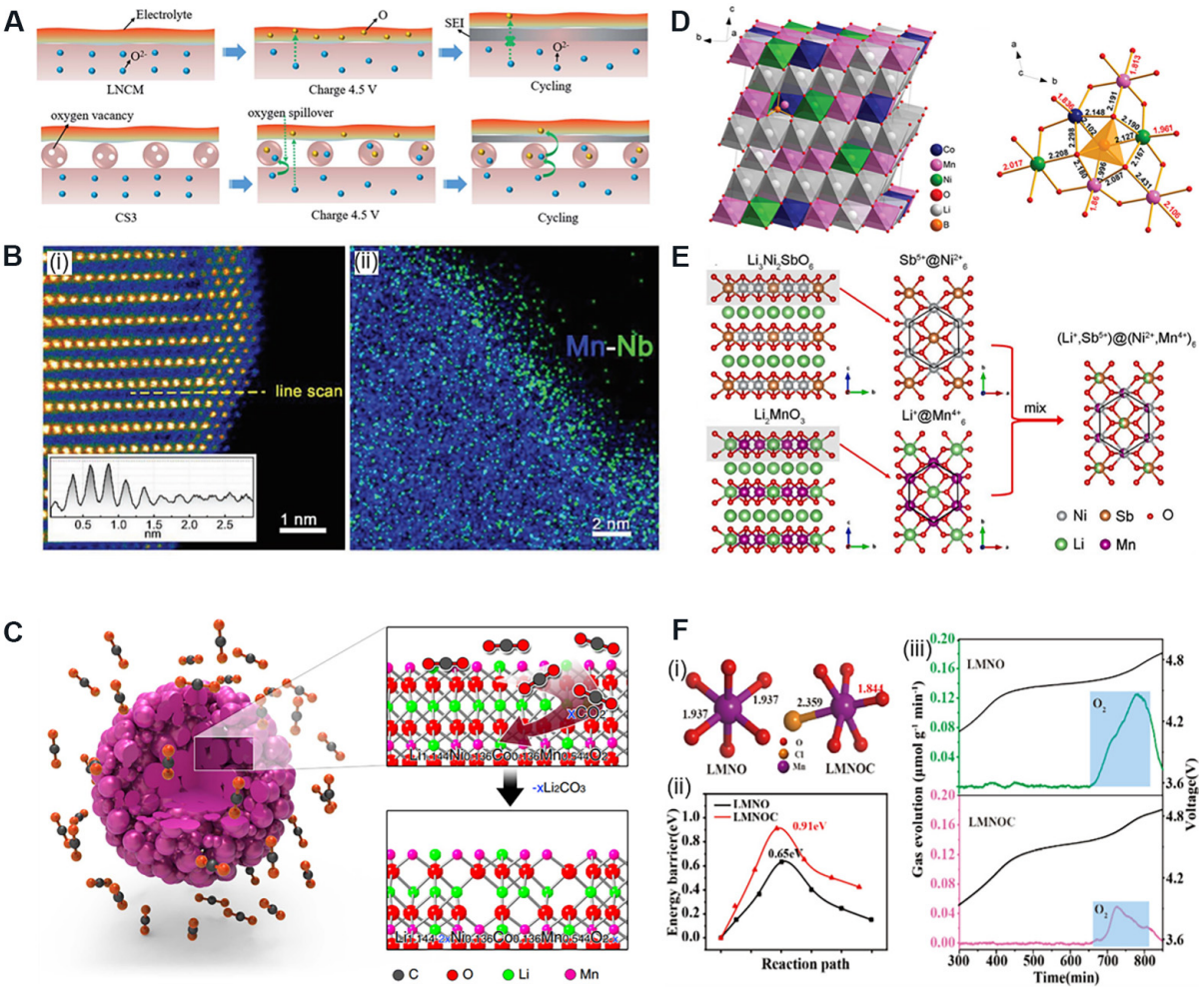

Figure 13. (A) Schematic illustration of oxygen vacancies in $Ce_{0.2}Sn_{0.8}O_{2-\sigma}$ and its protective effect on an LRMO material[159]. (B) HAADF image near the surface (i) and the EDS mapping of Mn and Nb (ii) of the LRMO particle by Nb surface doping[170]. (C) Schematic of gas-solid interface reaction between Li-rich layered oxides and carbon dioxide[173]. (D) Optimized structure of BO_4^{5-}-doped LRMO (left), in which B atoms occupy the tetrahedral interstitial sites. The simulated local structure (right) around the boracic polyanion, showing that the M-O bonds are lengthened due to the strong B-O bond[182]. (E) Schematic illustration of Li-rich layered material with composited $LiMn_6$ and $SbNi_6$ superstructures[186]. (F) (i) Length of TM-O (Cl) bonds of $Li_{1.2}Mn_{0.53}Ni_{0.27}O_2$ (LMNO) and $Li_{1.2}Mn_{0.53}Ni_{0.27}O_{1.976}Cl_{0.024}$ (LMNOC), (ii) energy barriers of TM migrating from the TM layer to the Li layer and (iii) operando differential electrochemical mass spectrometry curves of O_2 for LMNO and LMNOC[187]. LRMO: Lithium-rich manganese-based layered oxide; HAADF: high-angle annular dark-field.

Surface doping is based on surface coating. By increasing the calcination temperature, the coated elements spontaneously diffuse into the surface layer lattice of the material to form localized interface doping[165-167]. Surface doping can enhance the interaction between the doped elements and the host material and stabilize the surface interface without affecting the bulk structure[168,169]. Liu *et al.*[170] modified the surface of $Li_{1.2}Mn_{0.54}Co_{0.13}Ni_{0.13}O_2$ by Nb^{5+} surface doping. The doped Nb^{5+} is located in the Li layer near the surface of the material, thereby inhibiting lattice distortion and deactivating the surface oxygen, which is beneficial to preventing cation mixing and improving the structural stability [Figure 13B]. Zhong *et al.*[171] doped PO_4^{3-} on the surface of $Li_{1.2}Mn_{0.54}Co_{0.13}Ni_{0.13}O_2$, where the PO_4^{3-} inhibited the irreversible release of lattice oxygen on the surface of the material. Moreover, PO_4^{3-}-M with a stronger binding energy effectively reduced the migration of TMs to the Li layer and a fast ionic conductor, Li_3PO_4, was also formed on the interface of the host material by the interdiffusion of ions. Thus, the ionic conductivity of the modified material was

improved and the generation of the CEI film was reduced.

In addition, other surface treatments, such as mild acid treatments[172], can achieve H^+/Li^+ exchange and remove Li^+ and O^{2-} in the Li_2MnO_3 component in advance to reduce oxygen release and irreversible capacity loss during the initial cycle. Simultaneously, the residual Li_2CO_3, LiOH and other impurity components on the surface of the host material were removed, which improves the reaction activity of the cathode interface. Gas phase[73,173,174] (NH_3, CO_2, CO and so on) treatment can produce certain element doping or oxygen vacancy generation on the surface of the material, inhibit the oxygen release and promote the Li^+ diffusion [Figure 13C]. After molten salts or other highly reactive solutions are used to act on LRMOs[175-177], epitaxial heterostructures[150] (spinel and cation disordered rock-salt phases) are inclined to form on the surface. These structures formed by the phase transformation of layered materials exhibit higher thermodynamic stability, can inhibit the activity of surface oxygen and stabilize the interface to avoid the migration of structural defects from the surface to the bulk.

Bulk doping

Compared with the surface layer, the structural stability and electrochemical reversibility of the bulk phase of the material are relatively good. However, due to its intrinsic anion redox reaction, there are still problems such as TM migration, oxygen vacancy transfer and phase structural transformation. Therefore, bulk doping of the material is expected to improve the electrochemical performance and structural stability of the material radically. Generally, bulk doping can be carried out at three positions: Li sites[178]; TM sites[107]; oxygen active sites[96,179,180], which can produce different effects and results.

Liu *et al.*[181] prepared $Li_{1.167-x}K_xMn_{0.583}Ni_{0.25}O_2$ by ball milling and solid-phase sintering, using K^+ to partially replace Li^+ in the material. The rate performance and cycle performance of the pristine material are significantly improved. Studies have found that the doped K^+ is pinned at the Li site, which hinders the migration path of part of the Mn and inhibits the formation of the spinel phase. Zhang *et al.*[178] successfully incorporated Na^+ into the $Li_{1.23}[Ni_{0.2464}Mn_{0.462}Co_{0.0616}]O_2$ crystal through a solid-phase reaction to partially replace Li^+ in bulk. Tests showed that Na^+ doping significantly improved the electrochemical performance of the material. The main reason is that Na^+ doping into the layered structure expanded the layer spacing, which promoted the rapid diffusion of Li^+ and reduced the release of oxygen in the crystal lattice. Meanwhile, Mn^{4+} in Li_2MnO_3 was further activated after Na^+ doping and provided reversible capacity in subsequent electrochemical cycles.

Li *et al.*[182] successfully doped boron polyanions into a cathode material to synthesize $Li[Li_{0.2}Ni_{0.13}Co_{0.13}Mn_{0.54}](BO_4)_{0.75x}(BO_3)_{0.25x}O_{2-3.75x}$. First-principles calculations show that the doped borate anion can reduce the O 2p orbital energy level, due to the doping of B in the tetrahedral position of the transition metal layer [Figure 13D]. This reduced the covalency of the TM-O bond, inhibited the precipitation of oxygen in the LRMO and prevented structural damage of the material during charge-discharge cycling. Wu *et al.*[183] successfully synthesized a Fe-doped $Li_{1.2}Mn_{0.585}Ni_{0.185}Fe_{0.03}O_2$ material. The doped Fe instead of Co is located in the TM layer, which increased the lattice distance and enhanced the diffusion of Li^+ in the host structure. Simultaneously, it inhibited the migration of TMs to the Li layer and hindered the transformation of the crystal structure from the layered to spinel and rock-salt structures. Nayak *et al.*[184] successfully synthesized $Li_{1.2}Ni_{0.16}Mn_{0.51}Al_{0.05}Co_{0.08}O_2$ as a cathode material using Al^{3+} instead of Mn^{4+}. Al doping can suppress the phase change of the material from laminar to spinel during the cycle, thereby stabilizing the crystal structure. The electrochemical impedance of the doped material did not change significantly during cycling, indicating that Al doping exhibits a certain surface effect.

Jiang *et al.*[185] used F^- to replace O^{2-} in $Li_{1.2}Ni_{0.2}Mn_{0.6}O_2$, which changed the local electronic environment of Mn, reduced the release of oxygen and caused a change in the surface structure. The symmetry of the MnO_6 octahedron is destroyed because of the shorter Mn-F bond than the Mn-O bond, thereby alleviating the Jahn-Teller effect. The expansion of the interlayer spacing after doping caused Li^+ to be inserted/extracted faster, thereby suppressing the increase in charge transfer resistance during cycling. In addition, the conversion of the layered structure to the spinel phase during cycling was inhibited, which finally improved the electrochemical performance. Li *et al.*[186] successfully prepared $Li(Li_{1/6}Mn_{1/3}Ni_{1/3}Sb_{1/6})O_2$ materials with mixed $Li@Mn_6$ and $Sb@Ni_6$ superstructure elements [Figure 13E]. The study found that the coordination environment of local oxygen changes, which reduces the energy barrier for Li^+ diffusion and provides additional capacity. Wang *et al.*[187] partially replaced oxygen with anion Cl to change the coordination environment of the TMs, which stabilized the TM-O bond and effectively inhibited the irreversible O_2 release and TM migration [Figure 13F], thereby enabling the material to exhibit excellent capacity and voltage retention.

Other electrode/electrolyte scope

In order to ensure that an electrode exhibits good electrochemical performance, a certain amount of conductive agent is usually added during the production of the electrode slice to reduce the contact resistance and improve the electronic conductivity. The conductive agent should possess good dispersibility and a high specific surface area and electrolyte adsorption capacity to further improve the ionic conductivity of the electrode. The main conductive additive in traditional cathodes is acetylene black; however, acetylene black is difficult to disperse and exhibits strong oil absorption, resulting in an uneven local composition of the slurry. Yu *et al.*[188] used carbon nanotubes (CNTs) to prepare composite LRMO cathode electrodes, which displayed the characteristics of a binder, lightweight and self-standing [Figure 14A]. Based on long-period electrochemical tests, the self-supporting structure can reduce polarization, stabilize the electrode to inhibit structural deformation and simultaneously promote the rapid transmission of electrons/ions. Luo *et al.*[189] prepared a binder-free $LiCoO_2$ electrode with excellent flexibility and conductivity by constructing a continuous 3D super-aligned CNT frame with embedded $LiCoO_2$ particles. This binder-free cathode electrode showed better cycle stability, rate performance and energy density than the typical electrode with a binder.

As an inactive ingredient, the binder cannot provide capacity. Currently, the matching binder for LRMOs is mainly based on a fluorocarbon (PVDF). PVDF is sensitive to the water content during the electrode preparation process and will swell in the electrolyte. Furthermore, its exothermic reaction with metal lithium and Li_xC_6 at higher temperatures is unfavorable from a safety perspective. Therefore, designing and synthesizing a binder with excellent conductivity and viscosity is very important for improving the energy density, rate and cycle performance. Zhang *et al.*[190] used guar gum (GG) as the binder of a LRMO, which exhibited low solubility and swelling ability in the electrolyte [Figure 14B] and effectively reduced the volume expansion of the electrode during cycling. Polyacrylic acid (PAA) was also used by Yang *et al.*[191] as a binder for LRMO electrodes [Figure 14C]. The H^+/Li^+ exchange between the LRMO and PAA generates protons on the surface layer of the cathode, which effectively suppress the migration of TMs, thereby forming a stable structure. This surface modification represents a new method for stabilizing LRMOs.

Currently, microporous polyolefin membranes, such as polyethylene and polypropylene, are the most commonly used separators for lithium-rich cathode materials, because of their excellent mechanical strength and chemical stability. However, the low melting point of polyolefin membranes results in high thermal shrinkage at high temperatures, causing an internal short circuit and even explosion. Simultaneously, the non-polar polyolefin separator exhibits poor wettability, which has a negative impact

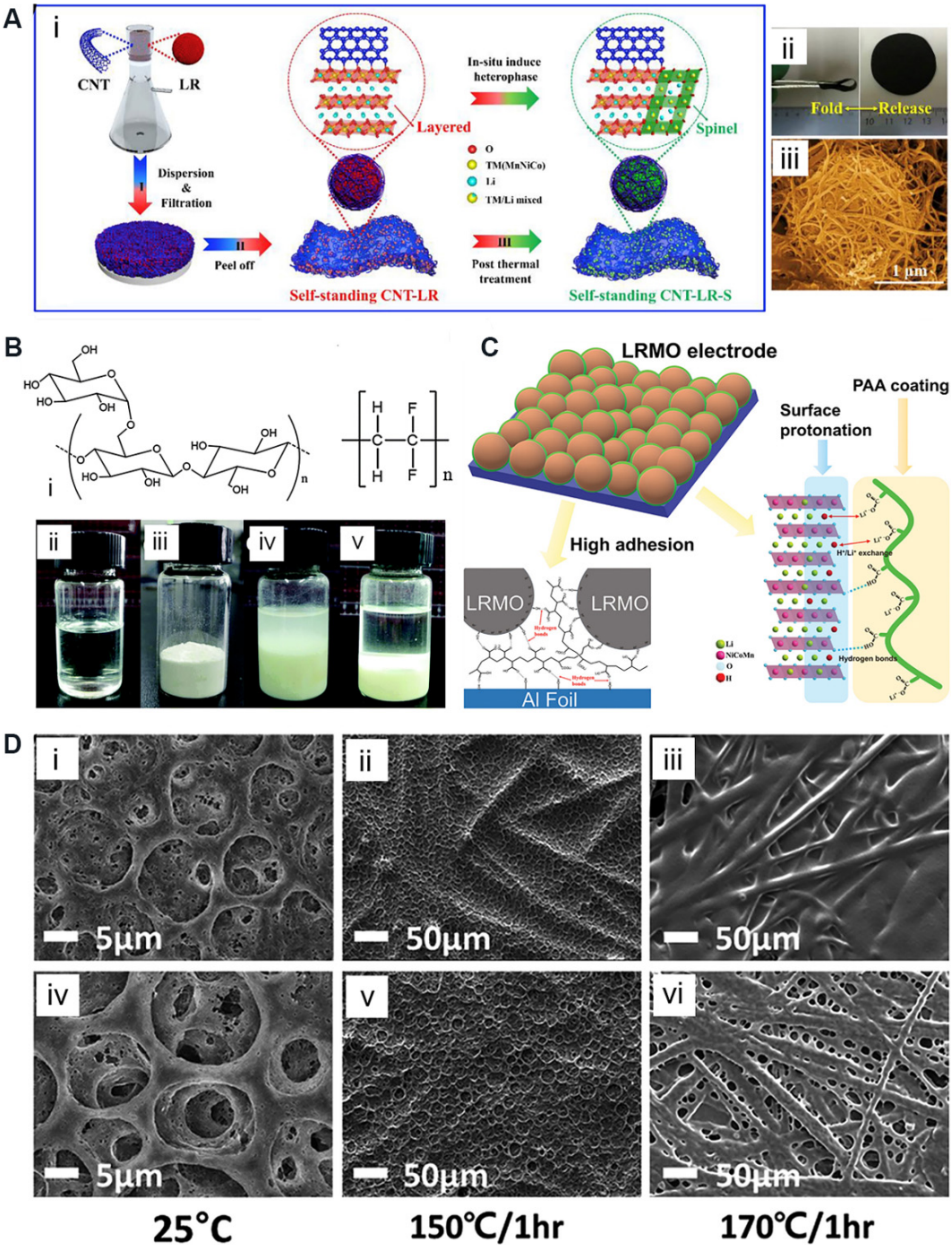

Figure 14. (A) Schematic synthesis process of self-standing CNT-LRMO (i) with photographic (ii) and SEM images (iii)[188]. (B) Chemical structure of GG and PVDF (i), photographs of electrolyte (ii) and GG (iii) and the mixture of GG and electrolyte after 0 h (iv) and 24 h (v)[190]. (C) Schematic of the effect of PAA binder for LRMO electrode[191]. (D) SEM micrograph of PVDF-HFP separator (i-iii) and modified PVDF-HFP/GO nanosheet (iv-vi) in its original state and stored at 150/170 °C for 1 h[192]. CNT-LRMO: Carbon nanotube-lithium-rich manganese-based layered oxide; GG: guar gum; PAA: polyacrylic acid; HFP: hexachloropropylene; GO: graphene oxide.

on the rate and cycle performance of the battery. Choi *et al.*[192] incorporated graphene oxide (GO) nanosheets into a PVDF-hexachloropropylene (HFP) framework through phase inversion during the pore formation process [Figure 14D]. The addition of GO greatly improves the thermal stability of the composite

separator. Shin *et al.*[193] reported a new concept of coating nitrogen and sulfur co-doped graphene (NSG) nanosheets on a polyethylene separator. The thin NSG layer acts as a physical barrier to inhibit Li dendrite growth due to its excellent mechanical properties. Due to the local strain caused in the carbon skeleton, the incorporation of N and S can cause structural deformation, thereby improving ion migration while maintaining a uniform ion flux on the surface of the Li metal.

The high working voltage of an LRMO exceeding 4.5 V causes the traditional carbonate-based electrolyte[194,195] to decompose severely on the surface of the cathode materials[196], forming an uneven, unstable and unprotected CEI, which hinders the diffusion of Li^+ and reduces the electrochemical efficiency. Liu *et al.*[21] studied the effect of concentrated electrolyte (with a solute concentration of 3 mol L^{-1}) on the surface structure of a cobalt-free LRMO and found that high-concentration electrolytes can form a CEI rich in LiF and other inorganic species on the surface of the electrode, which significantly inhibited the dissolution of TM and effectively protected the cathode material from corrosion. Cui *et al.*[197] added lithium difluoro(oxalato)borate to a perfluorinated electrolyte and the strong fluorinated CEI formed *in situ* effectively reduced the side reaction between the O2-type LRMO electrode and electrolyte, and further suppressed O2 structural transformation and oxygen release. Lou *et al.*[198] first studied methyl diphenyl phosphonate as an electrolyte additive to form a strong artificial mesophase layer *in situ* on the surface of the cathode electrode. The intermediate phase can effectively inhibit the decomposition of the electrolyte and greatly improve the stability of the interface between $Li_{1.16}Ni_{0.2}Co_{0.1}Mn_{0.54}O_2$ and the electrolyte under high voltage and temperature.

TESTING AND CHARACTERIZATION METHODS

The unique anion charge compensation mechanism of LRMO cathode materials causes a series of complex scientific problems, such as TM migration, oxygen release, surface densification, lattice distortion and energy band reconstruction. It is therefore necessary to employ multiscale and omni-directional characterization methods for in-depth research and effectively carry out materials design to develop new high specific energy cathode materials based on anionic redox reactions.

Electrochemical methods

Galvanostatic charge-discharge tests can act on the electrode material in a certain voltage range and obtain electrochemical properties, such as the charge and discharge curve, capacity, cycle and rate performance, of the material. The charge and discharge curve of the material can be differentiated to obtain dQ/dV, which can identify the redox reaction occurring at different potentials. The electrochemical behavior and evolution of the material can be obtained by analyzing the position and migration of the redox peaks. Yue *et al.*[199] conducted galvanostatic charge-discharge tests under different voltage ranges. By analyzing and comparing different dQ/dV curves [Figure 15A], the electrode reaction potentials and reaction ranges of different redox couples were easily and effectively obtained.

The principle of cyclic voltammetry (CV) is to apply a linearly varying cyclic voltage on a working electrode to record the change in potential. According to the peak current and peak potential in the cycle diagram, the electrochemical reaction of the electrode within this potential range can be analyzed. It can read the reaction type, steps and mechanism, judge the reversibility of the reaction and even study the chemical reaction that occurs on the electrode surface. Yu *et al.*[200] prepared Ga-doped $Li[Li_{0.2}Mn_{0.54}Co_{0.13}Ni_{0.13-x}Ga_x]O_2$ and used CV to test the material at a scan rate of 0.2 mV s^{-1} at 2.0-4.8 V to evaluate its electrochemical stability. By comparing the peak position, peak and potential in the initial two circles of the CV curve with the original electrode, the Ga-doped cathode material exhibited a larger reduction peak current, indicating that Ga doping can help improve the Mn^{4+}/Mn^{3+} reactive activation. The apparent D_{Li^+} of LRMO materials can also

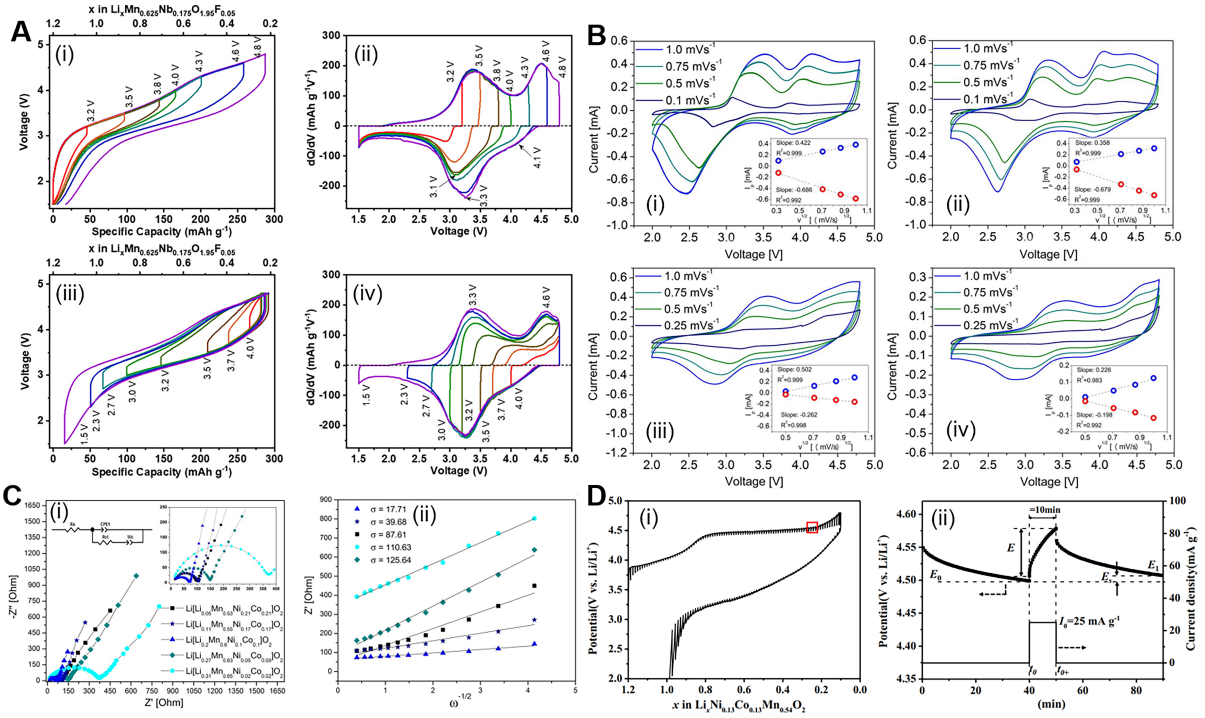

Figure 15. (A) Different electrochemical redox couples judged by regulating the voltage range. Charge-discharge curves (i) and corresponding d*Q*/d*V* (ii) by fixing the lower cut-off voltage and gradually increasing the upper cut-off voltage. Charge-discharge curves (iii) and corresponding d*Q*/d*V* (iv) by fixing the upper cut-off voltage and gradually decreasing the lower cut-off voltage[199]. (B) CV curves of different LRMO materials at different scanning rates and the linear fit of the i_p and $v^{1/2}$ in the illustration[201]. (i) $Li[Li_{0.31}Mn_{0.65}Ni_{0.02}Co_{0.02}]O_2$; (ii) $Li[Li_{0.27}Mn_{0.63}Ni_{0.05}Co_{0.05}]O_2$; (iii) $Li[Li_{0.2}Mn_{0.6}Ni_{0.1}Co_{0.1}]O_2$; (iv) $Li[Li_{0.11}Mn_{0.55}Ni_{0.17}Co_{0.17}]O_2$. (C) (i) EIS Nyquist plots of the tested LRMO materials with the corresponding equivalent circuit. (ii) Linear relationship between Z' and ω(angular frequency)$^{-1/2}$ in the low-frequency region with σ (the slopes of the simulated lines)[201]. (D) Overall GITT curve (i) for $Li_{1.2}Ni_{0.13}Co_{0.13}Mn_{0.54}O_2$ during the initial charge and discharge with the (ii) schematic diagram in a single GITT titration curve[110]. CV: Cyclic voltammetry; LRMO: lithium-rich manganese-based layered oxide; EIS: electrochemical impedance spectroscopy; GITT: galvanostatic intermittent titration technique.

be calculated through CV tests with different scanning rates:

$$i_p = 0.4463nFAC\left(\frac{nFvD}{RT}\right)^{\frac{1}{2}}$$

where i_p represents the current maximum in amps, n is the number of electrons transferred in the redox process, A is the electrode area, C is the ion concentration, F is the Faraday constant, R is the gas constant, T is the test temperature, v refers to the scan rate of CV and D is the diffusion coefficient [Figure 15B].

EIS is based on the application of a small amplitude sine wave potential (or current) disturbance signal to the electrode, so that the electrode system produces an approximately linear response and information, such as impedance, of the electrode can be obtained through these signals. In a LIB system with a LRMO cathode material, the side reactions of the interface cause the formation and accumulation of electrochemical inert materials on the electrode surface and the structural phase transition also causes changes in the internal resistance of the battery. Therefore, the use of EIS to characterize the diffusion capacity of Li^+ inside the material and the surface charge transfer resistance of the material is of great significance. EIS was adopted by Xue *et al.*[156] to further analyze the influence of polyaniline (PANI)-coated LRMO cathode materials on

Li^+ diffusion and electron migration. The equivalent circuit model calculation based on the EIS spectrum showed that the surface film resistance of the cathode material coated with PANI decreased and the growth of the charge transfer resistance slowed down, indicating that the electrochemical activity of the interface was significantly improved after coating. The AC impedance method can also use the following formula to calculate the ion diffusion coefficient:

$$D = \frac{R^2T^2}{2A^2n^4F^4C^2\sigma^2}$$

where σ is the Warburg coefficient and the other coefficients are consistent with those in the above CV method [Figure 15C]. Redel *et al.*[201] systematically studied the electrode reaction kinetics and calculated the D_{Li^+} of different molar amounts of LRMO materials through CV and EIS. They found that $Li[Li_{0.2}Mn_{0.6}Ni_{0.1}Co_{0.1}]O_2$ exhibited the highest kinetic conditions.

The galvanostatic intermittent titration technique (GITT) is a common method for measuring D_{Li^+} in LIB electrode materials. The principle is to apply a constant current to the electrode for a certain period of time and record and analyze the potential corresponding curve after the current pulse. This method eliminates the ohmic potential drop that is difficult to avoid in methods, such as constant potential intermittent titration techniques, and can quickly calculate the D_{Li^+} of the electrode material at any potential. The formula for calculating the diffusion coefficient is:

$$\widetilde{D}=\frac{4}{\pi\tau}\left(\frac{m_B V_m}{M_B S}\right)^2\left(\frac{\Delta E_s}{\Delta E_t}\right)^2 \qquad (\tau \ll L^2/\widetilde{D})$$

where τ is the time of the current pulse, m_B, M_B, V_m and S represents the mass, molecular weight, partial molar volume and the surface area of the electrode materials, respectively, and ΔE_τ and ΔE_s are the voltage changes during the current pulse and standing process, respectively [Figure 15D]. Yang *et al.*[110] conducted a GITT test on the initial charge and discharge process of the cathode and found that the value dropped sharply at ~4.5 V, thereby confirming the slow kinetics of anion charge transfer in LRMO materials.

Physical characterization

The anion redox mechanism is unique to LRMOs among layered cathode materials. The main test methods introduced in this section are used to characterize the complex charge compensation behavior of oxygen.

Shell-isolated nanoparticle-enhanced Raman spectroscopy (SHINERS) can obtain information on molecular vibration and rotation and apply it to molecular structure research by analyzing scattering spectra with different frequencies from the incident light. Li *et al.*[87] successfully detected the peroxygen signal of $Li_{0.66}[Li_{0.12}Ni_{0.15}Mn_{0.73}]O_2$ through the *in-situ* SHINERS, which confirmed the formation of oxidized lattice oxygen species during the initial two charge-discharge processes [Figure 16A]. In addition, the shift of the related peaks of the oxidized lattice oxygen indicates the contraction of the O-O bond after Li^+ deintercalation. When discharged to 2.0 V, the disappeared signal shows that the oxidized oxygen species can be reversibly reduced back to the initial state, which further proves the reversibility of the lattice oxygen redox. Hy *et al.*[202] also used SHINERS to study the evolution of Li_2O in a LRMO and clarified the reaction mechanism of oxygen activation.

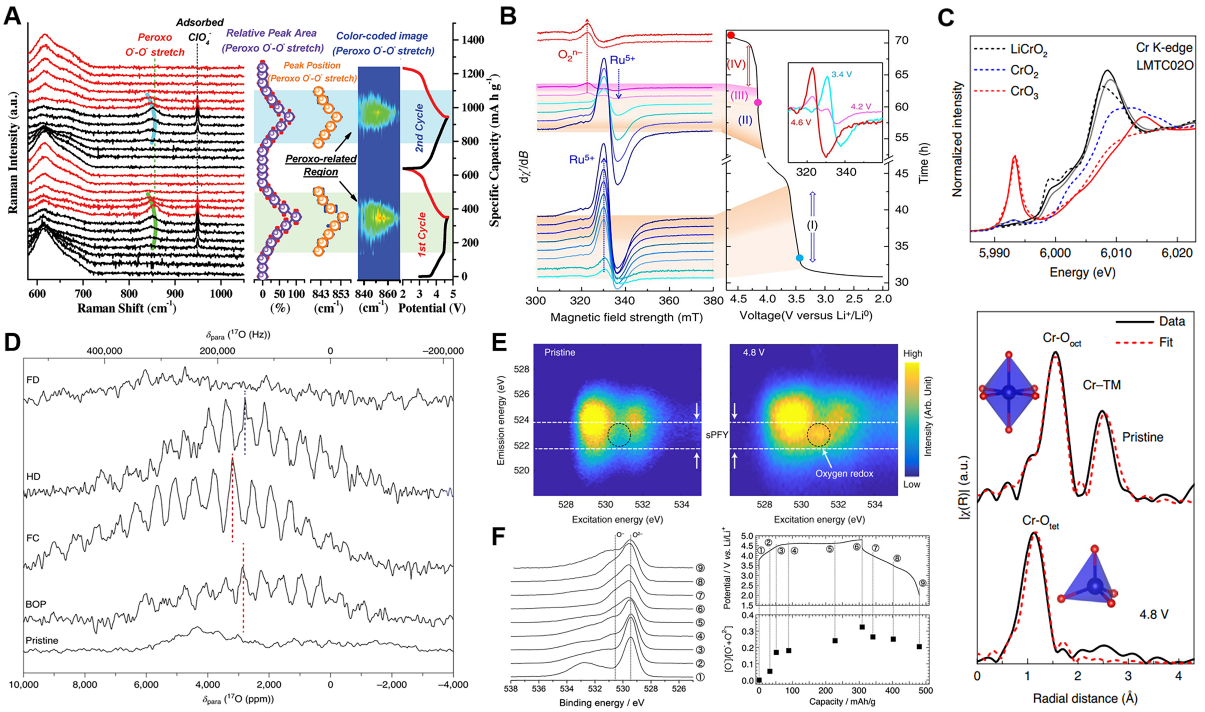

Figure 16. (A) *In-situ* SHINERS spectra recorded during initial two cycles with reversible generation and migration of peroxo O^--O^- at high voltage[87]. (B) X-band *in-situ* EPR spectra of $Li_2Ru_{0.75}Sn_{0.25}O_3$ during the initial charge between 2.0 and 4.6 V. $Ru^{4+}/^{5+}$ charge compensation occurs in the low-voltage plateau area and the reductive coupling of Ru and oxygen occurs in the first half of the high-voltage plateau with the oxidation process of pure O^{2-} in the second half[203]. (C) Cr K-edge XAS spectra (top) of $Li_{1.2}Mn_{0.2}Ti_{0.4}Cr_{0.2}O_2$ in pristine (black solid line), 4.8 V-charged (red solid line) and 1.5 V-discharged states (gray solid line). $LiCrO_2$, CrO_2 and CrO_3 standard spectra are plotted as dashed lines. Fitted Cr K-edge EXAFS spectra (bottom) of $Li_{1.2}Mn_{0.2}Ti_{0.4}Cr_{0.2}O_2$ in pristine and 4.8 V-charged states. Peaks at ~1.0, ~1.5 and ~2.5 Å correspond to the tetrahedral Cr-O, octahedral Cr-O and Cr-TM coordinations, respectively[109]. (D) Solid-state ^{17}O MAS NMR spectra showing the molecular O_2 trapped in the bulk of the cathode particles in the state of full charge[41]. (E) Soft X-ray RIXS data proves that oxygen redox occurs when $Li_{1.2}Ni_{0.13}Co_{0.13}Mn_{0.54}O_2$ is charged to 4.8 V[205]. (F) O 1s HAX-PES spectra (left) of $Li[Li_{0.25}Ni_{0.20}Mn_{0.55}]O_{1.93}$ electrodes for the 1st cycle. The sampling points correspond to the image on the right with the intensity ratio of $[O^-]/[O^- + O^{2-}]$[207]. SHINERS: Shell-isolated nanoparticle-enhanced Raman spectroscopy; EPR: electron paramagnetic resonance; XAS: X-ray absorption spectroscopy; EXAFS: extended X-ray absorption fine structure; NMR: nuclear magnetic resonance; RIXS: resonant inelastic X-ray scattering; HAX-PES: hard X-ray photoelectron spectroscopy.

Electron paramagnetic resonance (EPR) can be used to qualitatively and quantitatively detect the unpaired electrons contained in the atoms or molecules of substances and to explore the structural characteristics of the surrounding environment. Sathiya *et al.*[203] reported the results of the EPR operation spectroscopy and *in-situ* imaging of $Li_2Ru_{0.75}Sn_{0.25}O_3$ [Figure 16B]. By operando monitoring of the EPR signal of Ru^{5+} and paramagnetic oxygen, the formation of reversible O_2^{n-} species can be clearly proved. Tang *et al.*[86] used EPR to *in-situ* detect the cation-anion redox correlation and found that the coupling between Mn and oxygen produces the necessary synergy to stabilize O_2^{n-} species, activates more Mn to participate in the electrochemical reaction and ensures the high specific capacity of the LRMO material.

The structural information in the extended X-ray absorption fine structure (EXAFS) spectrum comes from the interference between the photoelectron wavefunction and nearby atoms. The structural information, such as the coordination structure around different element atoms and the types of coordination atoms, contained in the spectrum can be interpreted using Fourier transform. Huang *et al.*[109] analyzed the coordination environment of Cr in lithium-rich disordered rock salt phase materials by EXAFS spectroscopy and found that during the charging process, Cr migrates from the initial octahedral position to the tetrahedral coordination environment [Figure 16C]. This non-topological reaction mechanism

promotes the transformation of the Li^+ migration path from the 1-TM to 0-TM channel and realizes rapid Li^+ diffusion. After analyzing the EXAFS spectrum of the TM and oxygen in different charge-discharge stages, Yin *et al.*[71] revealed the evolution of their coordination structure and studied the effect of different nickel contents on anion redox. They showed that an appropriate increase in Ni content not only changed the redox center of the LRMO cathode but also enhanced the reversibility of Mn migration through the shielding effect.

NMR is one of the most powerful tools to qualitatively analyze the composition and structure of materials through the absorption of radio-frequency radiation by the atomic nucleus and sometimes can also be used for quantitative analysis. In order to independently verify the formation and reduction of molecular O_2, House *et al.*[41] labeled $Li_{1.2}Ni_{0.13}Co_{0.13}Mn_{0.54}O_2$ samples with ^{17}O. The results showed a large shift in the peak position and an ^{17}O paramagnetic shift. In addition, the ^{17}O sideband shift composed of a series of spikes indicates that the molecular O_2 is strictly confined in its local environment [Figure 16D], consistent with the clustering of defect vacancies and clearly explaining the formation of molecular O_2 and its position in bulk LRMO.

RIXS provides information regarding the intrinsic excitation of materials by detecting the energy and momentum differences of scattered photons. It is mostly used to study the conduction band, valence band and low-energy excited state, as well as the electronic structure of the electronic transition and charge transfer information. Xu *et al.*[204] used RIXS technology to reveal the attenuation information of soft XAS excitation energy, which provided higher sensitivity and clarity for defining the chemical state of oxygen and explained the charge compensation mechanism of the TMs in two compounds ($Li_{1.2}Ni_{0.2}Mn_{0.6}O_2$ and $Li_{1.2}Ni_{0.2}Ru_{0.6}O_2$). Simultaneously, Zhang *et al.*[205] applied RIXS to find that O^{-1} was formed in the subsurface transition layer of the material when charged to a high voltage [Figure 16E]. The irreversible loss of oxygen during the charging process decreases the valence of the TM cations and leave the oxygen vacancies around simultaneously, explaining why the valence state of TMs in the LRMO is different from the traditional NCM material. Dai *et al.*[206] distinguished the redox process of lattice oxygen and TM through mRIXS, quantified the contribution of lattice oxygen redox reaction to electrochemical capacity and revealed the inner behavior of oxygen redox in LRMOs.

Hard X-ray photoelectron spectroscopy (HAX-PES) uses high-energy hard X-rays as the excitation source (such as Cr K_α, energy 5414.9 eV, or a synchrotron radiation source), which can obtain several times the depth of conventional XPS analysis. The chemical information greatly reduces the interference from the surface contamination layer and can analyze the material interface layer non-destructively. It is a very important characterization method for the surface/interface chemical analysis of solid materials. Shimoda *et al.*[207] studied the oxidation/reduction behavior of lattice oxygen and TMs in $Li[Li_{0.25}Ni_{0.2}Mn_{0.55}]O_{1.93}$ using HAX-PES [Figure 16F], which clearly confirmed the formation of a large amount of oxygen species in the active material. Assat *et al.*[208] used HAX-PES to directly track the changes in the lattice oxygen electronic state and quantified the reversibility of oxygen redox to show its long-term cycling durability in the LRMO.

SUMMARY AND OUTLOOK

Anion charge compensation contributes to the ultra-high specific capacity and energy density of LRMOs; however, it is accompanied by problems, such as capacity attenuation and voltage decay, derived from complex and rapid phase structural evolution. It is also noteworthy that the intrinsic initial Coulombic efficiency and sluggish electrochemical dynamics cannot be ignored. In the past two decades, researchers have devoted significant efforts to studying the key scientific issues behind these problems, as well as to

improving electrochemical performance through various optimization methods, with impressive progress having been made. However, there are still a series of challenges hindering the further development and commercialization of LRMOs:

(1) Current detection methods are still unable to *in-situ* non-destructively monitor the evolution of materials at the electronic/atomic scale during charge and discharge. It is necessary to develop deeper and more accurate detection methods to obtain clearer structural information and verify the results of theoretical simulations. More importantly, powerful and versatile characterization methods need to be developed.

(2) The modified results of the materials are varied, although the electrochemical performance of some materials has improved significantly, the performance of the contrast samples may be very poor.

(3) Although O2-type lithium-rich materials can significantly inhibit the voltage attenuation caused by TM migration and exhibit ultra-high specific capacity, the preparation method of molten salt ion exchange is cumbersome and costly and is therefore difficult to realize practical applications.

(4) Components, such as electrolytes, binders and conductive agents, compatible with LRMOs still need to improve their high-voltage tolerance and coordination.

For pristine LRMOs, the Li/O and the ratio between TM ions should be adjusted, the advantages and defects of each chemical ratio of the material should be clarified clearly. Through electrochemical regulation of voltage and current, select suitable materials to meet the needs of different working conditions. For modification methods, such as doping and coating, it is necessary to focus on the uniformity and consistency of the modified material and eliminate the interference of human factors and randomness during the characterization process. The regulation of highly active near-surface structure should be emphatically considered. The $LiMn_6$ honeycomb superstructure triggers anion charge compensation and voltage hysteresis, so it is necessary to seek effective element substitution or structural adjustment (such as ribbon-like and mesh-like superstructures)[209,210] to achieve stable superstructure and reversible oxygen redox. For the voltage attenuation caused by the irreversible migration of TM to the Li layer, it is vital to focus on suppressing the migration of TM from the transitional state tetrahedral position to the final state octahedral Li vacancy. The O2 type structure is a good choice, but the preparation method still needs to be improved. Other oxygen stacking design[128,211] (such as T*2/O4/O6 type, stacking fault and so on) are also worthy of discussion. For other components, such as electrolyte and binder, functional design is required to stabilize the interface of lithium-rich materials and suppress battery flatulence and safety hazards caused by oxygen release.

Energy density is an eternal goal and the development of commercial cathode materials has been relatively slow. As the embedded cathode materials for LIBs with the highest energy density at present, LRMOs are the most promising next-generation cathode materials for popularization and application in the near future. Compared with NCM materials, LRMOs exhibit considerable advantages in cost and thermal stability but with similar preparation method and equipment. Practical applications can be attempted under the conditions of high energy density and less cycle number requirements. Of course, safety issues caused by high voltage and oxygen release should be considered. The unique oxygen charge compensation mechanism has opened a new field for the realization of high energy density LIBs. It can also provide a reference for other alkali ion batteries, such as Na^+/K^+ and even Li-S, Li-O_2 and other energy storage systems with anion charge compensation. Promoting continuous development of LIBs and even electrochemical energy devices

requires constant efforts and exploration from scientific researchers.

DECLARATIONS

Authors' contributions

Investigation, writing-original draft, review & editing: Yang Z
Investigation: Zheng C, Wei Z, Liu H, Feng J
Language check: Zhong J
Supervision funding supporting: Li J
Supervision: Kang F

Availability of data and materials

Not applicable.

Financial support and sponsorship

This work is financially supported by the National Natural Science Foundation of China (Grants 51972023).

Conflicts of interest

All authors declared that there are no conflicts of interest.

Ethical approval and consent to participate

Not applicable.

Consent for publication

Not applicable.

REFERENCES

1. Choi C, Ashby DS, Butts DM, et al. Achieving high energy density and high power density with pseudocapacitive materials. *Nat Rev Mater* 2020;5:5-19. DOI
2. Nitta N, Wu F, Lee JT, Yushin G. Li-ion battery materials: present and future. *Mater Today* 2015;18:252-64. DOI
3. Winter M, Barnett B, Xu K. Before Li ion batteries. *Chem Rev* 2018;118:11433-56. DOI PubMed
4. Liu C, Neale ZG, Cao G. Understanding electrochemical potentials of cathode materials in rechargeable batteries. *Mater Today* 2016;19:109-23. DOI
5. Assat G, Tarascon J. Fundamental understanding and practical challenges of anionic redox activity in Li-ion batteries. *Nat Energy* 2018;3:373-86. DOI
6. Moghadam Y, Masoudpanah S, Alamolhoda S, Daneshtalab R. Electrochemical properties of $LiMn_{1.5}Ni_{0.5}O_4$ powders synthesized by solution combustion method: Effect of CTAB as a fuel. *Advanced Powder Technology* 2020;31:639-44. DOI
7. Moghadam Y, El Kharbachi A, Diemant T, Melinte G, Hu Y, Fichtner M. Toward better stability and reversibility of the Mn^{4+}/Mn^{2+} double redox activity in disordered rocksalt oxyfluoride cathode materials. *Chem Mater* 2021;33:8235-47. DOI
8. Hu S, Pillai AS, Liang G, et al. Li-rich layered oxides and their practical challenges: recent progress and perspectives. *Electrochem Energ Rev* 2019;2:277-311. DOI
9. Thackeray MM, Kang S, Johnson CS, Vaughey JT, Benedek R, Hackney SA. Li_2MnO_3-stabilized $LiMO_2$ (M = Mn, Ni, Co) electrodes for lithium-ion batteries. *J Mater Chem* 2007;17:3112. DOI
10. Sathiya M, Rousse G, Ramesha K, et al. Reversible anionic redox chemistry in high-capacity layered-oxide electrodes. *Nat Mater* 2013;12:827-35. DOI PubMed
11. McCalla E, Abakumov AM, Saubanère M, et al. Visualization of O-O peroxo-like dimers in high-capacity layered oxides for Li-ion batteries. *Science* 2015;350:1516-21. DOI PubMed
12. Zhou YN, Ma J, Hu E, et al. Tuning charge-discharge induced unit cell breathing in layer-structured cathode materials for lithium-ion batteries. *Nat Commun* 2014;5:5381. DOI PubMed
13. Li B, Jiang N, Huang W, Yan H, Zuo Y, Xia D. Thermodynamic Activation of charge transfer in anionic redox process for Li-Ion batteries. *Adv Funct Mater* 2018;28:1704864. DOI
14. House RA, Marie J, Pérez-osorio MA, Rees GJ, Boivin E, Bruce PG. The role of O_2 in O-redox cathodes for Li-ion batteries. *Nat*

Energy 2021;6:781-9. DOI

15. Hu E, Yu X, Lin R, et al. Evolution of redox couples in Li- and Mn-rich cathode materials and mitigation of voltage fade by reducing oxygen release. *Nat Energy* 2018;3:690-8. DOI
16. Lei Y, Ni J, Hu Z, et al. Surface modification of Li-rich Mn-based layered oxide cathodes: challenges, materials, methods, and characterization. *Adv Energy Mater* 2020;10:2002506. DOI
17. Sun Z, Xu L, Dong C, et al. Enhanced cycling stability of boron-doped lithium-rich layered oxide cathode materials by suppressing transition metal migration. *J Mater Chem A* 2019;7:3375-83. DOI
18. Chen L, Su Y, Chen S, et al. Hierarchical $Li_{1.2}Ni_{0.2}Mn_{0.6}O_2$ nanoplates with exposed {010} planes as high-performance cathode material for lithium-ion batteries. *Adv Mater* 2014;26:6756-60. DOI PubMed
19. Sun G, Yu F, Que L, et al. Local electronic structure modulation enhances operating voltage in Li-rich cathodes. *Nano Energy* 2019;66:104102. DOI
20. Hwang J, Myeong S, Lee E, et al. Lattice-oxygen-stabilized Li- and Mn-rich cathodes with sub-micrometer particles by modifying the excess-Li distribution. *Adv Mater* 2021;33:e2100352. DOI PubMed
21. Liu W, Li J, Li W, Xu H, Zhang C, Qiu X. Inhibition of transition metals dissolution in cobalt-free cathode with ultrathin robust interphase in concentrated electrolyte. *Nat Commun* 2020;11:3629. DOI PubMed PMC
22. Ji X, Xia Q, Xu Y, Feng H, Wang P, Tan Q. A review on progress of lithium-rich manganese-based cathodes for lithium ion batteries. *J Power Sources* 2021;487:229362. DOI
23. Cui S, Gao M, Li G, Gao X. Insights into Li-rich Mn-based cathode materials with high capacity: from dimension to lattice to atom. *Adv Energy Mater* 2022;12:2003885. DOI
24. He W, Guo W, Wu H, et al. Challenges and recent advances in high capacity Li-rich cathode materials for high energy density lithium-ion batteries. *Adv Mater* 2021;33:e2005937. DOI PubMed
25. Seo DH, Lee J, Urban A, Malik R, Kang S, Ceder G. The structural and chemical origin of the oxygen redox activity in layered and cation-disordered Li-excess cathode materials. *Nat Chem* 2016;8:692-7. DOI PubMed
26. Wang Q, Mariyappan S, Rousse G, et al. Unlocking anionic redox activity in O_3-type sodium 3d layered oxides via Li substitution. *Nat Mater* 2021;20:353-61. DOI PubMed
27. Song J, Yoon G, Kim B, et al. Anionic redox activity regulated by transition metal in lithium-rich layered oxides. *Adv Energy Mater*. DOI
28. Zhuo Z, Dai K, Wu J, et al. Distinct oxygen redox activities in Li_2MO_3 (M = Mn, Ru, Ir). *ACS Energy Lett* 2021;6:3417-24. DOI
29. Hong J, Gent WE, Xiao P, et al. Metal-oxygen decoordination stabilizes anion redox in Li-rich oxides. *Nat Mater* 2019;18:256-65. DOI PubMed
30. Zhang K, Jiang Z, Ning F, et al. Metal-ligand π interactions in lithium-rich Li_2RhO_3 cathode material activate bimodal anionic redox. *Adv Energy Mater* 2021;11:2100892. DOI
31. Yu Z, Qu X, Dou A, Su M, Liu Y, Wu F. Synthesis and redox mechanism of cation-disordered, rock-salt cathode-material Li-Ni-Ti-Nb-O compounds for a Li-Ion battery. *ACS Appl Mater Interfaces* 2019;11:35777-87. DOI PubMed
32. Xie Y, Saubanère M, Doublet M. Requirements for reversible extra-capacity in Li-rich layered oxides for Li-ion batteries. *Energy Environ Sci* 2017;10:266-74. DOI
33. Ouyang C, Shi S, Lei M. Jahn-Teller distortion and electronic structure of $LiMn_2O4$. *J Alloys Compd* 2009;474:370-4. DOI
34. Liu S, Wang B, Zhang X, Zhao S, Zhang Z, Yu H. Reviving the lithium-manganese-based layered oxide cathodes for lithium-ion batteries. *Matter* 2021;4:1511-27. DOI
35. Jarvis KA, Deng Z, Allard LF, Manthiram A, Ferreira PJ. Atomic structure of a lithium-rich layered oxide material for lithium-ion batteries: evidence of a solid solution. *Chem Mater* 2011;23:3614-21. DOI
36. Yu X, Lyu Y, Gu L, et al. Understanding the rate capability of high-energy-density Li-rich layered $Li_{1.2}Ni_{0.15}Co_{0.1}Mn_{0.55}O_2$ cathode materials. *Adv Energy Mater* 2014;4:1300950. DOI
37. Yu H, Ishikawa R, So YG, et al. Direct atomic-resolution observation of two phases in the Li(1.2)Mn(0.567)Ni(0.166)Co(0.067)O2 cathode material for lithium-ion batteries. *Angew Chem Int Ed Engl* 2013;52:5969-73. DOI PubMed
38. Xiao L, Xiao J, Yu X, et al. Effects of structural defects on the electrochemical activation of Li_2MnO_3. *Nano Energy* 2015;16:143-51. DOI
39. Sun Y, Cong H, Zan L, Zhang Y. Oxygen vacancies and stacking faults introduced by low-temperature reduction improve the electrochemical properties of Li_2MnO_3 nanobelts as lithium-ion battery cathodes. *ACS Appl Mater Interfaces* 2017;9:38545-55. DOI PubMed
40. Shunmugasundaram R, Arumugam RS, Dahn JR. A study of stacking faults and superlattice ordering in some Li-rich layered transition metal oxide positive electrode materials. *J Electrochem Soc* 2016;163:A1394-400. DOI
41. House RA, Rees GJ, Pérez-osorio MA, et al. First-cycle voltage hysteresis in Li-rich 3d cathodes associated with molecular O_2 trapped in the bulk. *Nat Energy* 2020;5:777-85. DOI
42. Zhuo H, Liu Y, Wang Z, et al. Insight of reaction mechanism and anionic redox behavior for Li-rich and Mn-based oxide materials from local structure. *Nano Energy* 2021;83:105812. DOI
43. Zhang J, Cheng F, Chou S, et al. Tuning oxygen redox chemistry in Li-rich Mn-based layered oxide cathodes by modulating cation arrangement. *Adv Mater* 2019;31:e1901808. DOI PubMed
44. Song J, Li B, Chen Y, et al. A high-performance Li-Mn-O Li-rich cathode material with rhombohedral symmetry via intralayer Li/Mn disordering. *Adv Mater* 2020;32:e2000190. DOI PubMed
45. Ning F, Li B, Song J, et al. Inhibition of oxygen dimerization by local symmetry tuning in Li-rich layered oxides for improved

stability. *Nat Commun* 2020;11:4973. DOI PubMed PMC

46. Li X, Qiao Y, Guo S, Jiang K, Ishida M, Zhou H. A new type of Li-rich rock-salt oxide $Li_2Ni_{1/3}Ru_{2/3}O_3$ with reversible anionic redox chemistry. *Adv Mater* 2019;31:e1807825. DOI
47. Liu S, Liu Z, Shen X, et al. Li-Ti cation mixing enhanced structural and performance stability of Li-rich layered oxide. *Adv Energy Mater* 2019;9:1901530. DOI
48. Li N, Sun M, Kan WH, et al. Layered-rocksalt intergrown cathode for high-capacity zero-strain battery operation. *Nat Commun* 2021;12:2348. DOI PubMed PMC
49. Zhao E, Li Q, Meng F, et al. Stabilizing the oxygen lattice and reversible oxygen redox chemistry through structural dimensionality in lithium-rich cathode oxides. *Angew Chem Int Ed Engl* 2019;58:4323-7. DOI PubMed
50. Lee J, Yang Y, Jeong M, et al. Superior rate capability and cycling stability in partially cation-disordered co-free Li-rich layered materials enabled by an initial activation process. *Chem Mater* 2021;33:5115-26. DOI
51. Liang C, Kong F, Longo RC, et al. Unraveling the origin of instability in Ni-rich $LiNi_{1-2x}Co_xMn_xO_2$ (NCM) cathode materials. *J Phys Chem C* 2016;120:6383-93. DOI
52. Zheng J, Gu M, Genc A, et al. Mitigating voltage fade in cathode materials by improving the atomic level uniformity of elemental distribution. *Nano Lett* 2014;14:2628-35. DOI PubMed
53. Liu Q, Zhu H, Liu J, et al. High-performance lithium-rich layered oxide material: effects of preparation methods on microstructure and electrochemical properties. *Materials (Basel)* 2020;13:334. DOI PubMed PMC
54. Wu T, Liu X, Zhang X, et al. Full concentration gradient-tailored Li-rich layered oxides for high-energy lithium-ion batteries. *Adv Mater* 2021;33:e2001358. DOI PubMed
55. Toney MF. Li gradients for Li-rich cathodes. *Nat Energy* 2019;4:1014-5. DOI
56. Xu CL, Xiang W, Wu ZG, et al. Constructing a protective pillaring layer by incorporating gradient Mn^{4+} to stabilize the surface/interfacial structure of $LiNi_{0.815}Co_{0.15}Al_{0.035}O_2$ cathode. *ACS Appl Mater Interfaces* 2018;10:27821-30. DOI PubMed
57. Zhu Z, Yu D, Yang Y, et al. Gradient Li-rich oxide cathode particles immunized against oxygen release by a molten salt treatment. *Nat Energy* 2019;4:1049-58. DOI
58. Yang J, Xia Y. Suppressing the phase transition of the layered Ni-rich oxide cathode during high-voltage cycling by introducing low-content Li_2MnO_3. *ACS Appl Mater Interfaces* 2016;8:1297-308. DOI PubMed
59. Song Y, Zhao X, Wang C, et al. Insight into the atomic structure of Li_2MnO_3 in Li-rich Mn-based cathode materials and the impact of its atomic arrangement on electrochemical performance. *J Mater Chem A* 2017;5:11214-23. DOI
60. Liu J, Liu J, Wang R, Xia Y. Degradation and structural evolution of $xLi_2MnO_3 \cdot (1-x)LiMn_{1/3}Ni_{1/3}Co_{1/3}O_2$ during cycling. *J Electrochem Soc* 2013;161:A160-7. DOI
61. Shi JL, Xiao DD, Ge M, et al. High-capacity cathode material with high voltage for Li-ion batteries. *Adv Mater* 2018;30:1705575. DOI PubMed
62. Shen S, Hong Y, Zhu F, et al. Tuning electrochemical properties of Li-rich layered oxide cathodes by adjusting Co/Ni ratios and mechanism investigation using in situ X-ray diffraction and online continuous flow differential electrochemical mass spectrometry. *ACS Appl Mater Interfaces* 2018;10:12666-77. DOI PubMed
63. Hua W, Wang S, Knapp M, et al. Structural insights into the formation and voltage degradation of lithium- and manganese-rich layered oxides. *Nat Commun* 2019;10:5365. DOI PubMed PMC
64. Sun G, Yu FD, Zhao C, et al. Decoupling the voltage hysteresis of Li-rich cathodes: electrochemical monitoring, modulation anionic redox chemistry and theoretical verifying. *Adv Funct Mater* 2020;31:2002643. DOI
65. Zhou Y, Cui H, Qiu B, et al. Sufficient oxygen redox activation against voltage decay in Li-rich layered oxide cathode materials. *ACS Materials Lett* 2021;3:433-41. DOI
66. Wu F, Tian J, Su Y, et al. Effect of Ni(2+) content on lithium/nickel disorder for Ni-rich cathode materials. *ACS Appl Mater Interfaces* 2015;7:7702-8. DOI PubMed
67. Ji H, Wu J, Cai Z, et al. Ultrahigh power and energy density in partially ordered lithium-ion cathode materials. *Nat Energy* 2020;5:213-21. DOI
68. Boivin E, Guerrini N, House RA, et al. The role of Ni and Co in suppressing O-loss in Li-rich layered cathodes. *Adv Funct Mater* 2021;31:2003660. DOI
69. Huang W, Lin C, Zhang M, et al. Revealing roles of Co and Ni in Mn-rich layered cathodes. *Adv Energy Mater* 2021;11:2102646. DOI
70. Xiang X, Knight JC, Li W, Manthiram A. Understanding the effect of Co^{3+} substitution on the electrochemical properties of lithium-rich layered oxide cathodes for lithium-ion batteries. *J Phys Chem C* 2014;118:21826-33. DOI
71. Yin C, Wan L, Qiu B, et al. Boosting energy efficiency of Li-rich layered oxide cathodes by tuning oxygen redox kinetics and reversibility. *Energy Storage Mater* 2021;35:388-99. DOI
72. Okubo M, Mizuno Y, Yamada H, et al. Fast Li-Ion insertion into nanosized LiMn(2)O(4) without domain boundaries. *ACS Nano* 2010;4:741-52. DOI PubMed
73. Peng H, Zhao SX, Huang C, Yu LQ, Fang ZQ, Wei GD. In situ construction of spinel coating on the surface of a lithium-rich manganese-based single crystal for inhibiting voltage fade. *ACS Appl Mater Interfaces* 2020;12:11579-88. DOI PubMed
74. Su Y, Chen G, Chen L, et al. Exposing the {010} planes by oriented self-assembly with nanosheets to improve the electrochemical performances of Ni-rich $Li[Ni_{0.8}Co_{0.1}Mn_{0.1}]O_2$ microspheres. *ACS Appl Mater Interfaces* 2018;10:6407-14. DOI PubMed
75. Wei GZ, Lu X, Ke FS, et al. Crystal habit-tuned nanoplate material of $Li[Li_{1/3-2x/3}Ni_xMn_{2/3-x/3}]O_2$ for high-rate performance lithium-ion batteries. *Adv Mater* 2010;22:4364-7. DOI

76. Liu Y, Wang J, Wu J, et al. 3D cube-maze-like Li-rich layered cathodes assembled from 2D porous nanosheets for enhanced cycle stability and rate capability of lithium-ion batteries. *Adv Energy Mater* 2019;10:1903139. DOI
77. Shi S, Wang T, Cao M, Wang J, Zhao M, Yang G. Rapid self-assembly spherical $Li_{1.2}Mn_{0.56}Ni_{0.16}Co_{0.08}O_2$ with improved performances by microwave hydrothermal method as cathode for lithium-ion batteries. *ACS Appl Mater Interfaces* 2016;8:11476-87. DOI PubMed
78. Trevisanello E, Ruess R, Conforto G, Richter FH, Janek J. Polycrystalline and single crystalline NCM cathode materials-quantifying particle cracking, active surface area, and lithium diffusion. *Adv Energy Mater* 2021;11:2003400. DOI
79. Xu X, Huo H, Jian J, et al. Radially oriented single-crystal primary nanosheets enable ultrahigh rate and cycling properties of $LiNi_{0.8}Co_{0.1}Mn_{0.1}O_2$ cathode material for lithium-ion batteries. *Adv Energy Mater* 2019;9:1803963. DOI
80. Csernica PM, Kalirai SS, Gent WE, et al. Persistent and partially mobile oxygen vacancies in Li-rich layered oxides. *Nat Energy* 2021;6:642-52. DOI
81. Koga H, Croguennec L, Ménétrier M, et al. Operando X-ray absorption study of the redox processes involved upon cycling of the Li-rich layered oxide $L_{1.20}Mn_{0.54}Co_{0.13}Ni_{0.13}O_2$ in Li ion batteries. *J Phys Chem C* 2014;118:5700-9. DOI
82. Nakayama K, Ishikawa R, Kobayashi S, Shibata N, Ikuhara Y. Dislocation and oxygen-release driven delithiation in Li_2MnO_3. *Nat Commun* 2020;11:4452. DOI PubMed PMC
83. Luo K, Roberts MR, Hao R, et al. Charge-compensation in 3d-transition-metal-oxide intercalation cathodes through the generation of localized electron holes on oxygen. *Nat Chem* 2016;8:684-91. DOI PubMed
84. Yabuuchi N, Yoshii K, Myung ST, Nakai I, Komaba S. Detailed studies of a high-capacity electrode material for rechargeable batteries, Li_2MnO_3-LiCo(1/3)Ni(1/3)Mn(1/3)O2. *J Am Chem Soc* 2011;133:4404-19. DOI PubMed
85. Strehle B, Kleiner K, Jung R, et al. The role of oxygen release from Li- and Mn-rich layered oxides during the first cycles investigated by on-line electrochemical mass spectrometry. *J Electrochem Soc* 2016;164:A400-6. DOI
86. Tang M, Dalzini A, Li X, et al. Operando EPR for Simultaneous monitoring of anionic and cationic redox processes in Li-rich metal oxide cathodes. *J Phys Chem Lett* 2017;8:4009-16. DOI PubMed
87. Li X, Qiao Y, Guo S, et al. Direct visualization of the reversible O^{2-}/O^- redox process in Li-rich cathode materials. *Adv Mater* 2018;30:e1705197. DOI PubMed
88. Gent WE, Lim K, Liang Y, et al. Coupling between oxygen redox and cation migration explains unusual electrochemistry in lithium-rich layered oxides. *Nat Commun* 2017;8:2091. DOI PubMed PMC
89. Liu H, Chen Y, Hy S, et al. Operando lithium dynamics in the Li-rich layered oxide cathode material via neutron diffraction. *Adv Energy Mater* 2016;6:1502143. DOI
90. Mohanty D, Sefat AS, Kalnaus S, et al. Investigating phase transformation in the $Li_{1.2}Co_{0.1}Mn_{0.55}Ni_{0.15}O_2$ lithium-ion battery cathode during high-voltage hold (4.5 V) via magnetic, X-ray diffraction and electron microscopy studies. *J Mater Chem A* 2013;1:6249. DOI
91. Xu B, Fell CR, Chi M, Meng YS. Identifying surface structural changes in layered Li-excess nickel manganese oxides in high voltage lithium ion batteries: a joint experimental and theoretical study. *Energy Environ Sci* 2011;4:2223. DOI
92. Gao Y, Ma J, Wang Z, Lu G, Chen L. Vacancy-induced MnO_6 distortion and its impacts on structural transition of Li_2MnO_3. *Phys Chem Chem Phys* 2017;19:7025-31. DOI PubMed
93. Yu H, So YG, Ren Y, et al. Temperature-sensitive structure evolution of lithium-manganese-rich layered oxides for lithium-ion batteries. *J Am Chem Soc* 2018;140:15279-89. DOI PubMed
94. Radin MD, Vinckeviciute J, Seshadri R, Van der Ven A. Manganese oxidation as the origin of the anomalous capacity of Mn-containing Li-excess cathode materials. *Nat Energy* 2019;4:639-46. DOI
95. Kleiner K, Strehle B, Baker AR, et al. Origin of high capacity and poor cycling stability of Li-rich layered oxides: a long-duration in situ synchrotron powder diffraction study. *Chem Mater* 2018;30:3656-67. DOI
96. Cao S, Wu C, Xie X, et al. Suppressing the voltage decay based on a distinct stacking sequence of oxygen atoms for Li-rich cathode materials. *ACS Appl Mater Interfaces* 2021;13:17639-48. DOI PubMed
97. Zuo Y, Li B, Jiang N, et al. A high-capacity O_2-type Li-rich cathode material with a single-layer Li_2MnO_3 superstructure. *Adv Mater* 2018;30:e1707255. DOI
98. Eum D, Kim B, Kim SJ, et al. Voltage decay and redox asymmetry mitigation by reversible cation migration in lithium-rich layered oxide electrodes. *Nat Mater* 2020;19:419-27. DOI PubMed
99. Ma J, Zhou Y, Gao Y, et al. Feasibility of using Li_2MoO_3 in constructing Li-rich high energy density cathode materials. *Chem Mater* 2014;26:3256-62. DOI
100. Grenier A, Kamm GE, Li Y, Chung H, Meng YS, Chapman KW. Nanostructure transformation as a signature of oxygen redox in Li-rich 3d and 4d cathodes. *J Am Chem Soc* 2021;143:5763-70. DOI PubMed
101. Yan P, Zheng J, Tang ZK, et al. Injection of oxygen vacancies in the bulk lattice of layered cathodes. *Nat Nanotechnol* 2019;14:602-8. DOI PubMed
102. Lin R, Hu E, Liu M, et al. Anomalous metal segregation in lithium-rich material provides design rules for stable cathode in lithium-ion battery. *Nat Commun* 2019;10:1650. DOI PubMed PMC
103. Lee S, Jin W, Kim SH, et al. Oxygen vacancy diffusion and condensation in lithium-ion battery cathode materials. *Angew Chem Int Ed Engl* 2019;58:10478-85. DOI PubMed
104. Xiao B, Liu H, Chen N, et al. Size-mediated recurring spinel sub-nanodomains in Li- and Mn-rich layered cathode materials. *Angew Chem Int Ed Engl* 2020;59:14313-20. DOI PubMed
105. Zheng J, Xu P, Gu M, et al. Structural and chemical evolution of Li- and Mn-rich layered cathode material. *Chem Mater*

2015;27:1381-90. DOI

106. Zheng J, Ye Y, Liu T, et al. Ni/Li disordering in layered transition metal oxide: electrochemical impact, origin, and control. *Acc Chem Res* 2019;52:2201-9. DOI PubMed
107. Liu P, Zhang H, He W, et al. Lithium deficiencies engineering in Li-rich layered oxide $Li_{1.098}Mn_{0.533}Ni_{0.113}Co_{0.138}O_2$ for high-stability cathode. *J Am Chem Soc* 2019;141:10876-82. DOI PubMed
108. Yang M, Jin J, Shen Y, Sun S, Zhao X, Shen X. Cation-disordered lithium-excess Li-Fe-Ti oxide cathode materials for enhanced Li-ion storage. *ACS Appl Mater Interfaces* 2019;11:44144-52. DOI PubMed
109. Huang J, Zhong P, Ha Y, et al. Non-topotactic reactions enable high rate capability in Li-rich cathode materials. *Nat Energy* 2021;6:706-14. DOI
110. Yang Z, Zhong J, Liu Y, Li Z, Li J, Yang K. Unveiling the effect of voltage regulation system on the structure and electrochemical properties of lithium-rich cathode materials. *J Electrochem Soc* 2019;166:A1481-9. DOI
111. Nayak PK, Grinblat J, Levi M, Aurbach D. Electrochemical and structural characterization of carbon coated $Li_{1.2}Mn_{0.56}Ni_{0.16}Co_{0.08}O_2$ and $Li_{1.2}Mn_{0.6}Ni_{0.2}O2$ as cathode materials for Li-ion batteries. *Electrochimica Acta* 2014;137:546-56. DOI
112. Li N, Wu J, Hwang S, et al. Enabling facile anionic kinetics through cationic redox mediator in Li-rich layered cathodes. *ACS Energy Lett* 2020;5:3535-43. DOI
113. Saha S, Assat G, Sougrati MT, et al. Exploring the bottlenecks of anionic redox in Li-rich layered sulfides. *Nat Energy* 2019;4:977-87. DOI
114. Hou P, Li F, Sun Y, Li H, Xu X, Zhai T. Multishell precursors facilitated synthesis of concentration-gradient nickel-rich cathodes for long-life and high-rate lithium-ion batteries. *ACS Appl Mater Interfaces* 2018;10:24508-15. DOI PubMed
115. Sun YK, Myung ST, Park BC, Prakash J, Belharouak I, Amine K. High-energy cathode material for long-life and safe lithium batteries. *Nat Mater* 2009;8:320-4. DOI PubMed
116. Koga H, Croguennec L, Ménétrier M, Mannessiez P, Weill F, Delmas C. Different oxygen redox participation for bulk and surface: a possible global explanation for the cycling mechanism of $Li_{1.20}Mn_{0.54}Co_{0.13}Ni_{0.13}O_2$. *J Power Sources* 2013;236:250-8. DOI
117. Nie L, Liang C, Chen S, et al. Improved electrochemical performance of Li-rich layered oxide cathodes enabled by a two-step heat treatment. *ACS Appl Mater Interfaces* 2021;13:13281-8. DOI PubMed
118. Liu J, Chen H, Xie J, Sun Z, Wu N, Wu B. Electrochemical performance studies of Li-rich cathode materials with different primary particle sizes. *J Power Sources* 2014;251:208-14. DOI
119. Liu Y, Zhuo H, Yin Y, Lu S, Wang Z, Zhuang W. Remaining Li-content dependent structural evolution during high temperature re-heat treatment of quantitatively delithiated Li-rich cathode materials with surface defect-spinel phase. *ACS Appl Mater Interfaces* 2020;12:27226-40. DOI PubMed
120. Cui SL, Zhang X, Wu XW, et al. Understanding the structure-performance relationship of lithium-rich cathode materials from an oxygen-vacancy perspective. *ACS Appl Mater Interfaces* 2020;12:47655-66. DOI PubMed
121. Li Y, Feng X, Cui S, Shi Q, Mi L, Chen W. From α-$NaMnO_2$ to crystal water containing Na-birnessite: enhanced cycling stability for sodium-ion batteries. *CrystEngComm* 2016;18:3136-41. DOI
122. Liu Y, Chen Y, Wang J, et al. Hierarchical yolk-shell structured Li-rich cathode boosting cycling and voltage stabled LIBs. *Nano Res* 2021. DOI
123. Xu M, Fei L, Zhang W, et al. Tailoring anisotropic Li-ion transport tunnels on orthogonally arranged Li-rich layered oxide nanoplates toward high-performance Li-ion batteries. *Nano Lett* 2017;17:1670-7. DOI PubMed
124. Yabuuchi N, Hara R, Kajiyama M, et al. New O_2/P_2-type Li-excess layered manganese oxides as promising multi-functional electrode materials for rechargeable Li/Na batteries. *Adv Energy Mater* 2014;4:1301453. DOI
125. Heubner C, Matthey B, Lein T, et al. Insights into the electrochemical Li/Na-exchange in layered $LiCoO_2$ cathode material. *Energy Storage Mater* 2020;27:377-86. DOI
126. Shang H, Zuo Y, Shen F, et al. O_2-type $Li_{0.78}[Li_{0.24}Mn_{0.76}]O_2$ nanowires for high-performance lithium-ion battery cathode. *Nano Lett* 2020;20:5779-85. DOI PubMed
127. Yang Z, Zhong J, Feng J, Li J, Kang F. Highly reversible anion redox of manganese-based cathode material realized by electrochemical ion exchange for lithium-ion batteries. *Adv Funct Materials* 2021;31:2103594. DOI
128. Paulsen JM, Thomas CL, Dahn JR. Layered Li-Mn-oxide with the O_2 structure: a cathode material for Li-ion cells which does not convert to spinel. *J Electrochem Soc* 1999;146:3560-5. DOI
129. Robertson AD, Armstrong AR, Bruce PG. Layered $Li_xMn_{1-y}Co_yO_2$ intercalation electrodes influence of ion exchange on capacity and structure upon cycling. *Chem Mater* 2001;13:2380-6. DOI
130. Liu S, Zhu H, Zhang B, et al. Tuning the kinetics of zinc-ion insertion/extraction in V_2O_5 by in situ polyaniline intercalation enables improved aqueous zinc-ion storage performance. *Adv Mater* 2020;32:e2001113. DOI PubMed
131. Yi T, Han X, Yang S, Zhu Y. Enhanced electrochemical performance of Li-rich low-Co $Li_{1.2}Mn_{0.56}Ni_{0.16}Co_{0.08-x}Al_xO_2$ ($0 \leq x \leq 0.08$) as cathode materials. *Sci China Mater* 2016;59:618-28. DOI
132. Zhu J, Xiao G, Li X. Synthesis of $Li(Ni_{0.6}Co_{0.2}Mn_{0.2})O_2$ by a modified sol-gel method for lithium-ion batteries. *Synthetic Metals* 2021;281:116905. DOI
133. Xu G, Li J, Li X, et al. Understanding the electrochemical superiority of $0.6Li[Li_{1/3}Mn_{2/3}]O_2$-$0.4Li[Ni_{1/3}Co_{1/3}Mn_{1/3}]O_2$ nanofibers as cathode material for lithium ion batteries. *Electrochimica Acta* 2015;173:672-9. DOI
134. Yu R, Zhang Z, Jamil S, et al. Effects of nanofiber architecture and antimony doping on the performance of lithium-rich layered oxides: enhancing lithium diffusivity and lattice oxygen stability. *ACS Appl Mater Interfaces* 2018;10:16561-71. DOI PubMed
135. Zhou H, Ding X, Liu G, Gao Z, Xu G, Wang X. Characterization of cathode from $LiNi_xMn_{2-x}O_4$ nanofibers by electrospinning for Li-

ion batteries. *RSC Adv* 2015;5:108007-14. DOI

136. Ding X, Zhou H, Liu G, Yin Z, Jiang Y, Wang X. Electrochemical evaluation of $LiAl_{0.05}Ni_{0.05}Mn_{1.9}O_4$ cathode material synthesized via electrospinning method. *J Alloys Compd* 2015;632:147-51. DOI
137. Zhou H, Ding X, Liu G, Jiang Y, Yin Z, Wang X. Preparation and characterization of ultralong spinel lithium manganese oxide nanofiber cathode via electrospinning method. *Electrochimica Acta* 2015;152:274-9. DOI
138. Xu G, Li J, Li X, et al. The formation and electrochemical property of lithium-excess cathode material $Li_{1.2}Ni_{0.13}Co_{0.13}Mn_{0.54}O_2$ with petal-like nanoplate microstructure. *Ionics* 2017;23:2285-91. DOI
139. Liu H, Lei W, Tong Z, et al. Enhanced diffusion kinetics of Li ions in double-shell hollow carbon fibers. *ACS Appl Mater Interfaces* 2021;13:24604-14. DOI PubMed
140. Zhou X, Wang F, Zhu Y, Liu Z. Graphene modified $LiFePO_4$ cathode materials for high power lithium ion batteries. *J Mater Chem* 2011;21:3353. DOI
141. Watanabe A, Matsumoto F, Fukunishi M, et al. Relationship between electrochemical pre-treatment and cycle performance of a Li-rich solid-solution layered $Li_{1-\alpha}[Ni_{0.18}Li_{0.20+\alpha}Co_{0.03}Mn_{0.58}]O_2$ cathode for Li-ion secondary batteries. *Electrochemistry* 2012;80:561-5. DOI
142. Ito A, Li D, Ohsawa Y, Sato Y. A new approach to improve the high-voltage cyclic performance of Li-rich layered cathode material by electrochemical pre-treatment. *J Power Sources* 2008;183:344-6. DOI
143. Ito A, Li D, Sato Y, et al. Cyclic deterioration and its improvement for Li-rich layered cathode material $Li[Ni_{0.17}Li_{0.2}Co_{0.07}Mn_{0.56}]O_2$. *J Power Sources* 2010;195:567-73. DOI
144. Wei Z, Xia Y, Qiu B, Zhang Q, Han S, Liu Z. Correlation between transition metal ion migration and the voltage ranges of electrochemical process for lithium-rich manganese-based material. *J Power Sources* 2015;281:7-10. DOI
145. Yang J, Xiao L, He W, et al. Understanding voltage decay in lithium-rich manganese-based layered cathode materials by limiting cutoff voltage. *ACS Appl Mater Interfaces* 2016;8:18867-77. DOI PubMed
146. Nayak PK, Grinblat J, Levi E, Markovsky B, Aurbach D. Effect of cycling conditions on the electrochemical performance of high capacity Li and Mn-rich cathodes for Li-ion batteries. *J Power Sources* 2016;318:9-17. DOI
147. Pradon A, Caldes M, Petit P, et al. Revisiting the relevance of using a constant voltage step to improve electrochemical performances of Li-rich lamellar oxides. *J Power Sources* 2018;380:158-63. DOI
148. Yin W, Grimaud A, Rousse G, et al. Structural evolution at the oxidative and reductive limits in the first electrochemical cycle of $Li_{1.2}Ni_{0.13}Mn_{0.54}Co_{0.13}O_2$. *Nat Commun* 2020;11:1252. DOI PubMed PMC
149. Kaewmala S, Limphirat W, Yordsri V, et al. Rate dependent structural changes, cycling stability, and Li-ion diffusivity in a layered-layered oxide cathode material after prolonged cycling. *J Mater Chem A* 2021;9:14004-12. DOI
150. Wang E, Zhao Y, Xiao D, et al. Composite nanostructure construction on the grain surface of Li-rich layered oxides. *Adv Mater* 2020;32:e1906070. DOI PubMed
151. Yang K, Liu Y, Niu B, Yang Z, Li J. Oxygen vacancies in CeO_2 surface coating to improve the activation of layered $Li_{1.2}Mn_{0.54}Ni_{0.13}Co_{0.13}O_2$ cathode material for Li-ion batteries. *Ionics* 2019;25:2027-34. DOI
152. Li J, Li J, Yu T, et al. Stabilizing the structure and suppressing the voltage decay of $Li[Li_{0.2}Mn_{0.54}Co_{0.13}Ni_{0.13}]O_2$ cathode materials for Li-ion batteries via multifunctional Pr oxide surface modification. *Ceram Int* 2016;42:18620-30. DOI
153. Ding F, Li J, Deng F, et al. Surface heterostructure induced by $PrPO_4$ modification in $Li_{1.2}[Mn_{0.54}Ni_{0.13}Co_{0.13}]O_2$ cathode material for high-performance lithium-ion batteries with mitigating voltage decay. *ACS Appl Mater Interfaces* 2017;9:27936-45. DOI PubMed
154. Lu C, Wu H, Zhang Y, et al. Cerium fluoride coated layered oxide $Li_{1.2}Mn_{0.54}Ni_{0.13}Co_{0.13}O_2$ as cathode materials with improved electrochemical performance for lithium ion batteries. *J Power Sources* 2014;267:682-91. DOI
155. Lu C, Wu H, Chen B, Liu H, Zhang Y. Improving the electrochemical properties of $Li_{1.2}Mn_{0.52}Co_{0.08}Ni_{0.2}O_2$ cathode material by uniform surface nanocoating with samarium fluoride through depositional-hydrothermal route. *J Alloys Compd* 2015;634:75-82. DOI
156. Xue Q, Li J, Xu G, Zhou H, Wang X, Kang F. In situ polyaniline modified cathode material $Li[Li_{0.2}Mn_{0.54}Ni_{0.13}Co_{0.13}]O_2$ with high rate capacity for lithium ion batteries. *J Mater Chem A* 2014;2:18613-23. DOI
157. Chen Y, Wang X, Zhang J, et al. Al_2O_3-coated $Li_{1.2}Mn_{0.54}Ni_{0.13}Co_{0.13}O_2$ nanotubes as cathode materials for high-performance lithium-ion batteries. *RSC Adv* 2019;9:2172-9. DOI
158. Chen C, Geng T, Du C, et al. Oxygen vacancies in SnO_2 surface coating to enhance the activation of layered Li-rich $Li_{1.2}Mn_{0.54}Ni_{0.13}Co_{0.13}O_2$ cathode material for Li-ion batteries. *J Power Sources* 2016;331:91-9. DOI
159. Liu Y, Yang Z, Li J, Niu B, Yang K, Kang F. A novel surface-heterostructured $Li_{1.2}Mn_{0.54}Ni_{0.13}Co_{0.13}O_2@Ce_{0.8}Sn_{0.2}O_{2-\sigma}$ cathode material for Li-ion batteries with improved initial irreversible capacity loss. *J Mater Chem A* 2018;6:13883-93. DOI
160. Yang Z, Zhong J, Li J, Liu Y, Niu B, Kang F. Li-rich layered oxide coated by nanoscale MoO_x film with oxygen vacancies and lower oxidation state as a high-performance cathode material. *Ceram Int* 2019;45:439-48. DOI
161. Liu Y, Yang Z, Zhong J, et al. Surface-functionalized coating for lithium-rich cathode material to achieve ultra-high rate and excellent cycle performance. *ACS Nano* 2019;13:11891-900. DOI PubMed
162. Si M, Wang D, Zhao R, et al. Local electric-field-driven fast Li diffusion kinetics at the piezoelectric $LiTaO_3$ modified Li-rich cathode-electrolyte interphase. *Adv Sci (Weinh)* 2020;7:1902538. DOI PubMed PMC
163. Zhang W, Sun Y, Deng H, et al. Dielectric polarization in inverse spinel-structured Mg_2TiO_4 coating to suppress oxygen evolution of Li-rich cathode materials. *Adv Mater* 2020;32:e2000496. DOI
164. Hu S, Li Y, Chen Y, et al. Insight of a phase compatible surface coating for long-durable Li-rich layered oxide cathode. *Adv Energy Mater* 2019;9:1901795. DOI
165. Cao J, Xie H, Lv F, et al. Stable Li_2TiO_3 Shell-$Li_{1.17}Mn_{0.50}Ni_{0.16}Co_{0.17}O_2$ core architecture based on an in-site synchronous lithiation

method as a high rate performance and long cycling life lithium-ion battery cathode. *ACS Appl Energy Mater* 2020;3:5462-71. DOI PubMed

166. Yoon CS, Kim U, Park G, et al. Self-passivation of a $LiNiO_2$ cathode for a lithium-ion battery through Zr doping. *ACS Energy Lett* 2018;3:1634-9. DOI
167. Kong D, Hu J, Chen Z, et al. Ti□gradient doping to stabilize layered surface structure for high performance high-Ni oxide cathode of Li-ion battery. *Adv Energy Mater* 2019;9:1901756. DOI
168. Shang H, Ning F, Li B, Zuo Y, Lu S, Xia D. Suppressing voltage decay of a lithium-rich cathode material by surface enrichment with atomic ruthenium. *ACS Appl Mater Interfaces* 2018;10:21349-55. DOI PubMed
169. Lee Y, Shin J, Kang H, et al. Promoting the reversible oxygen redox reaction of Li-excess layered cathode materials with surface vanadium cation doping. *Adv Sci (Weinh)* 2021;8:2003013. DOI PubMed PMC
170. Liu S, Liu Z, Shen X, et al. Surface doping to enhance structural integrity and performance of Li-rich layered oxide. *Adv Energy Mater* 2018;8:1802105. DOI
171. Zhong J, Yang Z, Yu Y, Liu Y, Li J, Kang F. Surface substitution of polyanion to improve structure stability and electrochemical properties of lithium-rich layered cathode oxides. *Appl Surf Sci* 2020;512:145741. DOI
172. Xu G, Li J, Xue Q, et al. Enhanced oxygen reducibility of $0.5Li_2MnO_3{\cdot}0.5LiNi_{1/3}Co_{1/3}Mn_{1/3}O_2$ cathode material with mild acid treatment. *J Power Sources* 2014;248:894-9. DOI
173. Qiu B, Zhang M, Wu L, et al. Gas-solid interfacial modification of oxygen activity in layered oxide cathodes for lithium-ion batteries. *Nat Commun* 2016;7:12108. DOI PubMed PMC
174. Ye Z, Zhang B, Chen T, et al. A simple gas-solid treatment for surface modification of Li-rich oxides cathodes. *Angew Chem Int Ed Engl* 2021;60:23248-55. DOI PubMed
175. Zhang X, Cao S, Yu R, et al. Improving electrochemical performances of Li-rich layered Mn-based oxide cathodes through $K_2Cr_2O_7$ solution treatment. *ACS Appl Energy Mater* 2019;2:1563-71. DOI
176. Zhang XD, Shi JL, Liang JY, et al. Suppressing surface lattice oxygen release of Li-rich cathode materials via heterostructured spinel $Li_4Mn_5O_{12}$ coating. *Adv Mater* 2018:e1801751. DOI
177. Hu K, Lv G, Zhang J, et al. Na_2S treatment and coherent interface modification of the Li-rich cathode to address capacity and voltage decay. *ACS Appl Mater Interfaces* 2020;12:42660-8. DOI PubMed
178. Zhang K, Sheng H, Wu X, et al. Improving electrochemical properties by sodium doping for lithium-rich layered oxides. *ACS Appl Energy Mater* 2020;3:8953-9. DOI
179. Zhu Z, Wang H, Li Y, et al. A surface Se-substituted $LiCo[O_{2-\delta}Se_\delta]$ cathode with ultrastable high-voltage cycling in pouch full-cells. *Adv Mater* 2020;32:e2005182. DOI PubMed
180. Ahn J, Chen D, Chen G. A fluorination method for improving cation-disordered rocksalt cathode performance. *Adv Energy Mater* 2020;10:2001671. DOI
181. Liu C, Wu M, Guo Z, et al. Preparation and characterization of $Li_{1.167-x}K_xMn_{0.583}Ni_{0.25}O_2$ (x=0, 0.025, 0.05 and 0.075) as cathode materials for highly reversible lithium-ion batteries. *Electrochimica Acta* 2020;341:136014. DOI PubMed
182. Li B, Yan H, Ma J, et al. Manipulating the electronic structure of Li-rich manganese-based oxide using polyanions: towards better electrochemical performance. *Adv Funct Mater* 2014;24:5112-8. DOI
183. Wu F, Kim G, Kuenzel M, et al. Elucidating the effect of iron doping on the electrochemical performance of cobalt-free lithium-rich layered cathode materials. *Adv Energy Mater* 2019;9:1902445. DOI
184. Nayak PK, Grinblat J, Levi M, et al. Al doping for mitigating the capacity fading and voltage decay of layered Li and Mn-rich cathodes for Li-ion batteries. *Adv Energy Mater* 2016;6:1502398. DOI
185. Jiang Y, Sun G, Yu F, et al. Surface modification by fluorine doping to increase discharge capacity of $Li_{1.2}Ni_{0.2}Mn_{0.6}O_2$ cathode materials. *Ionics* 2020;26:151-61. DOI
186. Li Y, Xie L, Zheng Z, et al. Hybridizing $Li@Mn_6$ and $Sb@Ni_6$ superstructure units to tune the electrochemical performance of Li-rich layered oxides. *Nano Energy* 2020;77:105157. DOI
187. Wang T, Zhang C, Li S, et al. Regulating anion redox and cation migration to enhance the structural stability of Li-rich layered oxides. *ACS Appl Mater Interfaces* 2021;13:12159-68. DOI PubMed
188. Yu F, Que L, Xu C, et al. Dual conductive surface engineering of Li-Rich oxides cathode for superior high-energy-density Li-Ion batteries. *Nano Energy* 2019;59:527-36. DOI
189. Luo S, Wang K, Wang J, Jiang K, Li Q, Fan S. Binder-free $LiCoO_2$/carbon nanotube cathodes for high-performance lithium ion batteries. *Adv Mater* 2012;24:2294-8. DOI PubMed
190. Zhang T, Li JT, Liu J, et al. Suppressing the voltage-fading of layered lithium-rich cathode materials via an aqueous binder for Li-ion batteries. *Chem Commun (Camb)* 2016;52:4683-6. DOI PubMed
191. Yang J, Li P, Zhong F, et al. Suppressing voltage fading of Li-rich oxide cathode via building a well-protected and partially-protonated surface by polyacrylic acid binder for cycle-stable Li-ion batteries. *Adv Energy Mater* 2020;10:1904264. DOI
192. Choi Y, Zhang K, Chung KY, Wang DH, Park JH. PVdF-HFP/exfoliated graphene oxide nanosheet hybrid separators for thermally stable Li-ion batteries. *RSC Adv* 2016;6:80706-11. DOI
193. Shin WK, Kannan AG, Kim DW. Effective suppression of dendritic lithium growth using an ultrathin coating of nitrogen and sulfur codoped graphene nanosheets on polymer separator for lithium metal batteries. *ACS Appl Mater Interfaces* 2015;7:23700-7. DOI PubMed
194. Zhang J, Meng Z, Yang D, et al. Enhanced interfacial compatibility of FeS@N,S-C anode with ester-based electrolyte enables stable sodium-ion full cells. *J Energy Chem* 2022;68:27-34. DOI

195. Qi S, Mi L, Song K, et al. Understanding shuttling effect in sodium ion batteries for the solution of capacity fading: FeS_2 as an example. *J Phys Chem C* 2019;123:2775-82. DOI
196. Martha SK, Nanda J, Veith GM, Dudney NJ. Surface studies of high voltage lithium rich composition: $Li_{1.2}Mn_{0.525}Ni_{0.175}Co_{0.1}O_2$. *J Power Sources* 2012;216:179-86. DOI
197. Cui C, Fan X, Zhou X, et al. Structure and interface design enable stable Li-rich cathode. *J Am Chem Soc* 2020;142:8918-27. DOI PubMed
198. Lou S, Ma Y, Zhou Z, et al. Unravelling the enhanced high-temperature performance of lithium-rich oxide cathode with methyl diphenylphosphinite as electrolyte additive. *ChemElectroChem* 2018;5:1569-75. DOI
199. Yue Y, Li N, Li L, et al. Redox behaviors in a Li-excess cation-disordered Mn-Nb-O-F rocksalt cathode. *Chem Mater* 2020;32:4490-8. DOI
200. Yu T, Li J, Xu G, Li J, Ding F, Kang F. Improved cycle performance of $Li[Li_{0.2}Mn_{0.54}Co_{0.13}Ni_{0.13}]O_2$ by Ga doping for lithium ion battery cathode material. *Solid State Ionics* 2017;301:64-71. DOI
201. Redel K, Kulka A, Plewa A, Molenda J. High-performance Li-rich layered transition metal oxide cathode materials for Li-ion batteries. *J Electrochem Soc* 2019;166:A5333-42. DOI
202. Hy S, Felix F, Rick J, Su WN, Hwang BJ. Direct in situ observation of Li_2O evolution on Li-rich high-capacity cathode material, Li[Ni(x)Li((1-2x)/3)Mn((2-x)/3)]O2 ($0 \leq x \leq 0.5$). *J Am Chem Soc* 2014;136:999-1007. DOI
203. Sathiya M, Leriche JB, Salager E, Gourier D, Tarascon JM, Vezin H. Electron paramagnetic resonance imaging for real-time monitoring of Li-ion batteries. *Nat Commun* 2015;6:6276. DOI PubMed PMC
204. Xu J, Sun M, Qiao R, et al. Elucidating anionic oxygen activity in lithium-rich layered oxides. *Nat Commun* 2018;9:947. DOI PubMed PMC
205. Zhang J, Wang Q, Li S, et al. Depth-dependent valence stratification driven by oxygen redox in lithium-rich layered oxide. *Nat Commun* 2020;11:6342. DOI PubMed PMC
206. Dai K, Wu J, Zhuo Z, et al. High reversibility of lattice oxygen redox quantified by direct bulk probes of both anionic and cationic redox reactions. *Joule* 2019;3:518-41. DOI
207. Shimoda K, Minato T, Nakanishi K, et al. Oxidation behaviour of lattice oxygen in Li-rich manganese-based layered oxide studied by hard X-ray photoelectron spectroscopy. *J Mater Chem A* 2016;4:5909-16. DOI
208. Assat G, Iadecola A, Foix D, Dedryvère R, Tarascon J. Direct quantification of anionic redox over long cycling of Li-rich NMC via hard X-ray photoemission spectroscopy. *ACS Energy Lett* 2018;3:2721-8. DOI
209. Abate II, Pemmaraju CD, Kim SY, et al. Coulombically-stabilized oxygen hole polarons enable fully reversible oxygen redox. *Energy Environ Sci* 2021;14:4858-67. DOI
210. House RA, Maitra U, Pérez-Osorio MA, et al. Superstructure control of first-cycle voltage hysteresis in oxygen-redox cathodes. *Nature* 2020;577:502-8. DOI PubMed
211. Carlier D, Saadoune I, Ménétrier M, Delmas C. Lithium electrochemical deintercalation from O_2-$LiCoO_2$. *J Electrochem Soc* 2002;149:A1310. DOI PubMed